Structural Health Monitoring of Aircraft Composite Structures using Ultrasonic Guided Wave Propagation

Mohammad Hossein Sherafat

Department of Mechanical Engineering
McGill University, Montreal

A thesis submitted to McGill University in partial fulfilment of the requirements of the degree of doctor of philosophy

ABSTRACT

Despite enhancements in terms of specific strength and stiffness by using composite in aircraft structures, their susceptibility to hide damage is still a major point of concern. The objective of this work is to investigate guided wave propagation in composite structures to detect delaminations, disbond and impact damage.The majority of the work focuses on assessment of composite joints. Primarily, a simple composite structure configuration was chosen to evaluate the effect of artificial and real damage on guided wave behaviour. The results show that non-mid-plane artificial delamination can accurately represent real impact, particularly barely visible impact damage (BVID). Next, a composite skin-stringer assembly and a composite scarf repair were chosen in order to represent typical aerospace structural joint features. The reflection, transmission and scattering behaviour of the plane guided waves are studied as a function of mode, frequency, excitation angle and the quality of the joint. For the composite skin-stringer, two inspection strategies are applied. From the first strategy, the within-the-bond, it is concluded that the antisymmetric mode (A0) transmission is highly sensitive to the damage for frequencies below 350 kHz, while the symmetric mode (S0) reflection around 200 kHz could be employed for monitoring an echo induced by the disbond. For imaging the disbond based on the scattering of the waves, the S0 mode appears as the best candidate below 350 kHz, by inducing an increase of 60 % of the scattered field in the presence of a disbond. The results from the second strategy, the across-the-bond, indicate that the A0 mode behaves more directionally while S0 is more refracted, specifically at low frequencies. For damage imaging, the S0 mode appears to be sensitive enough to disbonds (an increase of 30 % of the scattered wave) at around 150 kHz. Comparison of the pristine and damaged repair joint indicates reflection at the tip of each layer in the scarf (the reflections from the steps' edges), which can be an indication for evaluation of the quality of the joint. The anti-symmetric mode in the pulse-echo configuration seems to be an efficient mode and strategy for disbond detection in composite repairs.

SOMMAIRE

Malgré toutes les améliorations en termes de résistance et de rigidité amenées par l'utilisation des structures composites, leur sensibilité à des défauts internes reste un sujet qui soulève des préoccupations. L'objective de ce projet est d'étudier l'interaction des ondes guidées pour la détection des défauts tels que les délaminations, les décollements et les endommagements par impact. Une première configuration a été choisie pour évaluer l'effet d'un défaut artificiel et d'un endommagement réel sur la propagation de l'onde guidée. Les résultats montrent qu'un défaut artificiel peut correctement simuler un défaut réel d'impact, surtout lorsqu'il s'agit d'un défaut à peine visible. Cependant, la majorité de ce travail de cette thèse de doctorat se focalise sur l'évaluation des joints en composite. Un assemblage composé d'une peau raidie en composite et un joint de réparation ont été choisis pour représenter des configurations typiques d'assemblage aéronautique. Les comportements des ondes guidées planes en transmission, réflexion et en dispersion ont été étudié en fonction des modes, fréquence, l'angle d'excitation et l'état du joint. Pour la plaque à raidisseur, deux stratégies d'inspection ont été appliquées. Dans la première stratégie, il a été conclu que le mode antisymétrique (A0) en transmission est très sensible à des défauts de décollement pour des fréquences inférieures à 350 kHz, alors que pour le mode symétrique (S0) la réponse en réflexion autour de 200 kHz présente un bon paramètre pour la surveillance de ce type défaut. Concernant la détection de ce défaut en se basant sur la réponse en dispersion, le mode S0 parait le mieux adapté pour des fréquences inférieures à 350KHz puisqu'il introduit une augmentation de la dispersion d'environ 60%. Les résultats obtenus de la deuxième stratégie, à travers le collage, montrent que le mode A0 à un comportement plus directif alors que le mode S0 est beaucoup plus réfracté particulièrement pour des basses fréquences. Pour la détection d'endommagement, le mode S0 parait suffisamment sensible pour un défaut de décollement (une augmentation de 30% de la dispersion de l'onde) à environ 150kHz. La comparaison entre un joint réparé avec et sans défaut montre que la réflexion à la pointe de chaque couche du recouvrement (les réflexions en provenance des bords) peut être un indicateur sur la qualité du joint. Le mode antisymétrique dans la configuration « pulse-echo » s'avère être un mode efficace et une bonne stratégie pour la détection des décollements dans les joints réparés en composite.

ACKNOWLEDGEMENT

I would like to express my sincere gratitude towards my supervisors, Professor Larry Lessard and Professor Pascal Hubert for their supervision, advice, and kindness throughout the course of this research. I would like to express special thanks to Professor Lessard for his friendly support, patient guidance, and constructive and timely feedbacks. I would also like to give my appreciation to Professor Hubert for his valuable time and insightful comments which contributed to the overall quality of this work. I also greatly appreciate their understanding during the last year of my research, facilitating my graduation in aviation management from McGill.

I would like to acknowledge the support of the Natural Sciences and Engineering Research Council of Canada (NSERC), the Consortium for Research and Innovation in Aerospace in Québec (CRIAQ) as well as the industry partners, Bombardier Aerospace, L-3 MAS, and Centre Technologique en Aérospatiale (CTA).

Technical Cooperation Bureau of International Civil Aviation Organization (ICAO), Fonds de recherche du Québec - Nature et technologies (FRQNT), and Mitacs are also gratefully acknowledged for their financial support.

I also owe many thanks to Professor Patrice Masson and Dr. Nicolas Quaegebeur for their guidance, assistance, and providing the experimental facilities. Finally, I would like to thank my friends and members of "McGill Composite Materials and Structures Laboratory" and "Groupe d'acoustique de l'Université de Sherbrooke (GAUS)" for their helpful support.

The support of my family has been very important to me, particularly that of my parents for their encouragements and prayers. Finally, my loving wife, Zahra, your patience – and sometimes your impatience, your interest in my work, the extra time you put into managing our household while doing your own PhD, and all your sacrifices – I could never have finished my PhD without all of this. Thank you so much.

CONTRIBUTION OF THE AUTHORS

First Manuscript (Chapter 3): "A Comparative Study of Guided Wave Interaction in Composites with Artificial Delamination and Impact Damage", Sherafat, M.H., Quaegebeur, N., Hubert, P., Lessard, L., Masson, P.

Sherafat, M.H.:

- Identified the design parameters (material, lay-up, size).
- Identified the defect parameters (location, size, severity).
- Designed the four composite test coupons.
- Conducted the experiments.
- Analysed and interpreted the results.
- Wrote the manuscript.

Quaegebeur, N.:

- Assisted in conducting the experiments.
- Assisted in the understanding of the experimental results.
- Developed the signal processing.
- Reviewed the manuscript.

Hubert, P.:

- Provided guidance to the general direction of the work.
- Reviewed the manuscript.

Lessard, L.:

- Provided guidance to the general direction of the work.

- Reviewed the manuscript.

Masson, P.:

- Decided the general objective of the work.
- Provided the required set-up for conducting the experiments.
- Reviewed the manuscript.

With acknowledgement of the support of the Centre Technologique en Aérospatiale (CTA) for manufacturing of the test coupons.

Second Manuscript (Chapter 4): “Structural Health Monitoring of a Composite Skin-Stringer Assembly using Within-the-bond Strategy of Guided Wave Propagation”, Sherafat, M.H., Guitel, R., Quaegebeur, N., Hubert, P., Lessard, L., Masson, P.

Third Manuscript (Chapter 5): “Guided Wave Scattering Behaviour in Composite Bonded Assemblies”, Sherafat, M.H., Guitel, R., Quaegebeur, N., Lessard, L., Hubert, P., Masson, P.

Sherafat, M.H.:

- Identified the design parameters (material, lay-up, size).
- Identified the defect parameters (location, size, severity).
- Designed the skin-stringer test coupon.
- Conducted the experiments.
- Analysed and interpreted the results.
- Wrote the manuscript.

Guitel, R.:

- Assisted in conducting the experiments.
- Assisted the signal processing.

Quaegebeur, N.:

- Assisted in conducting the experiments.
- Assisted in the understanding of the experimental results.
- Developed the signal processing.
- Reviewed the manuscript.

Hubert, P.:

- Provided guidance to the general direction of the work.
- Reviewed the manuscript.

Lessard, L.:

- Provided guidance to the general direction of the work.
- Reviewed the manuscript.

Masson, P.:

- Decided the general objective of the work.
- Provided the required set-up for conducting the experiments.
- Reviewed the manuscript.

Fourth Manuscript (Chapter 6): "Finite Element Modelling of Lamb Wave Propagation in Composite Stepped Joints", Sherafat, M.H., Quaegebeur, N., Lessard, L., Hubert, P., Masson, P.

Sherafat, M.H.:

- Identified the design parameters (material, lay-up, size).
- Identified the defect parameters (location, size).
- Designed the composite repair test coupon.

- Manufactured the test coupon.
- Conducted the experiments.
- Developed and conduct the numerical analysis.
- Developed the signal processing for numerical results.
- Analysed and interpreted the results.
- Wrote the manuscript.

Quaegebeur, N.:

- Assisted in conducting the experiments.
- Assisted in the understanding of the experimental results.
- Developed the signal processing.
- Reviewed the manuscript.

Hubert, P.:

- Provided guidance to the general direction of the work.
- Reviewed the manuscript.

Lessard, L.:

- Provided guidance to the general direction of the work.
- Reviewed the manuscript.

Masson, P.:

- Decided the general objective of the work.
- Provided the required set-up for conducting the experiments.
- Reviewed the manuscript.

TABLE OF CONTENTS

ABSTRACT ii

SOMMAIRE iii

ACKNOWLEDGEMENT iv

CONTRIBUTION OF THE AUTHORS v

TABLE OF CONTENTS ix

LIST OF TABLES xiii

LIST OF FIGURES xiv

1. CHAPTER 1. INTRODUCTION 1

1.1 Introduction to Composite Structures 1

1.1.1 Composite bonded joints 1

1.2 Structural Health Monitoring (SHM) 2

1.2.1 Guided wave propagation 6

1.3 Research Objectives 7

1.4 Structure of the Thesis 7

1.5 References 10

2. CHAPTER 2. LITERATURE REVIEW 12

2.1 Preface 12

2.2 Wave propagation fundamentals and principles 13

2.3 Actuators and sensors for Lamb waves 17

2.3.1 Ultrasonic probe 17

2.3.2 Laser-based Ultrasonics 17

2.3.3 Optical fibres 18

2.3.4 Interdigital Transducers 18

2.3.5 Piezoelectric Wafers and Piezocomposite Transducers 18

2.4 SHM using PZT generated-Lamb waves 20

2.4.1 Impedance based methods 20

2.4.1 Pitch-Catch method 21

2.4.2 Pulse-Echo Method 23

2.4.3 Piezoelectric phased-arrays 25
2.5 Processing of Lamb wave signals 25
2.5.1 Time domain analysis 26
2.5.2 Frequency domain analysis 28
2.6 Damage Identification 30
2.6.1 Damage Localization 31
2.6.2 DIs in Time Domain 32
2.6.3 DIs in Frequency Domain 33
2.7 Recent literature summary, research gap 34
2.8 References 37
3. CHAPTER 3. FIRST MANUSCRIPT 54
3.1 Preface 54
3.2 Abstract 55
3.3 Introduction 56
3.4 Structure description 59
3.5 Experimental methodology 61
3.5.1 Guided wave generation and sensing 62
3.6 Theoretical considerations, results, and discussion 64
3.6.1 Reflection and transmission 65
3.6.2 Scattering 68
3.7 Conclusion 71
3.8 Acknowledgments 72
3.9 References 72
4. CHAPTER 4. SECOND MANUSCRIPT 76
4.1 Preface 76
4.2 Abstract 77
4.3 Introduction 78
4.4 Structure description 80
4.5 Experimental methodology 81
4.5.1 Guided wave generation and sensing 82
4.6 Theoretical considerations, results, and discussion 84
4.6.1 Wavenumber extraction 84

4.6.2 Damping extraction ... 86
4.6.3 Reflection and transmission ... 88
4.6.4 Scattering at the disbond ... 90
4.7 Conclusion ... 92
4.8 Acknowledgments ... 93
4.9 References ... 93
5. CHAPTER 5. THIRD MANUSCRIPT ... 96
5.1 Preface ... 96
5.2 Abstract ... 97
5.3 Introduction ... 98
5.4 Structure description ... 100
5.5 Experimental methodology ... 101
5.5.1 Guided wave generation and sensing ... 102
5.6 Result and discussion ... 106
5.6.1 Influence of the mode and frequency of guided wave on scattering ... 106
5.6.2 The effect of the excitation orientation of guided waves on scattering ... 107
5.6.3 The effect of disbond on scattering ... 111
5.7 Conclusion ... 114
5.8 Acknowledgments ... 115
5.9 References ... 115
6. CHAPTER 6. FOURTH MANUSCRIPT ... 118
6.1 Preface ... 118
6.2 Abstract ... 119
6.3 Introduction ... 120
6.4 Numerical Modeling ... 122
6.4.1 Finite element modeling ... 122
6.4.2 Excitation of guided waves ... 124
6.5 Numerical results and discussion ... 125
6.5.1 Guided wave propagation and characterization ... 125
6.5.2 Reflection and transmission coefficients ... 127
6.6 Experimental setup ... 128
6.6.1 Structural description ... 128

6.6.2 Guided wave generation and sensing 129
6.6.3 Experimental results and discussion 131
6.7 Conclusion 134
6.8 Acknowledgments 135
6.9 References 135
7. CHAPTER 7. CONCLUSIONS AND FUTURE WORK 139
7.1 Preface 139
7.2 Summary of key findings 140
7.2.1 Interaction of artificial delamination and impact damage with guided waves 140
7.2.2 Within and across the bondline strategies of guided waves propagation in composite skin-stringer assembly 140
7.2.3 Guided waves propagation in composite scarf repair 141
7.3 Conclusions 143
7.4 Publications and presentations 144
7.5 Future Work 146

LIST OF TABLES

Table 1.1. Comparison of traditional NDI approach and SHM 5

Table 3.1. Composite samples with delamination and impact 61

Table 4.1. Material properties from manufacturers of woven CFRP (CYCOM 5320) and adhesive film (Cytec FM-300-2).. 80

Table 5.1. Material properties from manufacturers of woven CFRP (CYCOM 5320) and adhesive film (Cytec FM-300-2).. 100

Table 6.1. Material properties of woven CFRP (Newport NB 321 3K) and adhesive film [17]... 122

LIST OF FIGURES

Figure 1.1. Schematic representation of an SHM sensor network on a typical aircraft structure and its similarity to human nervous system network [16] 5

Figure 1.2. Schematic presentation of the thesis structure based on four research papers........ 9

Figure 2.1. Phase (C_p) and group velocities (C_g) of a pulse 13

Figure 2.2. Description of the first three symmetric (S) and anti-symmetric (A) mode shapes of Lamb waves, with the displacement profiles across the thickness of the plate........ 14

Figure 2.3. Dispersion curves (phase velocity ω/k depending on the frequency) obtained for a 1 mm thick, seven-ply [0/+45/90/-45/0/45/90/-45] Carbon-Epoxy plate. Anti-symmetric modes are represented by solid lines, and symmetric modes are represented by dotted lines 15

Figure 2.4. Slowness profiles of (a) symmetric; and (b) anti-symmetric Lamb modes in a [+456/-456]s CFRP laminate; (c) symmetric; and (d) anti-symmetric Lamb modes in a [+45/-45/0/90]s CFRP laminate (the angle refers to the inclination between the wave propagation direction and 0° in the carbon fibre) [4] 16

Figure 2.5. Illustration of the piezoceramic element (a) and excitation clamp (b)........ 20

Figure 2.6. Real part of the electro-mechanical impedance of a PZT bonded on a CFRP plate [34] with no damage and with a crack located in the near-field (3mm) (a). The probability of detection by integration of the differences in the 300 - 450 kHz band (b) 21

Figure 2.7. Ultrasonic damage detection techniques with pitch-catch method........ 22

Figure 2.8. Ultrasonic damage-detection techniques with Pulse-echo method........ 23

Figure 2.9. Comparative response of a pristine (solid line) and damaged (dashed line) CFRP sandwich beam after low-velocity impact [74] 24

Figure 2.10. Principle of use of a six channels piezoelectric phased-array for emission in the direction θ_{OUT} (left) and reception in the direction θ_{IN} (right)........ 25

Figure 2.11. An example of a Hilbert transform: (a) original constitutive signals: a sinusoid of frequency 1500 kHz and a 3-count tone-burst of 300 kHz; (b) the synthetic signal (A1≠A2,Ø1≠Ø2) and its envelope extracted by Hilbert transform [48] 26

Figure 2.12. Lamb wave signals captured in a CF/EP laminate: (a) before (benchmark); and (b) after the introduction of delamination; (c) correlation coefficient curves of two signals in (a) and (b); and (d) ratio of signal correlation coefficients of delaminated to benchmark laminate [81] 27

Figure 2.13. Concept of time reversal: (a) actuator A sends an input Lamb wave signal; (b) sensor B captures the response signal; (c) sensor B (now serving as an actuator) sends the reversed waveform of the signal that is captured in step (b); and (d) actuator A (now serving as a sensor) captures the response signal [83]........ 28

Figure 2.14. Time domain (a), Hilbert Transform (b) and Fourier Transform (c) of a typical signal used for signal processing comparison (5 cycles 100 kHz sinusoidal signal - 1Mhz sampling Frequency - Hanning window - repeated twice - additional white noise of 0.05 amplitude)............ 29

Figure 2.15. Detection of delamination location via direct algorithms [62]. Pseudo results (crosses) always accompany real delamination results (dots) 32

Figure 2.16. Definition of difference in the ToFs between the incident diagnostic wave and the damage-scattered wave [2] 32

Figure 3.1. Illustration of the piezoceramic element and excitation clamp (left) and the experimental setup (right) 62

Figure 3.2. Schematic representation of the scanning grid. Reflection (square blue), transmission (rectangular green) and diffraction (circle yellow) scanning points for 180° (left) 135° (middle) and 90° (right) excitation 63

Figure 3.3. Reflection coefficients of the A0 mode for the four damaged samples, excitation angle of 180° (dashed lines), 135° (solid lines) and 90°(dotted lines).. 66

Figure 3.4. Transmission coefficients of the A0 mode for the four damaged samples, excitation angle of 180° (dashed lines), 135° (solid lines) and 90° (dotted lines) 67

Figure 3.5. Diffraction pattern of the A0 mode excited at 50 kHz, 180° (left), 135° (middle), and 90°(right) for the four damaged plates: Teflon 3, 4 (black), Teflon 8, 9 (yellow), 10 J (blue), and 15 J (red) 69

Figure 3.6. Diffraction pattern of the A0 mode excited at 200 kHz, 180° (left), 135° (middle), and 90° (left) for the four damaged samples: Teflon 3, 4 (black), Teflon 8, 9 (yellow), 10 J (blue), and 15 J (red) 70

Figure 3.7. Diffraction pattern of the A0 mode excited at 350 kHz, 180° (left), 135° (middle), and 90° (right) for the four damaged samples: Teflon 3, 4 (black), Teflon 8, 9 (yellow), 10 J (blue), and 15 J (red) 70

Figure 4.1. Schematic view of the skin-stringer bonded joint configuration; undamaged (right) and damaged joint (left) 81

Figure 4.2. Illustration of the piezoceramic element and excitation clamp (a) and the experimental set up (b).. 83

Figure 4.3. Scanning grid of the undamaged joint (first scan grid) and the damaged joint (second scan grid). Reflection (square blue), transmission (rectangular green) and diffraction (circle yellow) scanning points 84

Figure 4.4. Frequency/wavenumber representation of the measured signals in the reflected path (see Fig. 4.3). The positive wavenumber domain corresponds to the incident field while the negative wavenumbers represent the reflected field. 86

Figure 4.5. Damping coefficient η of the A0 (blue) and S0 (red) modes in the bond line direction for the undamaged joint as a function of mode and frequency. The attenuation curves are obtained after smoothing of the raw estimated parameters 87

Figure 4.6. Reflection coefficients of A0 (top) and S0 (bottom) mode for both undamaged (solid blue) and damaged (dashed red) lines 89

Figure 4.7. Transmission coefficients of A0 (top) and S0 (bottom) mode for both undamaged (solid blue) and damaged (dashed red) lines 90

Figure 4.8. The effect of excitation frequency and propagating mode on the scattering behaviour: diffraction pattern of the A0 (left) and S0 modes (right) for the undamaged (solid blue) and the damaged joint (dashed red) 92

Figure 5.1. Schematic view of the skin-stringer bonded joint configuration; undamaged (right) and damaged joint (left) 101

Figure 5.2. Illustration of the piezoceramics element (a) and excitation clamp (b). 102

Figure 5.3. Schematic (a) and actual (b) illustration of the experimental setup 103

Figure 5.4. Scanning grid of the undamaged joint (first scan grid) and the damaged joint (second scan grid) 103

Figure 5.5. Schematic view (a) and actual representation (b) of the scanning grid details for 180° excitation incident angle 105

Figure 5.6. Schematic view (a) and actual representation (b) of the scanning grid details for 135° excitation incident angle 105

Figure 5.7. The effect of excitation frequency on the scattering behaviour: Diffraction pattern of the A0 (top) and S0 modes (bottom) for the undamaged (left) and the damaged joint (right) for an incident wave oriented at 180° 107

Figure 5.8. Diffraction pattern of the S0 mode at 150 kHz (top) 300 kHz (middle) and 500 kHz (bottom) for 180° and 135 ° excitation incident angles for the undamaged (left) and damaged joint (right) 109

Figure 5.9. Diffraction pattern of the A0 mode at 100 kHz (top) 300 kHz (middle) and 500 kHz (bottom) for 180° and 135 ° excitation incident angles for the undamaged (left) and damaged joint (right) 110

Figure 5.10. The sensitivity of the scattering field to the disbond: the difference between the undamaged and damaged scattering coefficients at every 50 kHz for 180° excitation angle 112

Figure 5.11. The effect of the disbond on the scattering behaviour: Diffraction pattern of the A0 mode (left) and S0 mode (right) for 180° excitation 113

Figure 6.1. Definition of the geometry of the structure (a), and detailed presentation of the undamaged (blue) and damaged (red) steps (b) used for 2-D FEM modelling of the scarf bonded joint 123

Figure 6.2. Mesh refinement representation around the steps 124

Figure 6.3. Dispersion curve for the composite scarf joint, green line (S0 mode), solid blue line (A0 mode undamaged) and dashed red line (A0 mode damaged) 125

Figure 6.4. Frequency/Wavenumber transform of the out-of-plane displacement for a propagating wave on the reflection side in the undamaged (top) and damaged (bottom) joint 126

Figure 6.5. Reflection coefficient (top) and transmission coefficient (bottom) of A0 mode for the undamaged (solid-blue) and damaged (dash-red) stepped joint as a function of frequency 127

Figure 6.6. Manufacturing of composite scarf joint using two stepped samples 129

Figure 6.7. Illustration of the piezoceramics and excitation clamp (a) and the experimental setup (b) 130

Figure 6.8. Two linear scanning grids, the pristine zone of the joint (a) and zone of the joint with disbond (b) 131

Figure 6.9. Frequency/Wavenumber transform for a propagating wave in the composite plate. Components in the x- (top) and z- direction (bottom) are presented for the case out-of-phase excitation 132

Figure 6.10. Reflection coefficients of A0 mode versus frequency (top) and wavelength (bottom) for the undamaged (blue) and damaged (red) stepped joint 132

Figure 6.11. Out-of-plane velocity response to a seven cycles Hanning windowed burst at 300 kHz before the joint in the case of undamaged (blue) and damaged (red) stepped joint 133

CHAPTER 1. INTRODUCTION

1.1 Introduction to Composite Structures

The use of composite materials in commercial aircraft structures has dramatically increased from nearly 5% in 1970 (Airbus 300) to more than 50% in 2010 (Airbus 350, Boeing 787) [1]. This shift is primarily due to the tailorability of composite materials, which enhances production rates by introducing large and integrated parts that require fewer joining operations. Also, composites are significantly lighter, stronger and can resist corrosion and fatigue damage better than traditional aluminium alloys. Moreover, they have low thermal expansion, enhanced fatigue life, improved in-service durability and lower maintenance costs [2, 3].

During the last decades, a wide range of composite manufacturing methods have been developed such as autoclave curing, filament winding, pultrusion, liquid composite moulding, out-of-autoclave and several other methods. Among these manufacturing methods, the out-of-autoclave (OOA) process is being increasingly used recently because it lowers manufacturing costs substantially. The OOA technology enables composites to be fabricated using only vacuum pressure, eliminating the cost of purchasing and operating an autoclave. Another potential cost saving element is the use of low-temperature tooling materials, such as wood or syntactic foam [5]. The OOA materials are specially designed so that the prepreg is partially impregnated to make a porous medium, which allows evacuating entrapped air prior the point where the resin infuses the fibres [6]. In this research, most of the CFRP test articles are manufactured using the OOA vacuum bagging process.

1.1.1 Composite bonded joints

Adhesive bonding of composite structural elements is intensively used in the aviation industry to restore structural integrity in repaired or assembled sub-structures. It allows large-area joining and potentially reduces or eliminates the need for bolts and fastened joints. Adhesive bonding processes are employed for joining polymeric composite elements (e.g. co-cured skin-stringers) or metallic and composite components (e.g. hybrid assemblies) [7]. The major advantages of adhesive bonding include greater fatigue resistance, fewer stress concentration zones, light weight, ability to join thin and dissimilar components, low manufacturing cost, good sealing, and good vibration and damping properties [8]. The most common adhesives used in the bonding of aircraft composite structures are thermosetting film adhesives, such as epoxies and nitrile-phenolics, which generally require elevated temperature curing. However thermoset adhesive systems are usually brittle and offer little resistance to crack growth, even though they offer high strength, good stiffness and are moisture and creep resistant.

Despite the advantages, adhesive bonding has had limited applications in primary structure in civil aircraft because of concerns with their durability and consistency. The joint area is known as a zone of potential weakness, because of load transferring phenomena taking place that may induce minor cracks and disbonds. Moreover, the adhesive is prone to degradation over time, harsh environment or improper installation, resulting in local disbonds or porosity. In composite bonded joints, aging, thermal, environmental and mechanical influences are just a few mechanisms that could lead to failure or damage. Failure of any component, specifically in the aerospace industry, could induce critical situations for humans, which is the most unwanted consequence of any possible incident. As a result, inspection, maintenance, and reliability become vital subjects. Since the adhesive bond itself is not usually accessible or visible, non-destructive inspection (NDI) methods are proposed to quantify the properties of hidden layers.

1.2 Structural Health Monitoring (SHM)

There are three main categories of damage that are taken into consideration in aircraft structural design, analysis, and maintenance. Fatigue Damage (FD) refers to the defects, mainly cracks or minor delaminations induced by cyclic loading of aircraft structures during flight. Physical deterioration of a structural element's strength or resistance as a result of chemical and/or thermal interaction with climate or the environment is classified as the Environmental Damage (ED), (e.g., corrosion). Accidental Damage (AD) refers to any physical deterioration of a structure caused by contact or impact with an object, which could be by another part of the aircraft or by human error during manufacturing, operation or maintenance activities (e.g., tool drop, ground handling impacts, etc.).

Even though an adhesively bonded joint can restore the strength of a repaired composite up to 80% of the original laminate strength [9], this structural feature is prone to three categories of damage: degradation of the adhesive, inappropriate installation or disbonding when submitted to fatigue loads. These types of defects can significantly jeopardize the integrity and performance of a structure, and subsequently safety of the flight. The recognition of safety, integrity, and durability as the principal priorities for engineered structures and materials has led to intensive research and development in the field of Non-Destructive Inspection (NDI) techniques.

Over the last 50 years, NDI techniques have attained maturity in engineering applications, playing a significant role in the assessment of the integrity and durability of the structures. The most common methods include visual inspection, detailed visual inspection using penetrant and magnetic particles, Eddy current, thermography, optical interferometry, radiography, ultrasonic inspection, acoustic emission and vibration/modal analysis. For composite structures (including bonded joints), the classical technique for inspection is based on a global scan of the structure (C-scan) using expensive ultrasonic equipment, or sometimes thermography is used. They are often considered as time-consuming diagnostic systems due to the requirement of point-to-point inspection performed by a technician. The NDI techniques are usually conducted at regularly scheduled intervals during the structure's lifetime. However, they sometimes cannot provide efficient access to appropriate critical sections of the structures in a real-time manner and provide limited information about structural integrity. For instance, the failure Air Transat Flight TS961 Airbus 310 composite rudder on a flight from Cuba to Quebec City in 2005 took place just five days after its routine A-check [10].

Structural Health Monitoring (SHM), as a retrofitted version of conventional NDI, has been proposed for continuous inspection of composite structural features to evaluate their health and integrity in a real-time manner. SHM is a major area of interest for the aerospace community, especially considering aging aircraft where the growing maintenance costs, estimated at $10.4 billion worldwide annually, can reduce their economic life [11]. The application of SHM may reduce these costs by allowing condition-based maintenance practices to replace the current interval-based maintenance approach [12]. The use of condition-based maintenance, benefiting from continuous on-line structural integrity monitoring, could significantly reduce the cost of the inspection phase. In other words, retirement-for-cause instead of retirement-as-planned could minimise the cost while maintaining a safe operation life for many aging aircraft structures. Also, the replacement of our present-day "manual inspection" with "automatic health monitoring" would substantially reduce the associated life-cycle costs (e.g. training and certification costs) as well as the risks related to human error. It has been demonstrated that an effective SHM technique can reduce the total maintenance cost compared to traditional NDE approaches by more than 30% for an aircraft fleet [13]. It has also been shown that life of the F-18 of the Canadian Air Force could be extended by 12 years, by monitoring the operational loads, thus leading to savings of 400 million Canadian dollars [14]. The comparison of SHM and traditional NDI approach is summarized in Table 1.1.

The idea of SHM is to employ sensor networks on the structure inspired by the human body and its nervous system. Fig. 1.1 shows the schematic representation of the sensor cluster on the different sections of a structure based on the idea of the human neural network. In aircraft structures, a signal generation unit generates desired signals and sends them to smart distribution of multiple communicating sensors, embedded or surface bonded to the structure under inspection. Sensors activate diagnostic elastic waves into the structures and subsequently receive them after travelling in certain targeted areas. The information is collected into a data acquisition and sent to the SHM central processing unit for diagnostic calculations. After integrating the data from other locations, the information is analysed, usually compared to the baseline data and eventually presented for final evaluation.

Table 1.1. Comparison of traditional NDI approach and SHM

Inspection approach	NDI	SHM
Maintenance Philosophy	- Interval-based maintenance - Baseline not available	- Condition-based maintenance - Baseline required [15]
Cost Elements	- Aircraft grounding, unnecessary removal, and installation of panels - Training and certification of the inspector	- No grounding time, cost saving up to 30% [13] - No training and certification costs
Safety Considerations	- Human interactions, human factors - Limited info. on structural integrity	- Limited human interactions - Efficient in integrity assessment
Other considerations	- Find existing damage	- Determine fitness for service and remaining useful time - Environmental data compensation method required [15]

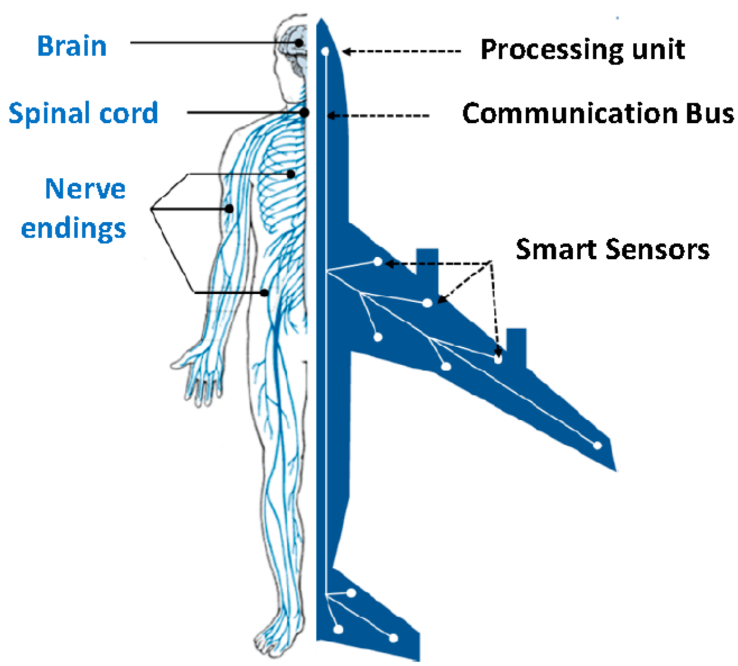

Figure 1.1. Schematic representation of an SHM sensor network on a typical aircraft structure and its similarity to human nervous system network [16]

1.2.1 Guided wave propagation

Typical approaches for performing SHM are modal-data-based (insensitive to small damage), electro-mechanical-impedance-based (unable to detect damage distanced from sensors and not highly accurate), static-parameter-based (insensitive to undersized damage), acoustic emission (prone to contamination and suitable for only small structures), and guided-wave-based [17]. Among the above-mentioned different approaches of SHM, the guided-wave-based strategies are cost effective, fast, repeatable, able to inspect large structures, sensitive to small damage size and able to detect both surface and internal damage [17]. Guided waves were first described by Lamb [18] for homogeneous isotropic materials, and were thus called "Lamb waves". They are ultrasonic waves that are guided between two parallel free surfaces, such as the upper and lower surfaces of a plate. However, the propagation of guided waves in anisotropic or viscoelastic media is complex. With a very fast velocity, waves reflected from boundaries may easily obscure damage-scattered components in the signals [19]. To have precision, the structure under inspection needs to be relatively large, and with a relatively small area for detection. In general, a Lamb wave-based approach has [20]:

- the capability to inspect relatively large structures with coating and insulation,
- the capacity to inspect the entire cross-sectional area of a structural element
- the limited necessity for and movement of the sensors
- excellent sensitivity to different defects types with high precision
- limited energy consumption and great cost-effectiveness [19]

Principles of guided wave propagation and its recent literature on applications to composite structures will be discussed in the second chapter. Various methods are available in order to generate and measure Lamb waves. The wave propagation methods usually make use of piezoelectric wafers as transducers to generate propagating waves and measure the signature of the echoes that may be influenced by any inhomogeneity (stiffener or defect). Interaction of guided waves with damage can significantly influence their propagation, accompanied by wave scattering effects such as reflection, transmission, and mode conversion. The above is the premise of elastic wave-based damage identification since different locations and severity of damage can cause unique scattering phenomena. Hence ultrasonic guided wave propagation has been proposed and reviewed for effective inspection of composite structures [20].

1.3 Research Objectives

The general objective of the proposed research is to provide SHM design criteria for damage detection using guided waves in aircraft composite structures. The specific objectives are to:

- Develop a standard process to characterize guided wave propagation in composite structures and understand if an artificial delamination can represent a real damage case
- Investigate the effect of disbonds on wave propagation in bonded joints and composite repairs
- Define some SHM guideline in terms of frequency range, excitation mode, excitation angle as well as an efficient strategy for effective monitoring of such structural features.

1.4 Structure of the Thesis

This thesis is composed of six chapters including the introduction. The second chapter includes studies of concepts and principles as well as a current literature review on guided wave propagation in composite structures. The principle concentration of the research is guided wave propagation in composite bonded joints. The rest of the thesis is based on four research papers (see Fig. 1.2).

It is crucial to characterize guided wave behaviour in composite plates with defects and to understand the extent that an artificial delamination (induced by Teflon tape) can properly simulate real damage. Thus, the third chapter investigates the comparison of wave behaviour interacting with artificial and real damage in composites. It experimentally scrutinizes the scattering, reflection, and transmission of guided waves through composite plates that contain the artificial delamination and impact damage.

In the fourth chapter, using the reflection, transmission and scattering of guided waves, the state of integrity of a composite skin-to-stringer is studied. The objective is to assess the quality of the joint and detect disbond. The appropriate inspection guidelines determine the excitation mode and frequency, and transducer locations using a within-the-bond strategy, for which the excitation is performed along the joint.

In the fifth chapter, the integrity state of a composite skin-stringer is evaluated by characterizing the scattered guided waves field through a bonded joint using an “across-the-bond strategy”. For a given frequency and mode, by comparing the sensitivity of the scattering field with respect to bonding condition, SHM design guidelines are extracted, justifying the guided wave method’s ability for disbond detection.

In the sixth chapter, the “across-the-bond” strategy, using anti-symmetric mode excitation, is used to examine a scarf joint made of two CFRP stepped samples as a general representative of a repair patch. The objective is to evaluate the effect of adhesive and steps on the wave behaviour to detect possible disbond as the structure represents a common defect feature found in scarf repairs. A two-dimensional Finite Element Analysis (FEA) is first developed for ultrasonic guided wave propagation in the structure. Experimental validation of propagation characteristics is also performed in the joint region in order to justify the selection of mode, frequency and inspection configuration for disbond detection.

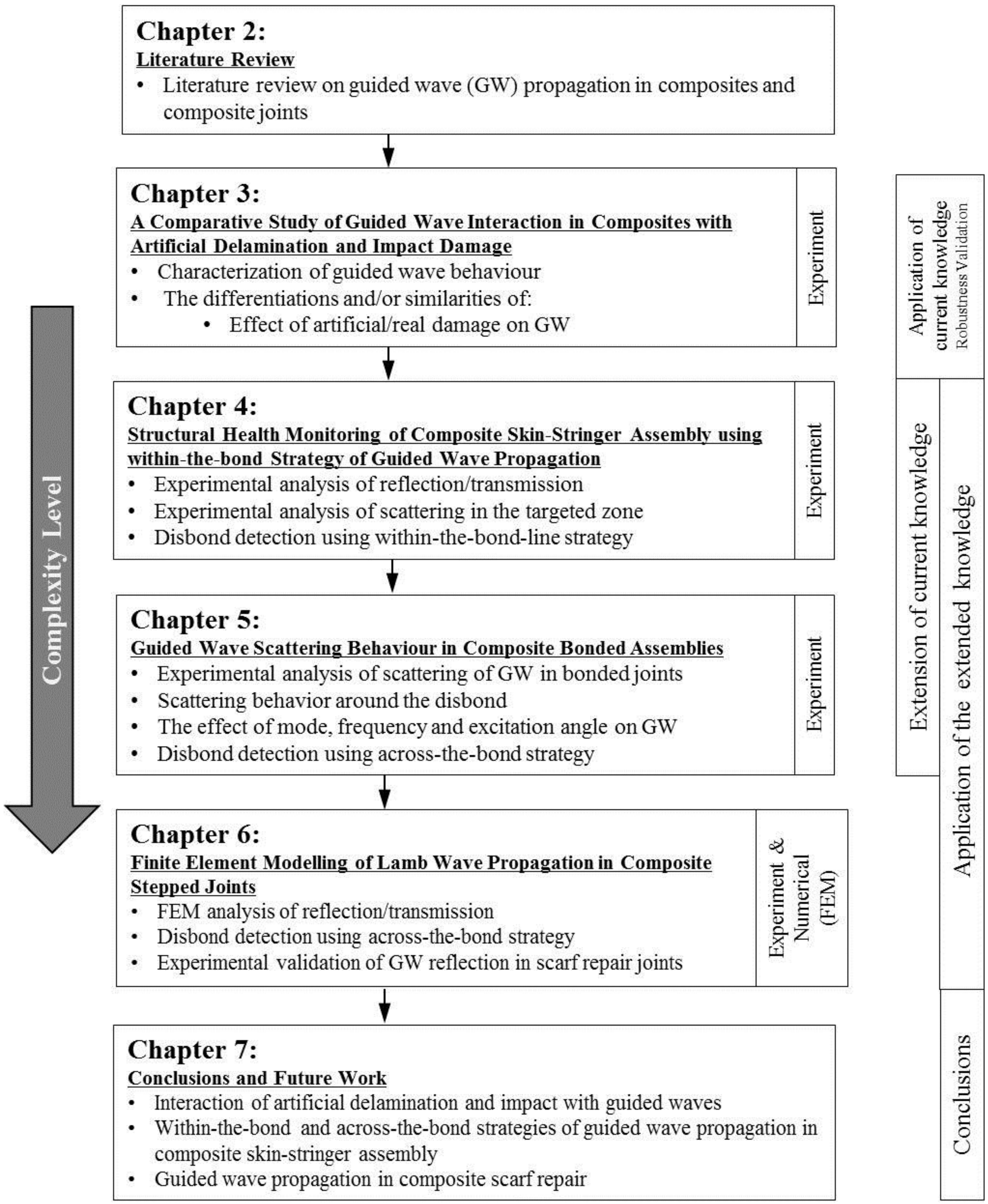

Figure 1.2. Schematic presentation of the thesis structure based on four research papers

1.5 References

[1] Lukaszewicz, D.H.J.A., Ward, C., Potter, K.D. The engineering aspects of automated prepreg layup: History, present and future, *Composites Part B: Engineering* 2012; 43:997-1009.

[2] Marsh, G. Airbus A350 XWB update, *Reinforced Plastics* 2010; 54: 20-4.

[3] Ovesy, H.R., Ghannadpour, S.A.M., Sherafat, M.H. Buckling analysis of laminated composite plates using higher order semi-analytical finite strip method, *Applied Composite Materials* 2010; 17: 69-80.

[4] Herakovich, C.T. Mechanics of fibrous composites, John Wiley & Sons, Inc., New York, 1998.

[5] Ridgard, C. Advances in low temperature curing prepregs for aerospace Structure, *45th International SAMPE Symposium*, 2000.

[6] Repecka, L., Boyd, J. Vacuum-bag-only-curable prepregs that produce void free parts, *47th International SAMPE Symposium,* 2002.

[7] National Research Council (U.S.). Committee on New Materials for Advanced Civil Aircraft, New materials for next-generation commercial transports, Washington, D.C.: National Academy Press, 1996.

[8] Samaratunga, D., Jha, R., Gopalakrishnan, S. Wave propagation analysis in adhesively bonded composite joints using the wavelet spectral finite element method, *Composite Structures* 2015; 122: 271-283.

[9] Soutis, C., Hu F.Z. Design and performance of bonded patch repairs of composite structures, *Proceedings of the Institution of Mechanical Engineers, Part G: Journal of Aerospace Engineering* 1997; 211: 263-271.

[10] Transportation Safety Board of Canada (TSB), Aviation Investigation Report, Loss of Rudder in Flight, Report Number A05F0047, Cat. No. TU3-5/05-2E ISBN 978-0-662-46783-0, 2007.

[11] Boeing Current Market Outlook 2010-2029(http://www.boeing.com/commercial/cmo/)

[12] Farrar C.R., Worden, K. An introduction to structural health monitoring, *Philosophical Transactions of the Royal Society* 2007; 365: 303-315.

[13] Chang, F.-K. Introduction to health monitoring: context, problems, solutions, First European Pre-workshop on Structural Health Monitoring, Paris, France, 2002.

[14] Caron, Y., Richard, Y. CF-188 Fatigue life management program, NATO publication RTO-MP-7, AC/323 (AVT) TP/4, Paper 4, 1998.

[15] Rose J. Ultrasonic Guided Waves in Solid Media, Cambridge University Press, New York, 2014.

[16] Boukabache H., Escriba C., Fourniols J.Y. Toward smart aerospace structures: Design of a piezoelectric sensor and its analog interface for flaw detection, *Sensors* 2014; 14: 543-561.

[17] Su, Z., Ye, L. Identification of damage using Lamb waves, from Fundamentals to Applications, Berlin: Springer-Verlag GmbH & Co., 2009.

[18] Lamb, H. On waves in an elastic plate, *Proceeding o*f *the Royal Society*. A. 1917; 93: 114-128.

[19] Su, Z., Ye, L., Lu, Y. Guided Lamb waves for identification of damage in composite structures: A review, *Journal of Sound and Vibration* 2006; 295:753-780.

[20] Worden, K., Manson, G., Allman D. Experimental validation of a structural health monitoring methodology: Part i. Novelty detection on a laboratory structure, *Journal of Sound and Vibration* 2003; 259(2): 323-343.

CHAPTER 2. LITERATURE REVIEW

2.1 Preface

Ultrasonic wave inspection techniques have been extensively employed in a wide range applications including aerospace engineering. This chapter aims to present the principles as well as a literature review of the ultrasonic guided-wave-based inspection approach for composite structures in industry. More attention will be given to the propagation of guided waves in composite bonded joints. The primary objective is to provide insight into the main fundamentals, addressing the advances and achievements as well as gaps that exist in the research.

2.2 Wave propagation fundamentals and principles

When an elastic perturbation occurs within a structure, the particles of the material propagate both parallel and perpendicular to the direction of propagation. This material vibration (i.e., particle movement) results in elastic waves that experience repeated reflections at the surfaces alternately, causing wave propagation phenomena. Discovered by Horace Lamb in 1917, Lamb waves (i.e., guided waves) exist in thin plate-like structural elements and are guided between the two parallel free surfaces of a plate [1]. They can travel over a long distance in materials, specifically, ones with a low attenuation ratio (e.g., metallic structures). Although the traveling distance is marginally limited in highly attenuated materials such as CFRP, Lamb waves are still highly beneficial to damage detection techniques, such as NDI and SHM approaches, for both metallic and composite structural elements.

Two of the most important parameters of the Lamb waves that characterize their behaviour are phase velocity (c_p) and group velocity (c_g). The phase velocity is associated with the velocity of a certain phase of a wave mode at a given frequency (see Fig. 2.1), which equals to ω/k, where ω is the angular frequency and k is the wave number [2]. The group velocity is defined as the velocity at which the overall shape of the amplitudes of the wave packet (a group of the waves) propagates. It is the actual velocity captured in experiments, and dependent on the frequency and plate thickness.

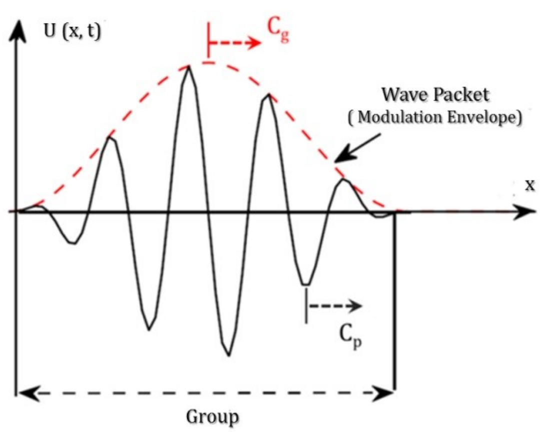

Figure 2.1. Phase (C_p) and group velocities (C_g) of a pulse

Guided waves can propagate in a symmetric or an anti-symmetric mode with respect to the neutral axis of the plate. The symmetric (S_i) modes predominantly have a radial in-plane displacement of particles, Fig. 2.2(a), while anti-symmetric (A_i) modes feature mostly out-of-plane displacement, Fig. 2.2(b). Therefore, a symmetric wave mode is often referred to as "compressional", resulting in thickness contraction and expansion; whereas an anti-symmetric mode displays constant-thickness flexing, usually referred to as "flexual" [2]. Under identical excitation conditions, the anti-symmetric modes are usually stronger, i.e., they have a greater magnitude than the symmetric modes.

In addition to the Ai and Si modes, another in-plane motion of the particles is sometimes present. Shear Horizontal (SH) mode, a transverse (shear) motion between layers of laminate, is identified as an in-plane movement perpendicular to the direction of wave propagation. Due to the complexity of the SH0 mode behaviour upon interaction with damage, most efforts are shifted towards the study of the two primary Lamb wave modes for damage identification.

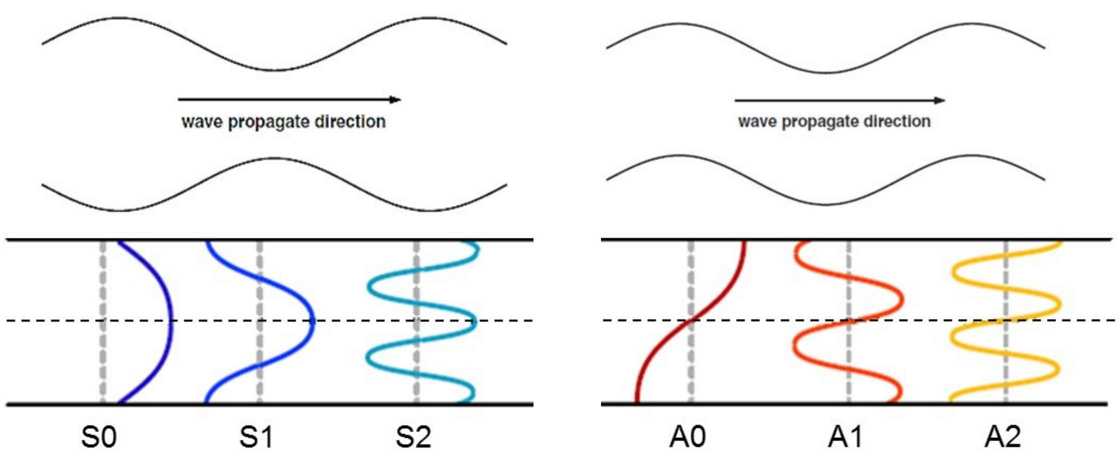

(a) (b)

Figure 2.2. Description of the first three symmetric (S) and anti-symmetric (A) mode shapes of Lamb waves, with the displacement profiles across the thickness of the plate

"Lamb waves are dispersive," meaning that their velocities depend on the frequency of propagation and plate thickness [2]. Dispersion curves portray the relationships between wave velocities, frequency (or equivalently the wavelength), and thickness for a given set of material properties. Fig. 2.3 depicts a dispersion curve for a seven-layer CFRP plate. Dispersion is often undesirable in practice for SHM applications because interpretation and processing of the data become complicated. Dispersion phenomenon causes an increase of the duration of the wave packet propagation, as well as a decrease in the amplitude of the waves. These two effects lead to the loss of resolution and sensitivity of the SHM system [3].

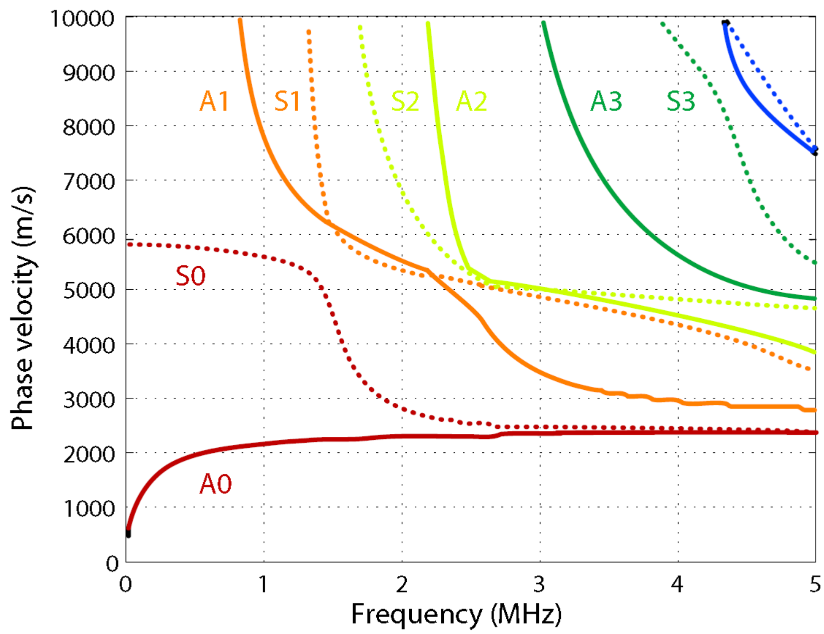

Figure 2.3. Dispersion curves (phase velocity ω/k depending on the frequency) obtained for a 1 mm thick, seven-ply [0/+45/90/-45/0/45/90/-45] Carbon-Epoxy plate. Anti-symmetric modes are represented by solid lines, and symmetric modes are represented by dotted lines

In isotropic plates, Lamb waves propagate with the same velocity in all directions (i.e., waves have constant velocity omnidirectionally), and the wavefront is in the form of a circle; whereas in non-isotropic materials such as CFRPs, the wave velocity is influenced by the direction [2]. Slowness profile is introduced to represent the velocity surface of propagating Lamb waves in different directions. The slowness is dependent on the direction as a function of the reciprocal of propagation velocity, $1/c_g(\theta)$, where θ is the wave propagation direction with respect to the 0° direction. The slowness profiles of the symmetric and anti-symmetric Lamb wave modes in two CFRP plates (angle ply and quasi-isotropic laminates) are presented in Fig. 2.4.

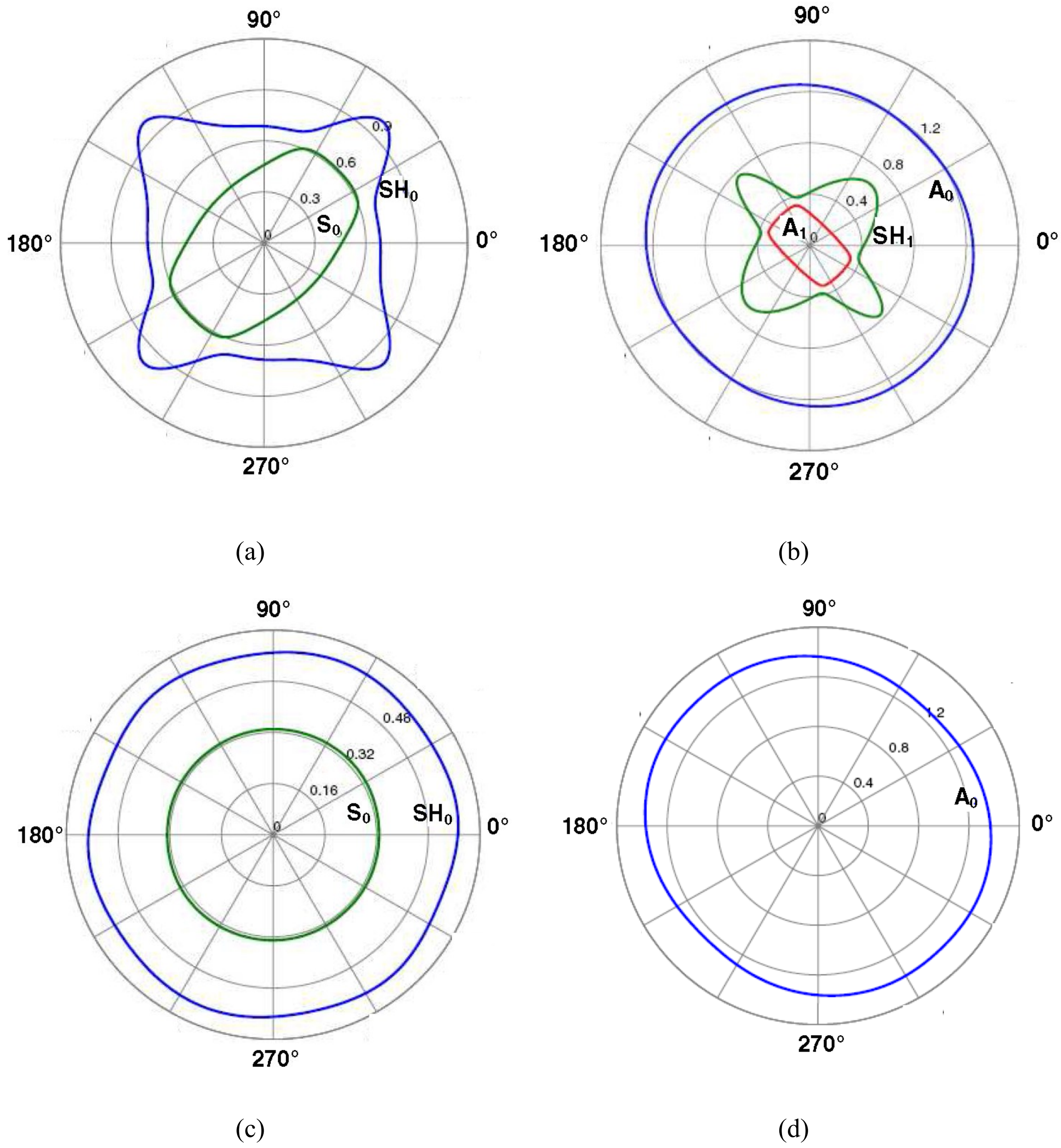

Figure 2.4. Slowness profiles of (a) symmetric; and (b) anti-symmetric Lamb modes in a [+45$_6$/-45$_6$]s CFRP laminate; (c) symmetric; and (d) anti-symmetric Lamb modes in a [+45/-45/0/90]s CFRP laminate (the angle refers to the inclination between the wave propagation direction and 0° in the carbon fibre) [4]

2.3 Actuators and sensors for Lamb waves

In practice, Lamb waves can be excited and received by different devices, which are categorized, and briefly described in the following five groups.

2.3.1 Ultrasonic probe

The most popular ultrasonic probes can be coupled with angle-adjustable Perspex wedges [5, 6]: comb ultrasonic probes [7] or Hertzian contact probes [8]. They can selectively produce a desirable Lamb wave mode according to Snell's law [9]. Thus, by eliminating the complexity of multimodal excitation, captured signals are more easily interpreted [10]. They are also widely employed to generate and collect a pure Lamb wave due to high precision and controllability advantages.

Several non-contact innovations such as air-coupled [11- 13], and fluid-coupled transducers [14] and electromagnetic acoustic transducers (EMATs) [15] were also introduced to the industry to address the issues of installation and couplant [10]. However, the precision of non-contact probes is sacrificed due to significant mismatches of the acoustical/mechanical impedance between the air/fluid and the structure. Moreover, such methods have only marginal effectiveness for detecting near-surface damage [16]. The requirement of accessibility from both sides of the structure and considerable weight/size of the probes [10] are the other factors may limit the applications of such ultrasonic probes in SHM techniques.

2.3.2 Laser-based Ultrasonics

Laser-Based Ultrasonics (LBU) activate waves using laser sources and collect structural responses using laser interferometers. It meets different resolution requirements using a flexibly controllable laser source and is particularly effective for irregular surfaces, complex geometry or stringent environments where direct access of transducers to the object is not feasible [10]. Selective generation of the desired wave mode [17] and high precision [15, 18, 19] are the other benefits; however, bulkiness and the high cost of equipment may lead to difficulties in adopting this method in practical industrial applications.

2.3.3 Optical fibres

With some competitive advantages such as light-weight, low power consumption, lower cost, durability, immunity to interference, wide bandwidth, and high compatibility, optical fibre sensors have been increasingly used in damage identification [20]. Although they are exceptionally efficient at capturing a static or quasi-dynamic strain, their applications as a sensor for dynamic Lamb wave signals in the ultrasonic range are limited [21, 22, 23] because of the low sampling rate of the normal Optical Spectrum Analyzer (OSA) [10]. It is demonstrated that this concern can be addressed using a Fibre Bragg Grating (FBG) filter connected to a photo-detector [24]. With the FBGs, the light intensity induced by the Lamb wave, not the strain itself, can be captured at a high sampling rate. It was demonstrated that an embedded FBG sensor is 20 times more sensitive to Lamb waves than a surface-bonded FBG sensor, although the surface-bonded sensor is more practical [25,26]. In this approach, the accuracy of measurement can be affected by environmental conditions and the alignment of sensors, necessitating a careful analysis of the output [2].

2.3.4 Interdigital Transducers

Interdigital transducers (IDTs), low-cost devices introduced to the NDI and SHM field, include polyvinylidene fluoride (PVDF) piezoelectric polymer films [27, 28]. PVDF is capable of producing Lamb waves with controllable wavelength by adjusting the space between interdigital electrodes [28]. PVDF also has better flexibility for adapting to curved surfaces, easier handling, higher dimensional stability, and more stable coefficients over time compared to piezoelectric transducers. PVDF-based IDTs have been mostly used as sensors only, although they were also employed as actuators within a low operating frequency range (up to 500 Hz) in a few studies [29, 30].

2.3.5 Piezoelectric Wafers and Piezocomposite Transducers

A piezoelectric lead zirconate titanate (PZT) element generates and receives Lamb waves directly through in-plane strain coupling, delivering wide frequency responses with low power consumption and cost [2,10]. Having negligible size and weight, the PZT element is especially beneficial for integration into aerostructural applications with good coupling capacity [2, 4, 10]. Moreover, a PZT element performs well for detecting damage close to its position. PZT has been extensively used in Lamb-wave-based approaches [31-37] because of their easy integration, excellent mechanical strength, and low acoustic impedance. Nevertheless, a PZT may display non-linearity under large strains (i.e., high voltages) or at high temperatures [2], resulting in weak driving force (or displacement), brittleness and sensitivity to the environment, which may narrow its application.

Robust packaging schemes have been designed and patented [38] to withstand typical aircraft environments. It is also shown that uneven waves caused by geometrical effects can be minimized by designing a disc-like PZT [36, 39]. Different shapes of piezoceramic patches have been used to generate Lamb waves. Many manufacturers produce a variety of piezoelectric elements from the rectangular PZT plate to circular patches with wrapped electrodes (in order to have the two electrodes on the same side).

In this research, in order to characterize the Lamb wave behaviour through composite structures (including bonded joints), a calibrated and repeatable device capable of generating a specific guided wave mode is required. For this purpose, plane wave generation was chosen in order to allow focusing the energy on the selected area and avoiding geometrical spread induced by finite size transducers. The designed device illustrated in Fig. 2.5 consists of two co-localized rectangular piezoceramics (50 x 5 x 0.45mm) maintained and aligned on both sides of the structure using high strength magnets and coupled to the host structure using a dedicated gel [40]. The dimensions are chosen in order to focus the energy within a 10-degree angle for wave numbers above 250 rad/m following the model presented in [36].

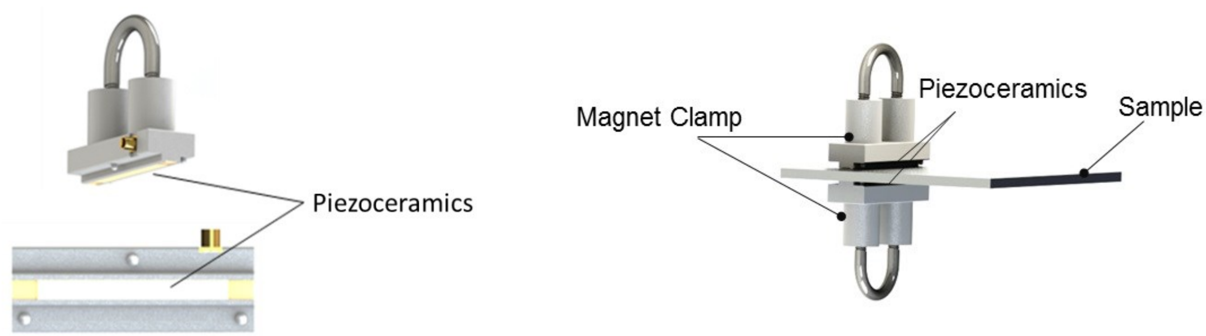

(a) (b)

Figure 2.5. Illustration of the piezoceramic element (a) and excitation clamp (b)

2.4 SHM using PZT generated-Lamb waves

2.4.1 Impedance based methods

The techniques based on elastic waves, such as mechanical impedance, or ultrasonics (Lamb waves), are the most important commonly used methods in the SHM field [34]. The impedance-based method uses high-frequency excitation (usually greater than 30 kHz) through surface-bonded PZT to evaluate changes in structural and mechanical impedance [41]. The electrical impedance of the PZT is a function of the mechanical impedance of the structure under inspection (assuming that the mechanical properties of the PZT do not vary over time). Any changes in the electrical impedance can be associated with mechanical properties, and then an indication of changes in the structural integrity. The theoretical development of impedance measurements for SHM application was proposed in [42] and then developed and extended for the case of beams [43], plates [34, 41, 44, 45] and multilayered media [46]. The method was recently patented [47]. It is shown that the electro-mechanical impedance approach and the wave propagation method are "complementary" techniques [48], since the former method works in the near field, whereas the latter acts in the far field; thus their simultaneous utilization ensures the complete coverage of the monitored structure. Fig. 2.6 represents a typical experiential result obtained for the sensor close to the crack (10 mm) in the case of a CFRP plate [34].

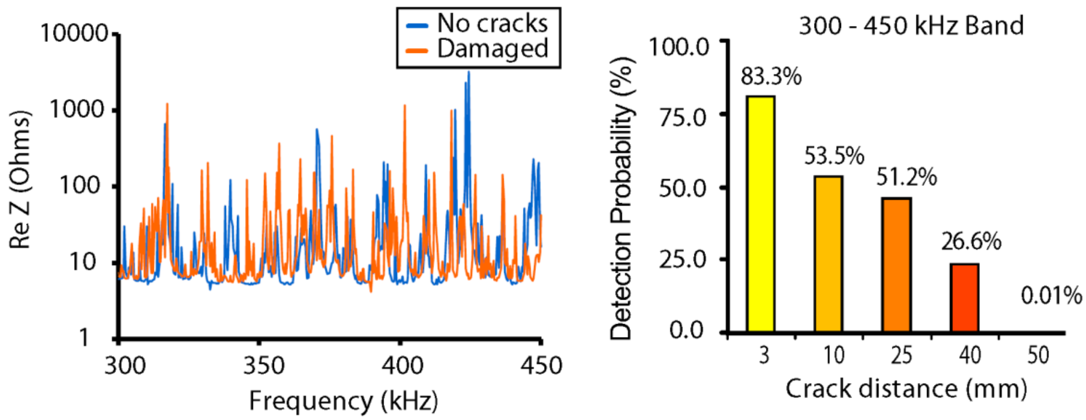

(a) (b)

Figure 2.6. Real part of the electro-mechanical impedance of a PZT bonded on a CFRP plate [34] with no damage and with a crack located in the near-field (3mm) (a). The probability of detection by integration of the differences in the 300 - 450 kHz band (b)

2.4.1 Pitch-Catch method

In the ultrasonic approaches, including guided wave propagation, actuator(s) and sensor(s) can be placed in pitch-catch configuration. In this method [49-53], a diagnostic Lamb wave signal is excited from an actuator and travels across the targeted area while a sensor on the other side of the inspection area receives the wave signal propagated through the wave path. Hence, the magnitude of the forward-scattering (transmitted) wave signal across the inspection zone governs the level of effectiveness [2]. This may necessitate multiple forward-scattering waves, using a network of transducers, for localization of damage. The pitch-catch method is capable of detecting defects that take place between a transmitter and a receiver [48].

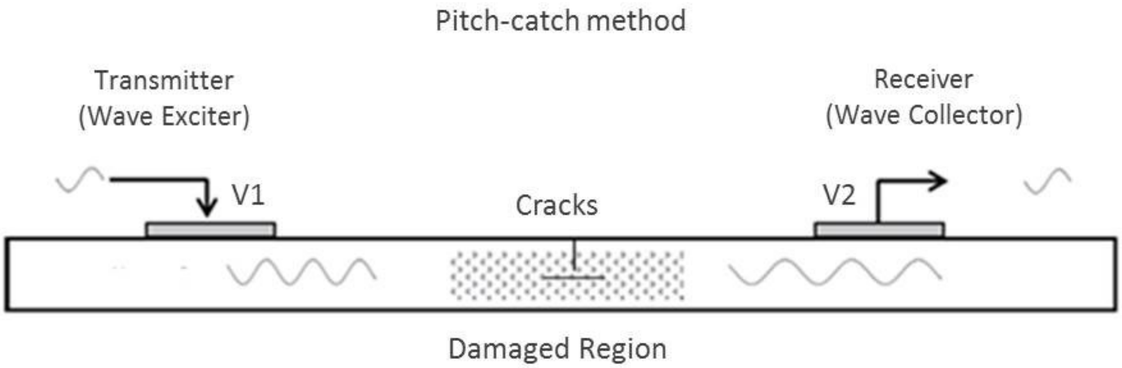

Figure 2.7. Ultrasonic damage detection techniques with pitch-catch method

The inspection is performed through the examination of the guided wave characteristics such as wave amplitude, wave phase, attenuation and transmission level in comparison with an undamaged case [48]. The studies in the literature that scrutinize the damage detection in composites using pitch-catch are numerous. The Lamb wave modes in pitch-catch configuration are significantly affected by small changes in the material properties and thickness. Therefore, they are well suited for detection of cracks in metallic structures [49, 54, 55, 56, 57], disbonds in adhesive joints as well as delamination in layered composites [53, 58-60]. A network of transmitter-receiver piezoelectric disks (5 mm diameter, 0.1 mm thick) was used earlier to detect delamination in composite structures [59, 60]. The incident S0 mode was scattered by the damage and converted into A0 and SH0 waves through mode conversion and diffraction. The received signals were analyzed, using discrete wavelet transformation, described in [61, 62], and compared with the undamaged signals. The incident A0 Lamb waves travelled in the composite plate, recorded by "SMART" layer, a network of piezoelectric disks embedded in a dielectric film, were scattered by the defect and caused the generation of new S0, and SH0 modes [58]. The embedded pitch-catch results compared very well with the X-ray image results.

The pitch-catch method has also been employed for disbond detection in composite wing skin-to-spar bonded joints [32, 33, 63]. Two carbon-epoxy samples representative of skin-to-spar joints were fabricated with $[0/\pm45/0]_s$ and $[0/\pm45/90]_s$ lay-up. After ensuring that the S0 was the mode generated and recorded by the PZTs with efficiency in a single composite plate, guided waves testing was performed in the joints and the assembly using the across-the-bond and the within-the-bond configurations [32]. The investigation successfully attributed the changes in energy transmission strength to the presence and type of the simulated disbond.

2.4.2 Pulse-Echo Method

In the traditional NDI technique, the pulse-echo method has mainly been used for through-the-thickness testing. Extending this configuration to SHM applications [34, 53, 64-67], the emitter and receiver (which could be one sensor) are placed on the same side of the targeted zone, and the sensor receives the wave signal echoed back from the damage [2] (see Fig. 2.8). Therefore, the sensitivity depends on the magnitude of the wave back-scattered (reflected) from the defect.

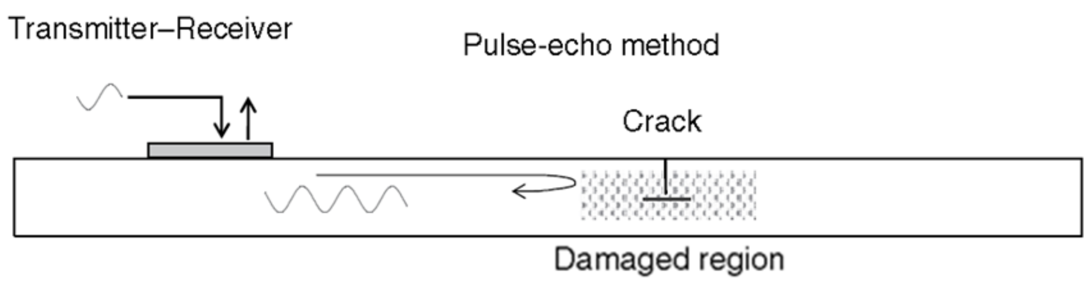

Figure 2.8. Ultrasonic damage-detection techniques with Pulse-echo method

Guided-wave pulse-echo is often more suitable for many applications, since wider areas could be covered from a single position [48]. However, in comparison with the pitch-catch configuration, the captured signal may not be sensitive enough to damage at a remote location, because the echoed waves from remote damage may lose significant information during long-distance travelling [2]. Thus, to benefit from the pulse-echo configuration, a low-dispersion guided wave needs to be employed. Such a wave is selected through either the Lamb-wave tuning methods [34, 36] or using piezoceramic wafers with interdigital electrodes [68]. Moreover, since in pulse-echo configuration, sensitivity to damage depends on the reflected signal, and the S0 mode often provides better damage-reflected waves rather than the transmitted signals [69], the pulse-echo setup and the S0 mode are often employed together for through-thickness crack detection [2].

In the literature, the pulse-echo method along with low-frequency A0 Lamb waves is also employed for detection of delamination in a composite beam [70], and again for composite plates [67, 71]. The presence of the delamination contributes to an additional echo. Furthermore, low-frequency A0 Lamb waves (10 and 20 kHz) were used to evaluate the effect of damage (hole) in the foam core of a sandwich plate with glass fibre skins in pulse-echo configuration [72]. It is shown that the echo analysis can evaluate the severity and location of the damage without the necessity of an analytical model.

The pulse-echo method was applied to detect impact damage in composites [73], and further to detect disbond in sandwich plates [74], using a high-frequency range of the S0 mode. It is noted that despite greater attenuation in sandwich plates, the dispersion curves at low frequencies are similar to those for free plates. The comparative response of a pristine and impacted CFRP sandwich illustrated in Fig 2.9 indicates that the disbond produces an additional echo.

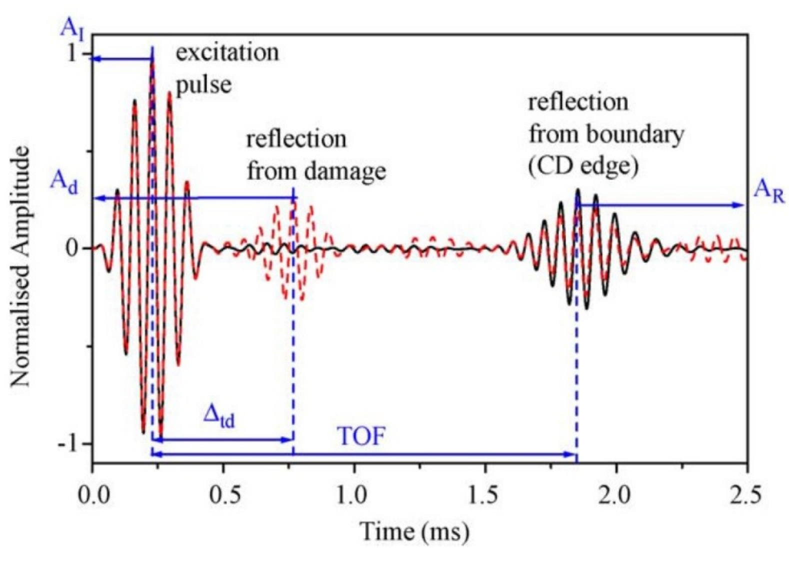

Figure 2.9. Comparative response of a pristine (solid line) and damaged (dashed line) CFRP sandwich beam after low-velocity impact [74]

2.4.3 Piezoelectric phased-arrays

A phased array benefits a group of sensors positioned at different locations in which the relative phases of the signals are varied (see Fig 2.10) to ensure that the effective propagation pattern of the array is augmented in a targeted direction [48]. It provides several benefits including saving time, resulting in quick scanning and reliable detection with more precision.

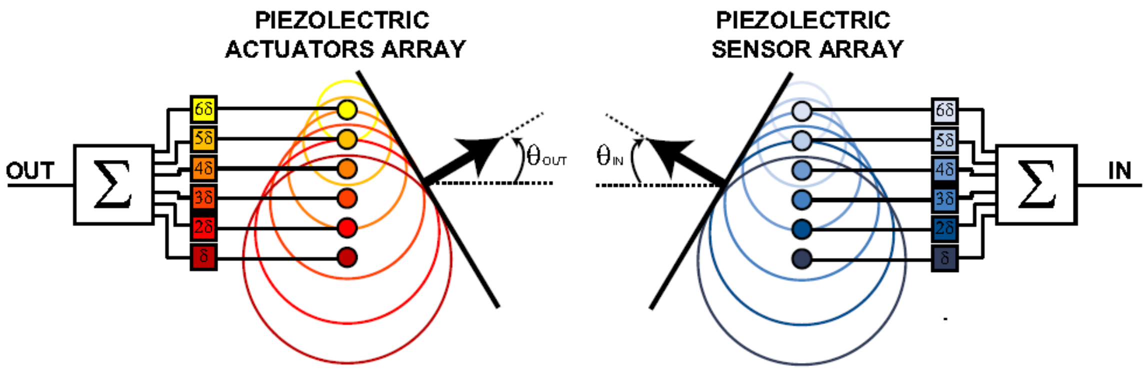

Figure 2.10. Principle of use of a six channels piezoelectric phased-array for emission in the direction θ_{OUT} (left) and reception in the direction θ_{IN} (right)

Phased arrays are employed in radar, sonar, oceanology, and medical imaging. Its applications are widely developed in NDI (e.g., cross-sectional inspection), and recently SHM using Rayleigh and Lamb waves [75, 76]. Phased arrays are developed for surface inspection using ultrasonic tomography imaging systems for aircraft structures [59, 77] or beam forming for composite laminates [78]. A 120 kHz A0 mode, implemented with a non-contact LDV sensing system, successfully indicates multiple surface defects and confirmed the potential effectiveness of guided waves phased array.

2.5 Processing of Lamb wave signals

The concept, principles and mathematical formulation of Digital Signal Processing (DSP) of elastic waves, the study of signals in digital forms, can be found in [79]. The main approaches, time domain, frequency domain, and time-frequency domain analysis, are briefly described in following sections.

2.5.1 Time domain analysis

The key features contained in a time-series Lamb wave signal, f(t), that have been used in the literature for DSP are the absolute value of magnitude (f(t)), energy distribution, the root mean square (RMS), standard deviation and time-of-flight (ToF). As the most prominent feature, ToF is defined as the time consumed for a specific wave mode to travel a certain distance. Delaminations can be detected and localized in composite beams [70] or plates [55, 62, 80] by measuring of the time of flight (ToF) in the acquired Lamb signal. DSP in the time domain mainly uses the Hilbert transform, correlation, and time reversal to extract the aforementioned parameters in a time-series signal.

The Hilbert transform improves a Lamb wave signal in the time domain [62, 53], in terms of its energy distribution, and allows extracting the envelope and phase of a signal precisely, thus benefits the ToF calculations [2]. Observing the envelope clearly facilitates the wave package recognition, helping to attribute them to the structural features and damage (see Fig 2.11).

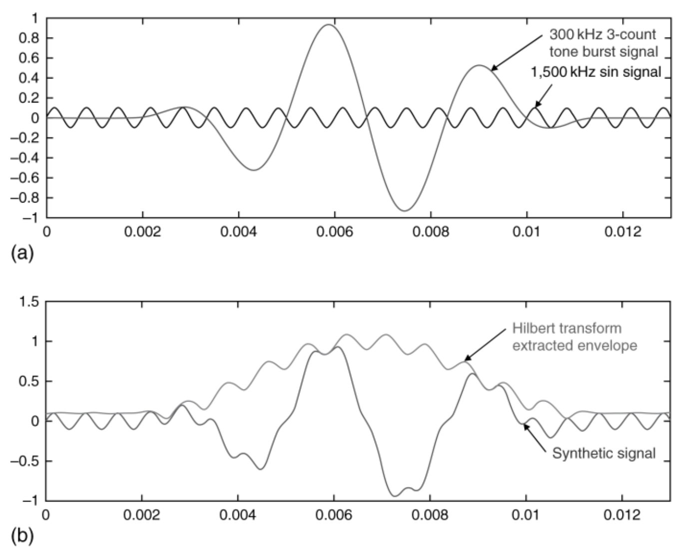

Figure 2.11. An example of a Hilbert transform: (a) original constitutive signals: a sinusoid of frequency 1500 kHz and a 3-count tone-burst of 300 kHz; (b) the synthetic signal (A1≠A2,Ø1≠Ø2) and its envelope extracted by Hilbert transform [48]

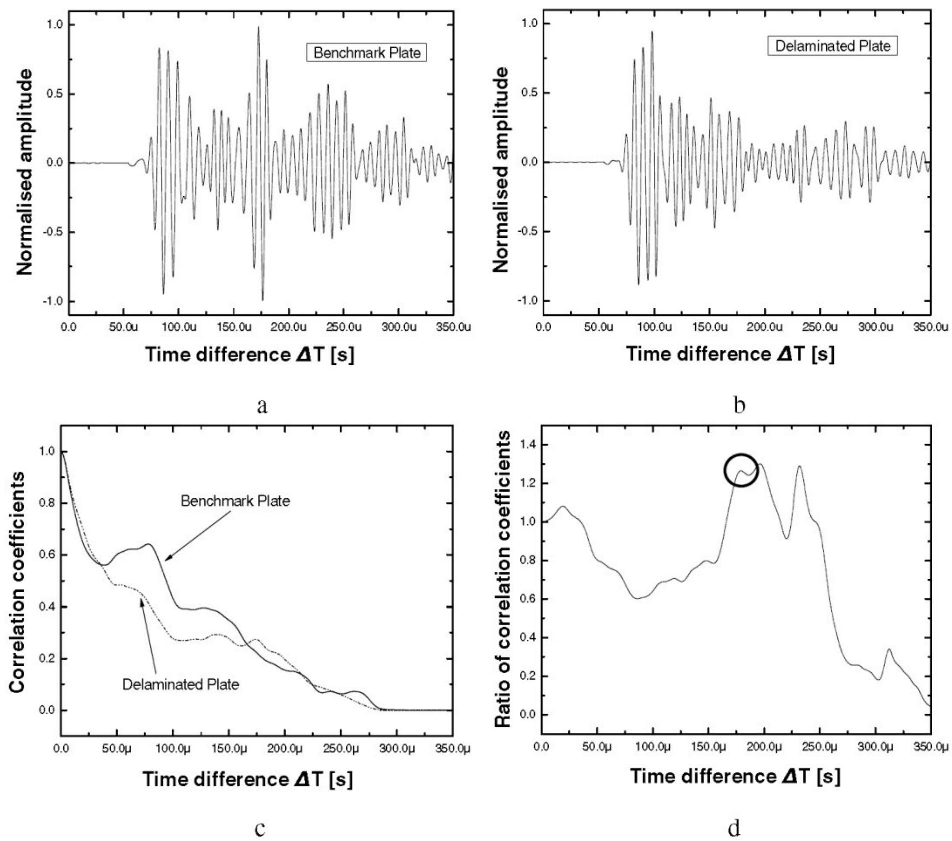

Figure 2.12. Lamb wave signals captured in a CF/EP laminate: (a) before (benchmark); and (b) after the introduction of delamination; (c) correlation coefficient curves of two signals in (a) and (b); and (d) ratio of signal correlation coefficients of delaminated to benchmark laminate [81]

The correction method enhances the comparison of damaged and healthy conditions, and highlights the difference between the two states, by introducing a correlation coefficient [2]. A time-series guided wave signal captured in a structure under examination is often compared to the same-length signal [81] in the benchmark structure using correlation processing (see Fig. 2.12).

The time reversal concept is based on “reciprocity of the wave equation” [2]. It implies for a given process that the solution to the wave equation at time (t) is the same as that at time (−t), even though the waves may be reflected, refracted by inhomogeneities in the medium where waves travel [82,83]. Based on this method, the captured signal is reversed first in the waveform, and then re-emitted from the sensing location (see Fig 2.13), and then the comparison is used for subsequent comparisons and defect identification. The quality of a Lamb wave signal can be much improved using time-reversal compensation [2, 82], which improves damage detection capabilities.

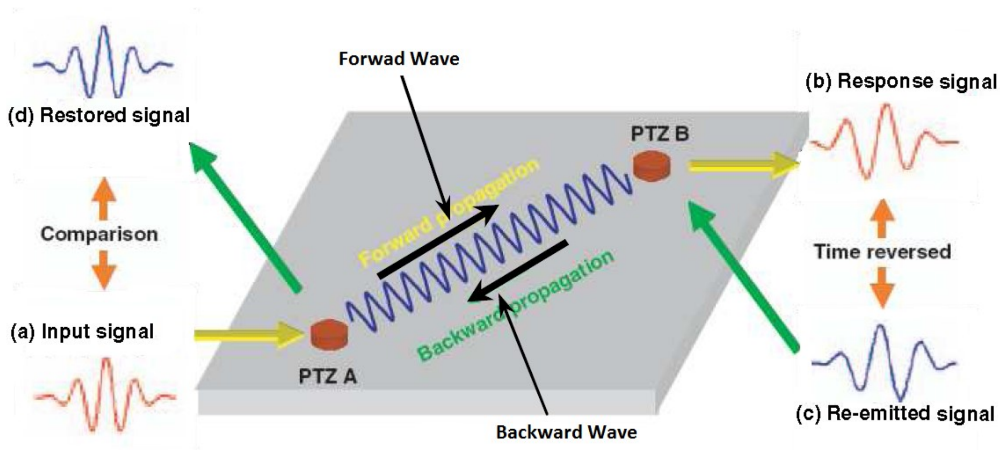

Figure 2.13. Concept of time reversal: (a) actuator A sends an input Lamb wave signal; (b) sensor B captures the response signal; (c) sensor B (now serving as an actuator) sends the reversed waveform of the signal that is captured in step (b); and (d) actuator A (now serving as a sensor) captures the response signal [83]

2.5.2 Frequency domain analysis

Working with wave packet signals in the time domain becomes challenging, particularly in complicated structures where guided waves interact with the structure's features. It is more common to examine a dynamic signal in the frequency domain via Fourier transform (FT) [84] that transforms a time-dependent Lamb wave signal f (t), into the frequency space F_f (ω) where ω denotes the angular frequency:

$$F_f(\omega) = \int_{-\infty}^{+\infty} f(t).\, e^{J\omega t} dt \qquad (2\text{-}1)$$

where ω and J are the angular frequency and unit complex, respectively. Fig. 2.14 shows the comparison of time domain, Hilbert Transform, and Fourier Transform of a typical signal used for signal processing.

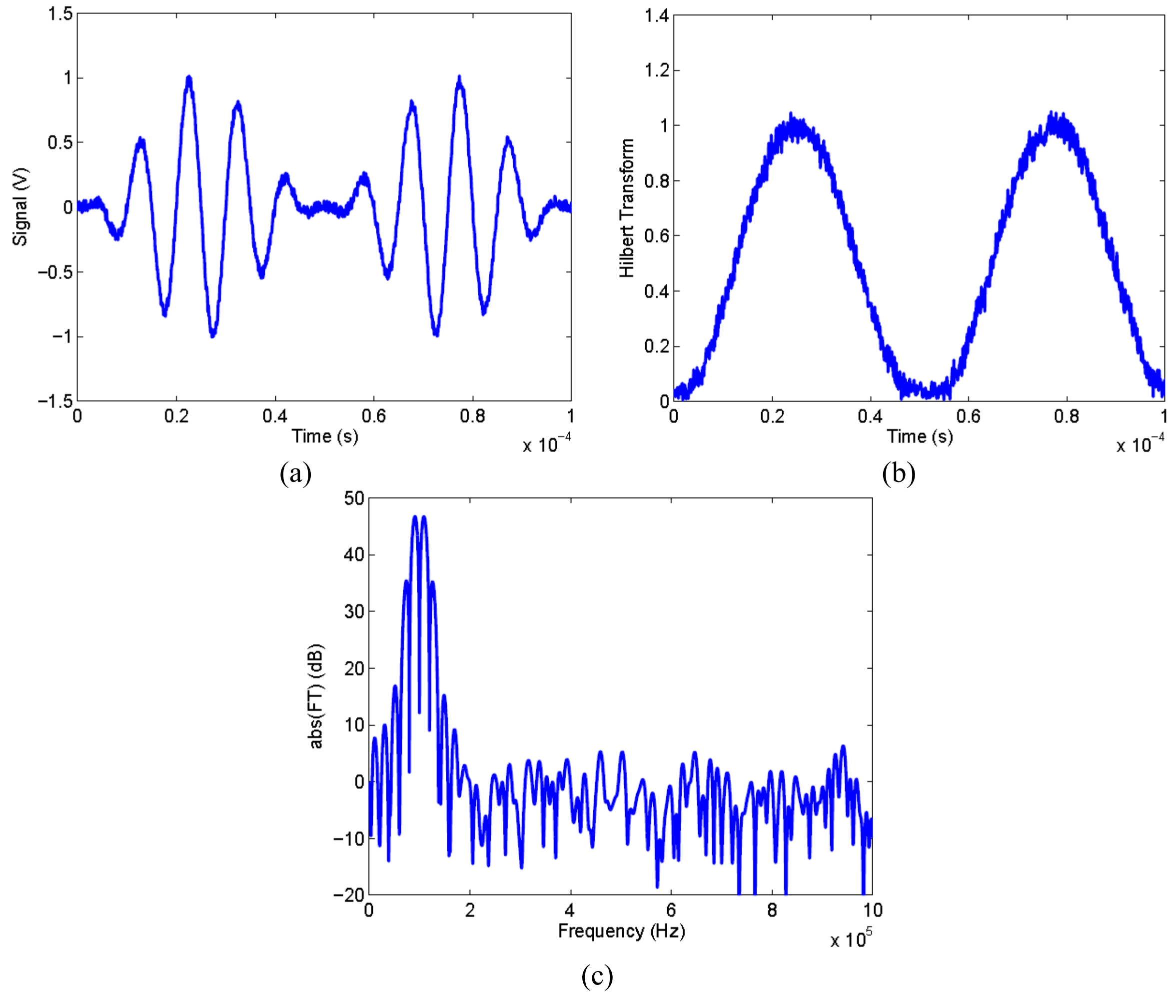

Figure 2.14. Time domain (a), Hilbert Transform (b) and Fourier Transform (c) of a typical signal used for signal processing comparison (5 cycles 100 kHz sinusoidal signal - 1Mhz sampling Frequency - Hanning window - repeated twice - additional white noise of 0.05 amplitude)

More often, a two-dimensional Fast Fourier Transform (2D-FFT) algorithm is applied to enhance the capacity of calculation of FFT [85-88], and to depict amplitude versus wavenumber and frequency [2]. Measuring the response of the plate at a series of equally spaced positions on the surface and applying 2D-FT [89], different modes at different frequencies can be isolated in the frequency-wavenumber domain, facilitating an explicit analysis of multi-mode Lamb waves. The propagation characteristics (e.g. the amplitude and real/imaginary part of the wavenumber) can be extracted using this method, resulting in a wavenumber/frequency representation along the different paths. Since 2D-FT needs a significant volume of signals captured from various positions, a great number of transducers must be ensured to scan the whole structural surface [2]. Using 2D-FT and benefiting from its capabilities, this shortcoming is accommodated using a Laser Doppler Vibrometer (LDV) for scanning dense measuring points, as used in this research.

Another main category of digital signal processing is Time-Frequency transformation. To overcome deficiencies of either time- or frequency-domain analysis of the Lamb wave signal, the combination of time information with frequency data is proposed in several studies. For instance, short-time Fourier transform (STFT) was first introduced in [90], then developed in [91] and applied for inspection of a structural beam [92] and recently in plate-like structures [49]. Moreover, for a Lamb wave signal, Continuous Wavelet Transform (CWT) described in [91] is particularly effective in terms of signal analysis, filtration, feature extraction, and visualization rather than Discrete Wavelet Transform (DWT) [93, 94]. This approach has been applied to delamination in composite laminate beams and plates [59, 60, 80, 95-97] and extended to the case of bonded joints [32, 33, 98] where the increase of transmitted energy due to a disbond is directly measured from wavelet coefficients.

2.6 Damage Identification

The final goal of guided wave characterization is to detect and triangulate damage. In composite structures, defects can be initiated by minor cracks induced by fabrication imperfections or by being subjected to low-velocity impact; subsequently propagated by cyclic fatigue loading in service, resulting in a delamination or disbond. These forms of damage may produce wave diffraction (including reflection and transmission) and mode conversion that can be analyzed and compared to the pristine case. The presence and evolution of the defect can be attributed to changes in the guided wave characteristics. Methodologies have been developed to define signal features in the two domains for identifying structural damage in composites [99-104]; however, the focus is mainly on the disbond detection in bonded joints and repairs [105-114]. These extracted features are often termed the damage index (DI), serving as an indicator to describe the damage. Some of the algorithms for damage identification, such as Time-of-Flight, magnitude level, time reversal, artificial intelligence, probability-based diagnostic imaging, migration technique, Lamb wave tomography, phased-array, and beam forming are elaborated in detail in [2, 9, 48]. The following sections briefly review the algorithms of the most prominent DI-based damage localization/identification techniques in the time and frequency domains.

2.6.1 Damage Localization

The changes associated with the main features of a Lamb wave signal, before and after the damage, are used through appropriate identification algorithms (direct and inverse) to calibrate the difference between unhealthy and pristine states of a structure. A direct algorithm is an analysis conducted logically; and in most cases, its solution is unique and sufficient for a few simple cases. In contrast, an inverse problem is difficult to solve by rational means, and the solution can be ambiguous. Details of the two different algorithms can be found in [2, 9, 48]. As an application of a 2-D expansion of the direct algorithm for defects localizing in composites, a series of PZT sensors was employed to cover the inspection area, and then, ToFs were extracted from signals captured from each possible actuator-sensor path [59, 62, 115]. The diagnosis system includes four PZT sensors, each serving as both actuators as well as sensors, attached to the four corners of a CFRP plate (see Fig 2.15), exciting and collecting the S0 mode [62]. It is shown that the position of the damage is well predicted. The accuracy and reliability of such a system are governed by the total number of the actuator-sensor paths. Therefore, increasing the number of the paths decreases the inspection error, along with increasing of the computing time and cost.

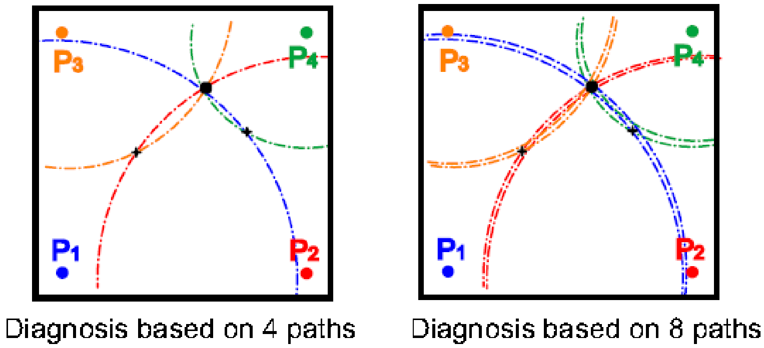

Figure 2.15. Detection of delamination location via direct algorithms [62]. Pseudo results (crosses) always accompany real delamination results (dots)

2.6.2 DIs in Time Domain

Time of Flight (ToF)

Time of flight (ToF), defined as the time lag from the moment when a sensor catches the damage-reflected signal in the case of pulse-echo setup (or -transmitted in the case of pitch-catch configuration) to the moment when the same sensor catches the incident signal. It can be one of the most straightforward methods for damage detection in composites [67, 70, 80, 116] and in metallic plates repaired with a bonded composite patch [55]. The difference in the ToFs between two wave components in a signal (as shown in Fig 2.16) describes the relative distance between the sensor and the damage.

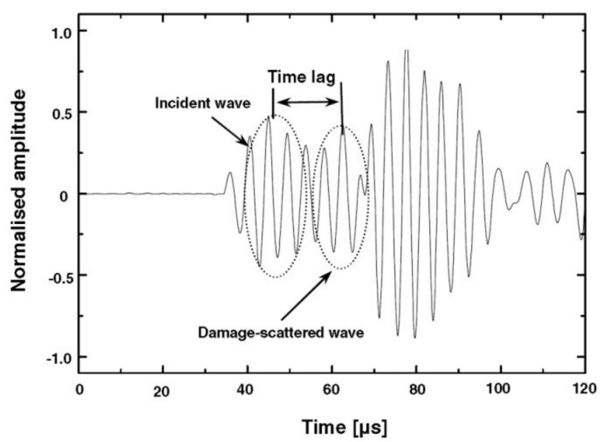

Figure 2.16. Definition of difference in the ToFs between the incident diagnostic wave and the damage-scattered wave [2]

Moreover, the change in magnitude (or amplitude) of the signal is another feature that can be evaluated, since the Lamb wave gets attenuated to a significant degree when passing through the damage. A damage index, benefiting from both ToF and magnitude level is introduced as Eq. 2-1 in [117]:

$$DI = (A1 - A2) \times (T1 - T2) \tag{2-1}$$

where A and T stand for the magnitude and the difference in extracted ToFs respectively, and subscripts 1 and 2 represent before and after the presence of damage. However, in relatively small samples or complex structural features, the interpretation of the wave packets is challenging because of the multimodal presence, mode conversion, attenuation and also unwanted reflections from the boundaries.

In the time domain analysis, other damage indices are also defined such as DI_{RMS} [118] and $DI_{Variance}$ [118]. The former is based on the root mean square and is associated with the signal energy, and the latter indicates the variability of the signal with respect to the mean value of the magnitude. Moreover, a combination of RMS-based and variance-based indices, DI_{RMSD}, attributed to the signal energy level [119], is also efficient for certain cases.

Regarding the correlation of the pristine and damaged signal, the DI based on correlation can be established as in [120, 121]. If the value of the DI is clearly lower than *one*, the two signals of the structures under inspection are not identical, indicating the presence of damage in the structure. Moreover, according to the damage index based on the time reversal method [83, 122], if the DI becomes *zero*, the Lamb wave signal is reversible; this indicates a healthy state of the structure. Whereas if the reconstructed signal mismatch the original signal, the non-zero DI shows the presence of a defect around the direct wave path.

2.6.3 DIs in Frequency Domain

In the frequency domain, the main DIs can be extracted from some features of a Lamb wave such as figure-of-merit (FoM) [123-125], spectral density [126], the peak of FFT amplitude, FFT coefficient [127], variance and kurtosis [128, 129]. With FFT analysis, the DI can also be defined as Eq. 2-2 in [127]:

$$DI = \frac{\sum_{i=1}^{N} \left| F_i^I - F_i^{II} \right|}{\sum_{i=1}^{N} \left| F_i^I \right|} \qquad (i = 1,2,\dots,N) \tag{2-2}$$

where F_i^I and F_i^{II} are the FFT coefficients (N in total) in the FFT spectra of two wave signals recorded in a structure when it is at the initial and later states, I and II, respectively. Thus, this DI represents the normalized difference between two moduli of guided wave signals in a targeted frequency bandwidth; and highlights the presence or absence of damage in the structure.

Moreover, the characteristics extracted from the signal energy spectrum obtained can be used for developing DIs in the joint time-frequency domain, which are introduced in [130] and applied to the different Lamb modes to identify structural damage [49,55]. It has been demonstrated that using the damage-scattered A0 mode to develop this DI, effectively examines delamination in composite laminates.

A summary of different DIs in time and frequency domain analysis has been introduced. Deciding on the appropriate and efficient methodology for damage identification, or DI, depends on the cases under inspection, the level of structural complexity, detectable defect size, availability of knowledge and logistics. Usually, a high sensitivity and accuracy require a higher level of signal features, resulting in a higher computational cost [2]. However, there is no explicit criterion in this respect; the desired DI, whatever its form, must be sensitive enough to the existence and evolution of the defect but robust against environmental noise. By evaluating a qualitative or quantitative relationship between alteration in an appropriate DI and defect parameters, the damage can be identified.

2.7 Recent literature summary, research gap

Guided wave propagation is still being characterized in the literature using different methods, such a semi-analytical approach [131,132], FEM [133-136] or linear 3-D elasticity [137]; most of the recent studies on this topic are inclined to try new approaches for damage detection in composite structures [138-146].

To simulate the damage (delamination or disbond) in composites, a widely used approach in SHM community is to insert one or two Teflon tapes of controlled dimensions and locations [140,145]. Whereas in reality, Accidental Damage (AD) is usually caused by contact or impact with an object [9, 48]. It is vitally important to investigate the extent to which a Teflon-tape delamination can represent a real damage case. In these regards, the size and level of severity of impact, as well as the location of the Teflon through-the-thickness, are significant characteristics require detailed attention. A handful of studies have considered scattering behaviour in composites [147-150]. The effect of the crack and inclusion [147], the influence of hole diameter to wavelength aspect ratios, different stacking sequences [148,149], and delamination size [150] on wave scattering characteristics are investigated. However, no comparative study of guided wave scattering with artificial delamination and impact damage has been performed yet. Thus, the present work marries "the study of scattering behaviour of guided waves" with "the effects of different types of damage and their attributed parameters on the diffraction patterns". To achieve that, the methodology used in this research is based on extracting the amplitude and real part of the wavenumber by performing a two-dimensional Fourier transform [89]. It measures the amplitude associated with each mode for defining reflection, transmission, and scattering coefficients. Thus, the third chapter develops an understanding of the 3-D behaviour of guided waves and targets highlighting the similarities and differences of artificial and real damage's scattering. It stimulates the understanding of the complex behaviour of the Lamb waves around damage and allows the NDI and SHM researchers to accurately model (numerically) or simulate (experimentally) the defects in composite structures.

The concentration of the many recent studies has shifted towards composite assemblies [151-158], sandwich structures [159-164] and joints and repairs [118, 165-169]. Defining the SHM design guidelines in terms of an appropriate mode (A or S) and frequency range (low, mid, high), excitation angle and approach (across-the-bond and within-the-bond) and features (reflection, transmission, and diffraction) are still concerns. Regarding propagating the effective mode, the A0 Lamb mode at a low frequency, together with correlation coefficients were used to define the damage index (DI), which were subsequently used to develop an imaging algorithm [161]. The S0 mode showed very good accuracy, and ease of use in sandwich structures [164], particularly on the reflection side [104], whereas the A0 mode resulted in a higher error and complexity. The joint configurations make the interpretation more challenging to find sensitive mode [169], proper excitation angle [155], and optimal excitation frequency and approach [32, 153] for efficient inspection. There are significant parameters affecting the ultrasonic results [155], and their effects on the 3-D scattering behaviour of guided waves have not been investigated in detail. Chapters 4 and 5 fill in the above-mentioned gaps in the literature for aircraft composite skin-stringer structures. They develop an efficient strategy for inspection of stiffened composites, looking at the important parameters' influcences on wave scattering. Using the within-the-bond and across-the-bond methodology, a disbond in composite bonded joints is identified. It is achieved through developing the reflection, transmission and scattering coefficients of the amplitude associated with each mode. Finally, Chapter 6 numerically and experimentally develops the reflection and transmission coefficients as the SHM guidelines for detecting a disbond in a composite scarf repair.

In this thesis, by understanding of the behaviour of guided wave behaviour while interacting with delaminations and other types of defects, the robustness of the inspection methodology is proven in simple composites and then extended into composite joints. As efficient SHM guidelines, the most sensitive guided wave features (reflection, transmission and diffraction) along with the best mode and frequency range, excitation approach, and incident angle, are identified for disbond detection in composite assemblies and scarf repairs.

2.8 References

[1] Lamb, H. On waves in an elastic plate, In Proceeding of the Royal Society 1917; A93: 114-128.

[2] Su, Z., Ye, L. Identification of damage using Lamb waves, from Fundamentals to Applications, Berlin: Springer-Verlag GmbH & Co. 2009.

[3] Wilcox, P., Lowe, M., Cawley, P. The effect of dispersion on long-range inspection using ultrasonic guided waves, *NDT & E International* 2001; 34(1): 1-9.

[4] Wang, L., Yuan, F.G. Group velocity and characteristic wave curves of Lamb waves in composites: modelling and experiments, *Composites Science and Technology* 2007; 67: 1370-1384.

[5] Guo, N., Cawley, P. Lamb waves for the NDE of Composite Laminates, in D.O. Thompson, D.E. Chimenti (Eds.), *Review of Progress in Quantitative Non-destructive Evaluation* 1992; 11: 1443-1450.

[6] Guo, N., Cawley, P. Lamb wave reflection for the quick nondestructive evaluation of large composite laminates, *Materials Evaluation* 1994; 52: 404-411.

[7] Rose, J. L. A baseline and vision of ultrasonic guided wave inspection potential, *Journal of Pressure Vessel Technology* 2002; 124: 273-282.

[8] Degertekin, F.L., Khuri-Yakub, B.T. Lamb wave excitation by Hertzian contacts with application in NDE. IEEE Transactions on Ultrasonics, *Ferroelectrics, and Frequency Control* 1997; 44: 769-779.

[9] Rose, J.L. Ultrasonic Waves in Solid Media. Cambridge University Press, New York, 2014.

[10] Su, Z., Ye, L., Lu, Y. Guided Lamb waves for identification of damage in composite structures: A review, *Journal of Sound and Vibration* 2006; 295: 753-780.

[11] Harb, M.S. Damage imaging in metallic and composite structures using scanning air-coupled and laser ultrasound, Ph.D. thesis, North Carolina State University, Nov 2015.

[12] Castaings, M., Cawley, P. The generation, propagation, and detection of Lamb waves in plates using air-coupled ultrasonic transducers, *Journal of the Acoustical Society of America* 1996; 100(5): 3070-3077.

[13] Brassier, P., Peres, P., Hosten, B., Castaings, M., Cinquin, M., Lourme, H. Health monitoring of composite structures using ultrasonic guided waves, In *NDT for Safety*, Nov. 2007.

[14] Ghosh, T., Kundu, T., Karpur, P. Efficient use of Lamb modes for detecting defects in large plates, *Ultrasonics* 1998; 36:791-801.

[15] Guo, Z., Achenbach, J.D., Krishnaswamy, S. EMAT generation and laser detection of single Lamb wave modes, *Ultrasonics* 1997; 35: 423-429.

[16] Achenbach, J.D. Quantitative nondestructive evaluation, *International Journal of Solids and Structures* 2000; 37: 13-27.

[17] Silva, M.Z., Gouyon, R., Lepoutre, F. Hidden corrosion detection in aircraft aluminium structures using laser ultrasonics and wavelet transform signal analysis, *Ultrasonics* 2003; 41: 301-305.

[18] Yoshimura, S., Yagawa, G., Oishi, A., Yamada, K. Neural network based inverse analysis for defect identification with laser ultrasonics, *Key Engineering Materials* 1998; 145(149): 443-452.

[19] Valle, C., Littles, J.W. Flaw localization using the reassigned spectrogram on laser-generated and detected Lamb modes, *Ultrasonics* 2002; 39: 536-542.

[20] Boller, C. Ways and options for aircraft structural health monitoring, *Smart Materials and Structures* 2001; 10: 432-440.

[21] Levin, K. Durability of embedded fibre optical sensors in composites, Ph.D. thesis, Royal
Institute of Technology, Sweden, 2001.

[22] Pierce, S.G., Philp, W.R., Culshaw, B., Gachagan, A., McNab, A., Hayward, G., Lecuyer, F. Surface-bonded optical fibre sensors for the inspection of CFRP plates using ultrasonic Lamb waves, *Smart Materials and Structures*1996; 5(6):776-787.

[23] Gachagan, A., Hayward, G., McNab, A., Reynolds, P., Pierce, S.G., Philp, W.R. Culshaw, B. Generation and reception of ultrasonic guided waves in composite plates using conformable piezoelectric transmitters and optical-fiber detectors, *IEEE Transactions on Ultrasonics, Ferroelectrics and Frequency Control* 1999; 46:72-81.

[24] Isuda, H., Toyama, N., Urabe, K., Takatsubo, J. Impact damage detection in CFRP using fiber bragg gratings, *Smart Materials and Structures* 2004; 13:719-724.

[25] Zhou, G., Sim, L.M. Damage detection and assessment in fibre-reinforced composite structures with embedded fibre optic sensors review, *Smart Materials and Structures* 2004; 11: 925-939.

[26] Pierce, S.G., Philp, W.R., Gachagan, A., McNab, A., Hayward, G., Culshaw, B. Surface-bonded and embedded optical fibers as ultrasonic sensors, *Applied Optics* 1996; 35(25): 5191-5197.

[27] Monkhouse, R.S.C., Wilcox, P.W., Lowe, M.J.S., Dalton, R., Cawley, P. The rapid monitoring of structures using interdigital lamb wave transducers, *Smart Materials and Structures* 2000; 9: 304-309.

[28] Monkhouse, R.S.C., Wilcox Cawley, P. Flexible interdigital PVDF transducers for the generation of lamb waves in structures, *Ultrasonics* 1997; 35: 489-498.

[29] Main, J.A. Smart material control without wire leads or electrodes: new methods and devices, In Proceedings of the ASME Design Engineering Technical Conference, Sacramento, CA, USA, September 14-17, 1997.

[30] Stobener, U., Gaul, L. Active vibration and noise control for the interior of a car body by PVDF actuator and sensor arrays, In Proceedings of the 10th International Conference on Adaptive Structures and Technologies; 457-464, 2000.

[31] Grondel, S., Paget, C., Delebarre, C., Assaad, J., Levin, K. Design of optimal configuration for generating A0 Lamb mode in a composite plate using piezoceramics transducers, *Journal of the Acoustical Society of America* 2002; 112:84-90.

[32] Matt, H., Bartoli, I., Lanza di Scaleaa, F. Ultrasonic guided wave monitoring of composite wing skin-to-spar bonded joints in aerospace structures, *Journal of the Acoustical Society of America* 2005; 118(4): 2240-2253.

[33] Matt, H., Structural Diagnostics of CFRP Composite Aircraft Components by Ultrasonic Guided Waves and Built-In Piezoelectric Transducers. Ph.D. thesis, University of California, San Diego, 2006.

[34] Giurgiutiu, V., Zagrai, A., Bao, J. Piezoelectric wafer embedded active sensors for aging aircraft structural health monitoring, *Structural Health Monitoring* 2002; 1(1): 41-61.

[35] Hailu, B., Hayward, G., Gachagan, A., Mcnab, A., Farlow, R. Comparison of different piezoelectric materials for the design of embedded transducers for structural health monitoring applications, In IEEE Ultrasonics Symposium; 1009-1013, 2000.

[36] Lanza di Scalea, F., Matt, H., Bartoli, I. The response of rectangular piezoelectric sensors to Rayleigh and Lamb ultrasonic waves, *Journal of the Acoustical Society of America* 2007; 121(1): 175-188.

[37] Grondel, S., Assaad, J., Delebarre, C., Moulin, E. Health monitoring of a composite wingbox structure, *Ultrasonics* 2004; 42: 819-824.

[38] Kessler, S.S., Jugenheimer, K.A., Size, A.B., Dunn, C.T. Piezoelectric damage detection, Technical Report, Unites States Patent 2008; US 7,469,595 B2.

[39] Kessler, S.S. Piezoelectric based in-situ damage detection of composite materials for structural health monitoring systems, Ph.D. thesis, Massachusetts Institute of Technology, 2002.

[40] Guitel, R., Quaegebeur, N., Micheau, P., Masson P. Clamped piezoelectric movable transducer for robust and selective guided wave mode generation, CanSmart/SMN Workshop, July 15, 2015, Vancouver, BC.

[41] Park, G. Sohn, H., Farra, C.R., Inman, D.J. Overview of Piezoelectric Impedance-Based Health Monitoring and Path Forward, *The Shock and Vibration Digest* 2003; 35(6): 451-463.

[42] Liang, C., Sun, F., Rogers, C. Electro-mechanical impedance modelling of active material systems, *Smart Materials and Structures* 1996; 5: 171-186.

[43] Sumant, P.S., Maiti, S.K. Crack detection in a beam using PZT sensors, *Smart Materials and Structures* 2006; 15: 695-703.

[44] Chaudhry, Z.A., Joseph, T., Sun, F.P., Rogers, C. Local-area health monitoring of aircraft via piezoelectric actuator/sensor patches, In *SPIE Structural Health Monitoring* 1995; 2443.

[45] Zagrai, A.N., Giurgiutiu, V., Electro-mechanical impedance method for crack detection in thin plates, *Journal of Intelligent Material Systems and Structures* 2001; 12:709-718.

[46] Pohl, J., Herold, S., Mook, G., Michel, F. Damage detection in smart CFRP composites using impedance spectroscopy, *Smart Materials and Structures* 2001; 10:834-842.

[47] Giurgiutiu, V., Xu, B. Self-processing integrated damage assessment sensor for structural health monitoring, Technical Report, United States Patent US 7,174,255 B2, 2007.

[48] Giurgiutiu, V. Structural health monitoring with piezoelectric wafer active sensors, Elsevier Academic Press, Boston, second edition 2014.

[49] In, J.-B., Chang, F.-K. Pitch-catch active sensing methods in structural health monitoring for aircraft structures, *Structural Health Monitoring: An International Journal* 2008; 7(1): 5-15.

[50] Qing, X.P., Beard, S.J., Kumar, A., Sullivan, K., Aguilar, R., Merchant, M., Taniguchi, M. The performance of a piezoelectric-sensor-based SHM system under a combined cryogenic temperature and vibration environment, *Smart Materials and Structures* 2008; 17: 055010-055021.

[51] Harri, K., Guillaume, P., Vanlanduit, S. On-line damage detection on a wing panel using transmission of multisine ultrasonic waves, *NDT&E International* 2008; 41(4): 312-317.

[52] Petculescu, G., Krishnaswamy, S., Achenbach, J.D. Group delay measurements using modally selective Lamb wave transducers for detection and sizing of delaminations in composites, *Smart Materials and Structures* 2008; 17: 015007-015016.

[53] Raghavan, A., Cesnik, C.E.S. Effects of elevated temperature on guided-wave structural health monitoring, *Journal of Intelligent Material Systems and Structures* 2008; 19: 1383-1398.

[54] Ihn, J.-B., Chang, F.-K. Multi crack growth monitoring at riveted lap joints using piezoelectric patches, In 7th Annual International Symposium on Non-destructive Evaluation for Health Monitoring and Diagnostics, 2002.

[55] Ihn, J.-B., Chang, F.-K. Detection and monitoring of hidden fatigue crack growth using a built-in piezoelectric sensor/actuator network. *Smart Materials and Structures* 2004; 13: 609-620.

[56] Boller, C., Ihn, J.-B., Staszewski, W.J., Speckmann, H. Design principles and inspection techniques for long life endurance of aircraft structures, In 3rd International Workshop on Structural Health Monitoring, Stanford/CA, USA, 2001.

[57] Seydel, R. Chang, F.-K. Impact identification of stiffened composite panels: I. system development, *Smart Materials and Structures* 2001; 10: 354-369.

[58] Giurgiutiu, V., Cuc, A. Embedded non-destructive evaluation for structural health monitoring, damage detection, and failure prevention, *The Shock and Vibration Digest* 2005; 37(2): 85-103.

[59] Lemistre, M., Balageas, D.L., Structural health monitoring system based on diffracted lamb wave analysis by multiresolution processing, *Smart Materials and Structures* 2001; 10: 504-511.

[60] Sohn, H. Park, G., Wait, J.R., Limback, N.P., Farrar, C.R. Wavelet-based active sensing for delamination detection in composite structures, *Smart Materials and Structures* 2004; 13: 153-160.

[61] Deng, X., Wang, Q., Giurgiutiu, V. Structural health monitoring using active sensors and wavelet transforms, In SPIE 6th Annual International Symposium on Smart Structures and Materials, 1999.

[62] Su, Z., Ye, L., Bu, X. A damage identification technique for CF/EP composite laminates using distributed piezoelectric transducers, *Composite Structures* 2002; 57: 465-471.

[63] Olson, S.E., Desimio, M.P., Brown, S., Derriso., M. Impact and disbond detection in composite wing structures, In 4th European Workshop on Structural Health Monitoring, 2008.

[64] Giurgiutiu, V. Tuned Lamb wave excitation and detection with piezoelectric wafer active sensors for structural health monitoring, *Journal of Intelligent Material Systems and Structures* 2005; 16: 291-305.

[65] Tan, K.S., Guo, N., Wong, B.S., Tui, C.G. Comparison of Lamb waves and pulse echo in detection of near-surface defects in laminate plates, *NDT&E International* 1995; 28(4):215-223.

[66] Giurgiutiu, V., Zagrai, A., Bao, J. Embedded active sensors for in-situ structural health monitoring of thin-wall structures, *Journal of Pressure Vessel Technology* 2002; 124:293-302.

[67] Diamanti, K., Hodgkinson, J.M., Soutis, C. Detection of low-velocity impact damage in composite plates using Lamb waves, *Structural Health Monitoring: An International Journal* 2004; 3(1): 33-41.

[68] Grondel, S., Paget, C., Delebarre, C., Assaad, J., Levin, K. Design of optimal configuration for generating a0 Lamb mode in a composite plate using piezoceramics transducers, *Journal of the Acoustical Society of America* 2002; 112: 84-90.

[69] Giurgiutiu, V., Bao, J., Zhao, W. Piezoelectric wafer active sensor embedded ultrasonics in beams and plates, *Experimental Mechanics* 2003; 43(4): 428-449.

[70] Diaz-Valdes, S.H., Soutis, C. Real-time non-destructive evaluation of fiber composite laminates using low-frequency lamb waves, *Journal of the Acoustical Society of America* 2002; 111(5): 2026-2033.

[71] Diamanti, K., Soutis, C., Hodgkinson, J.M. Piezoelectric transducer arrangement for the inspection of large composite structures, *Composites: Part A* 2007; 38: 1121-1130.

[72] Barnoncel, D. Monitoring of impact damages in sandwich plates with a foam core using bonded PZT discs: experimental and numerical studies, In 2nd European Workshop on Structural Health Monitoring, 2004.

[73] Barnoncel, D., Osmont, D., Dupont, M. Health monitoring of sandwich plates with real impact damages using PZT devices, In Structural Health Monitoring, Stanford/CA, USA, 2003 871-878.

[74] Diamanti, K., Soutis, C., Hodgkinson, J.M. Lamb waves for the non-destructive inspection of monolithic and sandwich composite beams, *Composites, Part A* 2005; 36:189-195.

[75] Deutsch, W.A.K., Cheng, A., Achenbach, J.D. Self-focusing of Rayleigh waves and Lamb waves with a linear phased array, *Research in Non-destructive Evaluation* 1997; 9: 81-95.

[76] Deutsch, W.A.K., Cheng, A., Achenbach, J.D. Focusing of Rayleigh waves: simulation and experiments, IEEE Transactions on Ultrasonics, *Ferroelectrics and Frequency Control* 1999; 46: 333-341.
[77] Schwarz, W.G., Read, M.E., Kremera, M.J., Hinders, M.K., Smith, B.T. Lamb wave tomographic imaging system for aircraft structural health assessment, In SPIE Conference on Non-destructive Evaluation of Aging Aircraft, 1999.
[78] Yu, L., Tian, Z. Guided wave phased array beamforming and imaging in composite plates, *Ultrasonics* 2016; 68:43-53
[79] Staszewski, W.J., Worden, K. Signal processing for damage detection, In Staszewski, W.J., Boller, C., Tomlinson, G.R. (eds.) Health Monitoring of Aerospace Structures: Smart Sensor Technologies and Signal Processing 2004; 5: 163-206. John Wiley & Sons, Inc., Chichester.
[80] Kessler, S.S., Spearing, S., Soutis, C. Damage detection in composite materials using Lamb wave methods, *Smart Materials and Structures* 2002; 11: 269-278.
[81] Su, Z., Wang, X., Chen, Z., Ye, L., Wang, D. A built-in active sensor network for health monitoring of composite structures, *Smart Materials and Structures* 2006; 15: 1939-1949.
[82] Prada, C., Kerbrat, E., Cassereau, D., Fink, M. Time reversal techniques in ultrasonic nondestructive testing of scattering media, *Inverse Problems* 2002; 18: 1761-1773.
[83] Sohn, H., Park, H.W., Law, K.H., Farrar, C.R. Combination of a time reversal process and a consecutive outlier analysis for baseline-free damage diagnosis, *Journal of Intelligent Material Systems and Structures* 2007; 18: 335-346.
[84] Boashash, B. Time-Frequency signal analysis, methods and applications, Longman Cheshire Press, Melbourne, 1992.
[85] Gao, W., Glorieux, C., Thoen, J. Laser ultrasonic study of Lamb waves: determination of the thickness and velocities of a thin plate, *International Journal of Engineering Science* 2003; 41: 219-228.
[86] Koh, Y.L., Chiu, W.K., Rajic, N. Integrity assessment of composite repair patch using propagating Lamb waves, *Composite Structures* 2002; 58: 363-37.

[87] Koh, Y.L., Chiu, W.K., Rajic, N. Effects of local stiffness changes and delamination on Lamb wave transmission using surface-mounted piezoelectric transducers, *Composite Structures* 2002; 57: 437-443.

[88] Heller, K., Jacobs, L.J., Qu, J. Characterization of adhesive bond properties using Lamb waves, *NDT&E International* 2000; 33: 555-563.

[89] Alleyne, D.N., Cawley, P. A 2-dimensional Fourier transform method for the quantitative measurement of Lamb modes, IEEE Transactions on Ultrasonics, *Ferroelectrics and Frequency Control* 1990; 2(3): 1143-1146.

[90] Gabor, D. Theory of Communication, *Journal of IEEE* 1946, 93, 429-457.

[91] Okumura, S. The short time Fourier transform and local signals, Ph.D. thesis, Carnegie Mellon University, June 2011.

[92] Kim, Y., Kim, E.H. Effectiveness of the continuous wavelet transform in the analysis of some dispersive elastic waves, *Journal of the Acoustical Society of America* 2001; 110: 86-95.

[93] Yu, L., Giurgiutiu, V., Advanced signal processing for enhanced damage detection with piezoelectric wafer active sensors, *Smart Materials and Structures* 2005; 1: 185-215.

[94] Lu, Y., Ye, L., Su, Z. Crack identification in aluminium plates using Lamb wave signals of a PZT sensor network, *Smart Materials and Structures* 2006; 15: 839-849.

[95] Yan, Y.J., Yam, L.H. Online detection of crack damage in composite plates using embedded piezoelectric actuators/sensors and wavelet analysis, *Composite Structures* 2002; 58: 29-38.

[96] Quek, S.T., Wang, Q., Zhang, L., Ang, K.K. Sensitivity analysis of crack detection in beams by wavelet technique, *International Journal of Mechanical Sciences* 2001; 43: 2899-2910.

[97] Grabowska, J., Palaczb, M., Krawczuk, M. Damage identification by wavelet analysis, *Mechanical Systems and Signal Processing* 2008; 22: 1623-1635.

[98] Lanza di Scalea, F., Rizzo, P., Marzani, A. Propagation of ultrasonic guided waves in lap-shear adhesive joints: Case of incident A0 Lamb wave, *Journal of the Acoustical Society of America* 2004, 115(1): 146-157.

[99] Su, Z., Yang, C., Pan, N., Ye, L., Zhou, L.M. Assessment of delamination in composite beams using shear horizontal (SH) wave mode, *Composites Science and Technology* 2007; 67: 244-251.

[100] Guo, N., Cawley, P. The interaction of Lamb waves with delaminations in composite laminates, *Journal of the Acoustical Society of America*. 1993; 94: 2240-2246.

[101] Basri, R., Chiu, W.K. Numerical analysis on the interaction of guided Lamb waves with a local elastic stiffness reduction in quasi-isotropic composite plate structures, *Composite Structures* 2004, 66: 87-99.

[102] Ostachowicz, W.M. Damage detection of structures using spectral finite element method, *Computers & Structures* 2008; 86(35): 454-462.

[103] Hayashi, T., Kawashima, K. Multiple reflections of Lamb waves at a delamination, *Ultrasonics* 2002; 40: 193-197.

[104] Jin, J., Quek, S.T., Wang, Q. Wave boundary element to study Lamb wave propagation in plates, *Journal of Sound and Vibration* 2005; 288(12):195-213.

[105] Diamanti, K., Soutis, C., Hodgkinson, J.M. Non-destructive inspection of sandwich and repaired composite laminated structures, *Composites Science and Technology* 2005; 65: 2059-2067.

[106] Chiu, W.K., Koh, Y.L., Galea, S.C., Rajic, N. Smart structure application in bonded repairs, *Composite Structures* 2000; 50: 433-444.

[107] Lowe, M.J.S., Challis, R.E., Chan, C.W. The transmission of Lamb waves across adhesively bonded lap joints, *Journal of the Acoustical Society of America* 2000; 107: 1333-46.

[108] Lowe, M.J.S., Cawley, P. The applicability of plate wave techniques for the inspection of adhesive and diffusion bonded joints, *Journal of Non-destructive Evaluation*, 1994; 13(4), 185-200.

[109] Seifried, R., Jacobs, L.J., Qu, J. Propagation of guided waves in adhesive bonded components, NDT&E International 2002; 35:317-328.

[110] Kundu, T., Maji, A., Ghosh, T., Maslov, K. Detection of kissing disbonds by Lamb waves, *Ultrasonics* 1998; 35:573-80.

[11] Nagy, P.B., Adler, L. Non-destructive evaluation of adhesive joints by guided waves, *Journal of Applied Physics* 1989; 66:4658-63.

[112] Soutis, C., Ihn, J.B. Design, analysis, and SHM of bonded composite repair and substructure2009, Encyclopaedia of Structural Health Monitoring, Chapter 11, 1-17.

[113] Soutis, C., Hu, F.Z. Design and performance of bonded patch repairs of composite structures, *Proceedings of the Institution of Mechanical Engineers, Part G: Journal of Aerospace Engineering* 1997; 211:263-71.

[114] Takahashi, I., Ito, Y., Takeda, S., Iwahori, Y., Takatsubo, J., Takeda, N. Impact damage detection on scarf-repaired composites using Lamb wave sensing, 16th International Conference on Composite Materials, July 2007, Japan.

[115] Gaul, L., Hurlebaus, S. Wavelet-transform to identify the location and force-time-history of transient load in a plate, in: F.-K. Chang (Ed.), Structural Health Monitoring, second ed., Technomic Publishing Co., Lancaster, 1999; 851-860.

[116] Diaz Valdes, S.H., Soutis, C. A structural health monitoring system for laminated composites, In Chang, F.-K. (ed.) Proceedings of the 3rd International Workshop on Structural Health Monitoring, Stanford, CA, USA, September 12-14, 2001, pp. 1476–1485. CRC Press, Boca Raton.

[117] Yuan, S., Liang, D., Shi, L., Zhao, X., Wu, J., Li, G., Qiu, L. Recent progress on distributed structural health monitoring research at NUAA, *Journal of Intelligent Material Systems and Structures* 2008; 19: 373-386.

[118] Rizzo, P., di Scalea, F.L. Feature extraction for defect detection in strands by guided ultrasonic waves, *Structural Health Monitoring: An International Journal* 2006; 5(3): 297-308.

[119] Park, S., Yun, C.-B., Roh, Y., Lee, J.-J. PZT-based active damage detection techniques for steel bridge components, *Smart Materials and Structures* 2006; 15: 957-966.

[120] Michaels, J.E. Detection, localization and characterization of damage in plates with an in situ array of spatially distributed ultrasonic sensors, *Smart Materials and Structures* 2008; 17: 035035-03548.

[121] Zhao, X., Gao, H., Zhang, G., Ayhan, B., Yan, F., Kwan, C., Rose, J.L. Active health monitoring of an aircraft wing with embedded piezoelectric sensor/actuator network: I.

defect detection, localization and growth monitorin, *Smart Materials and Structures* 2007; 16: 1208-1217.

[122] Park, H.W., Sohn, H., Law, K.H., Farrar, C.R. Time reversal active sensing for health monitoring of a composite plate, *Journal of Sound and Vibration* 2007; 302: 50-66.

[123] Keilers Jr, C. H., Chang, F.-K. Identifying delamination in composite beams using built-in piezoelectrics: part I - experiments and analysis, *Journal of Intelligent Material Systems and Structures* 1995; 6(5): 649-663

[124] Choi, K., Keilers Jr., C.H., Chang, F.-K. Impact Damage detection in composite structures using distributed piezoceramics. In Proceedings of the 35th AIAA/ASME/ASCE/AHS/ASC Structures, Structural Dynamics, and Materials Conference, April 18-20, 1994, 118-124.

[125] Tracy, M., Chang, F.-K. Identifying impacts in composite plates with piezoelectric strain sensors, part I: Theory, *Journal of Intelligent Material Systems and Structures* 1998; 9: 920-928.

[126] Halabe, U.B., Franklin, R. Ultrasonic signal amplitude measurement and analysis techniques for nondestructive evaluation of structural members, In Proceedings of the SPIE 1998; 3396: 84-94.

[127] Monnier, T. Lamb waves-based impact damage monitoring of a stiffened aircraft panel using piezoelectric transducers, *Journal of Intelligent Material Systems and Structures* 2006; 17: 411-421.

[128] Staszewski, W.J., Boller, C., Tomlinson, G.R. Health monitoring of aerospace structures: smart sensor technologies and signal processing, John Wiley & Sons, Inc, Chichester, 2004.

[129] Sohn, H., Farrar, C.R., Hunter, N.F., Worden, K. Structural health monitoring using statistical pattern recognition techniques, *ASME Journal of Dynamic Systems, Measurement and Control* 2001; 123: 706-711.

[130] Chang, F.-K., Markmiller, F.C., Ihn, J.-B., Cheng, K.Y. A potential link from damage diagnostics to health prognostics of composites through built-in sensors, *Journal of Vibration and Acoustics* 2007; 129: 718-729.

[131] Eremin , A.A., Glushkov, E.V., Glushkova, N.V., Lammering, R. Evaluation of effective elastic properties of layered composite fiber-reinforced plastic plates by piezoelectrically induced guided waves and laser Doppler vibrometry, *Composite Structures* 2015; 125: 449-458.

[132] Rekatsinas, C., Nastos, C., Theodosiou, T., Saravanos, D. A time-domain high-order spectral finite element for the simulation of symmetric and anti-symmetric guided waves in laminated composite strips with active piezoelectric sensors, EWSHM - 7th European Workshop on Structural Health Monitoring, Jul 2014, Nantes, France. 2014.

[133] Maio, L., Memmolo, V., Ricci, F., Boffa, N.D., Monaco, E., Pecora, R. Ultrasonic wave propagation in composite laminates by numerical simulation, *Composite Structures* 2015; 121: 64-74.

[134] Samaratunga, D., Jha, R., Gopalakrishnan, S. Wave propagation analysis in adhesively bonded composite joints using the wavelet spectral finite element method, *Composite Structures* 2015; 122: 271-283.

[135] Sause, M.G.R., Hamstad, M.A., Horn, S. Finite element modeling of Lamb wave propagation in anisotropic hybrid materials, *Composites: Part B* 2013; 53: 249-257.

[136] Ostiguy, P.C., Quaegebeur, N., Masson, P. Assessment of the excitelet algorithm for in-situ mechanical characterization of orthotropic structures, SPIE Smart Structures and Materials/NDE, 2012: 83480N.

[137] Pant, S. Lamb wave propagation and material characterization of metallic and composite aerospace structures for improved structural health monitoring (SHM), Ph.D. thesis, Carleton University, 2014.

[138] Li, B., Ye, L., Li, Z., Ma, Z., Kalhori, H. Quantitative identification of delamination at different interfaces using guided wave signals in composite laminates, *Journal of Reinforced Plastics and Composites* 2015; 34(18): 1506-1525.

[139] Wang, D., Ye, L., Tang, Y., Lu, Ye. Monitoring of delamination onset and growth during Mode I and Mode II interlaminar fracture tests using guided waves, *Composites Science and Technology* 2012; 72: 145-151.

[140] Quaegebeur, N., Micheau. P., Masson, P., Maslouhi, A. Structural health monitoring strategy for detection of interlaminar delamination in composite plates, *Smart Materials and Structures* 2010; 19 (8): 5-14.

[141] Sharif-Khodaei, Z., Aliabadi, M.H. Assessment of delay-and-sum algorithms for damage detection in aluminum and composite plates, *Smart Materials and Structures* 2014; 23, 2-27.

[142] Diamanti, K., Soutis, C. Structural health monitoring techniques for aircraft composites structures, *Progress in Aerospace Sciences* 2010; 46:342-52.

[143] Wang, D., Ye, L., Tang, Y., Lu, Ye. Monitoring of delamination onset and growth during Mode I and Mode II interlaminar fracture tests using guided waves, *Composites Science and Technology* 2012; 72: 145-151.

[144] Panda, R.S., Rajagopal, P., Balasubramaniam, K. An approach for defect visualization and identification in composite plate structures using air-coupled guided ultrasound, *AIP Conference Proceedings* 2015; 1650 (1299); 1299-1306.

[145] Ramadas, C., Balasubramaniam, K., Joshi, M., Krishnamurthy, C.V. Interaction of guided Lamb waves with an asymmetrically located delamination in a laminated composite plate, *Smart Materials Structures* 2010; 19: 65009-65020.

[146] Ramadas, C., Balasubramaniam, K., Joshi, M., Krishnamurthy, C.V. Interaction of the primary anti-symmetric Lamb mode (A0) with symmetric delaminations, numerical and experimental studies, *Smart Materials Structures* 2009; 18: 85011-18.

[147] Liu, G.R. A combined finite element-strip element method for analysing elastic wave scattering by cracks and inclusions in laminates, *Computational Mechanics* 2002; 28: 76-81.

[148] Veidt, M., Ng, C.T. Influence of stacking sequence on scattering characteristics of the fundamental anti-symmetric Lamb wave at through holes in composite laminates, *Journal of the Acoustical Society of America* 2011; 129(3): 1280-1287.

[149] Ng, C.T., Veidt, M., Rose L.R.F. et. Al. Analytical and finite element prediction of Lamb wave scattering at delaminations in quasi-isotropic composite laminates, *Journal of Sound and Vibration* 2012; 331(22): 4870-4883.

[150] Ng, C.T., Veidt, M. Scattering of the fundamental anti-symmetric Lamb wave at delaminations in composite laminates, *Journal of the Acoustical Society of America* 2011; 129(3): 1288-1296.

[151] Rathod, V.T. Mahapatra, D.R. Lamb wave based monitoring of plate-stiffener deboding using a circular array of piezoelectric sensors, *International Journal on Smart Sensing and Intelligent Systems* 2010; 3(1): 27-44.

[152] Ramadas, C., Balasubramaniam, K., Joshi, M., Krishnamurthy, C.V. Sizing of interface delamination in a composite T-joint using time-of-flight of Lamb waves, *Journal of Intelligent Material Systems and Structures* 2011; 22: 757-768.

[153] Quaegebeur, N., Micheau, P., Masson, P., Castaings, M. Methodology for optimal configuration in structural health monitoring of composite bonded joints, *Smart Materials and Structures* 2012, 21:105001-105011.

[154] Wu1, Z., Liu, K., Wang, Y., Zheng, Y. Validation and evaluation of damage identification using probability-based diagnostic imaging on a stiffened composite panel, *Journal of Intelligent Material Systems and Structures* 2014; 26: 2181-2195.

[155] Haynes, C., Todd, M., Nadabe, T., Takeda, N. Monitoring of bearing failure in composite bolted connections using ultrasonic guided waves: A parametric study, Structural Health Monitoring, An International Journal 2014, 13(1): 94-105.

[156] Vanniamparambila, P.A., Carmib, R., Khanc, F., Cuadraa, J., Bartolic, I., Kontsosa, A. An active-passive acoustics approach for bond-line condition monitoring in aerospace skin stiffener panels, *Aerospace Science and Technology* 2015; 43: 289-300.

[157] Ricci, F., Monaco, E. , Maio, L. , Boffa, N. D., Mal, A.K. Guided waves in a stiffened composite laminate with a delamination, *Structural Health Monitoring: An International Journal* 2015; 15 (3): 1-8.

[158] Padiyar, M.J., Balasubramaniam, K. Quantitative characterization of interface delamination in composite T-joint using couplant-free Lamb wave methods, *Journal of Reinforced Plastics and Composites* 2016; 35(4): 345-36.1

[159] Smelyanskiy, V.N., Hafiychuk, V., Luchinsky, D.G., Tyson, R., Miller, J., Banks, C. Modelling wave propagation in sandwich composite plates for structural health monitoring, Annual Conference of the Prognostics and Health Management Society, 2011.

[160] Hosseini, S.M.H., Gabbert, U. Numerical simulation of the Lamb wave propagation in honeycomb sandwich panels: A parametric study, *Composite Structures* 2013; 97:189-201.

[161] Mustapha, S., Ye ,L. Propagation behaviour of guided waves in tapered sandwich structures and debonding identification using time reversal, *Wave Motion* 2015; 57: 154-170.

[162] Mustapha, S., Ye, L., Dong, X., Alamdari, M.M. Evaluation of barely visible indentation damage (BVID) in CF/EP sandwich composites using guided wave signals, *Mechanical Systems and Signal Processing* 2016; 76-77497-517

[163] Sikdar, S., Banerjee, S. Identification of disbond and high density core region in a honeycomb composite sandwich structure using ultrasonic guided waves, *Composite Structures* 2016; 152: 568-578.

[164] Mustapha, S., Ye, L., Dong, W., Lu, Y. Debonding detection in composite sandwich structures based on guided waves, *AIAA Journal* 2012; 50(8): 1697-1706.

[165] Pavlopoulou, S., Soutis, C., Manson, G. Non-destructive inspection of adhesively bonded patch repairs using Lamb waves, *Plastics, Rubber and Composites* 2012; 4: 61-8.

[166] Jang, I., Park, I., Lee, U. Guided waves in a Timoshenko beam with a bonded composite patch: Frequency domain spectral element modeling and analysis, *Composites: Part B* 2014; 60: 248-260.

[167] Pavlopoulou, S. On structural health monitoring of aircraft adhesively bonded repairs, Ph.D. thesis, University of Sheffield, 2013.

[168] Habib, F., Martinez, M., Artemev, A., Brothers, M. Structural health monitoring of bonded composite repairs - A critical comparison between ultrasonic Lamb wave approach and surface mounted crack sensor approach, *Composites: Part B* 2013; 47: 26-34.

[169] Ren, B., Lissenden, C.J. Ultrasonic guided wave inspection of adhesive bonds between composite laminates, *International Journal of Adhesion and Adhesives* 2013; 45: 59-68.

CHAPTER 3. FIRST MANUSCRIPT

3.1 Preface

This chapter presents an investigation of the guided wave propagation in composite structures. It characterizes the guided wave behaviour regarding reflection, transmission, and scattering while interacting with delamination (introduced by Teflon tape) and impact. The experimental setup, the methodology of wave generation and data acquisition are examined and justified. Moreover, the comparison of the diffracted wave components with respect to damage cases (type, size, and location), mode and frequency and excitation angle contributes to the understanding of reflection, transmission and scattering behaviour of guided wave in composites.

A Comparative Study of Guided Wave Interaction in Composites with Artificial Delamination and Impact Damage*

*Manuscript submitted to Structural Health Monitoring, An International Journal (February 2016)

Mohammad H. Sherafat, Pascal Hubert, Larry Lessard

Department of Mechanical Engineering, McGill University, Macdonald Engineering Building, 817 Sherbrooke West, Montreal, QC, Canada, H3A 0C3

Nicolas Quaegebeur, Patrice Masson

GAUS, Department of Mechanical Engineering, Université de Sherbrooke, Sherbrooke, QC, Canada, J1K 2R1

3.2 Abstract

The objective of this paper is to compare the reflection, transmission and scattering behaviour of anti-symmetric mode of guided waves, caused by artificial and real damage in composite structures. The structures of interest are composed of unidirectional prepreg carbon fibre reinforced polymer (CFRP) with a quasi-isotropic layup. The artificial delamination is introduced into the laminate using two circular Teflon tapes during manufacturing, and the realistic damage is simulated by impacting the samples at two energy levels. Two co-localized rectangular piezoceramics are used to generate anti-symmetric mode, and non-contact measurement is performed using a 3-D laser Doppler vibrometer (LDV) to extract the required information for evaluation of the reflection, transmission as well as the scattering behaviour of the anti-symmetric mode. The corresponding coefficients as a function of frequency, excitation angle, and type of damage are extracted. It is found that the amplitude of the coefficients and directivity patterns of scattered waves are barely affected by excitation angle but significantly by the impact energy. Finally, SHM design guidelines based on comparing artificial and real damage effect on guided waves are proposed for efficient inspection of composite structures.

Keywords: Composite structures, Structural health monitoring (SHM), Guided wave propagation, Damage detection, Impact, Delamination

3.3 Introduction

Despite enhancements in terms of specific strength and stiffness using composites, their susceptibility to hide damage is still a major point of concern. The main types of damage (e.g. Fatigue Damage (FD), Environmental Damage (ED) and Accidental Damage (AD)) can significantly jeopardize the performance and safety of a structure with a little-advanced warning [1]. Therefore it is crucial to take necessary precautions by effectively detecting these types of damage at early stages and subsequently undertaking an appropriate action (e.g. repair) to prevent catastrophic failure. Since many of the kinds of damage cannot be easily detected by visual inspection, Non-Destructive Testing (NDT) methods are being employed for detailed inspection of structures. Conventional NDT approaches have attained maturity in engineering applications during the last decades [2], but since they are usually conducted at regularly scheduled intervals during the part's lifetime, they cannot provide descriptive information about structural integrity in a real-time manner. Moreover, most of the existing NDT methods require extremely time-consuming point-by-point inspection methods (e.g., C-Scan). Structural Health Monitoring (SHM) has been proposed as an improved and retrofitted version of traditional NDT for continuous inspection of structural features and to evaluate their health and integrity. SHM systems aim at replacing scheduled maintenance with condition-based maintenance, thus saving the cost of unnecessary maintenance as well as improving the level of safety through the consideration of working conditions updates [1]. SHM contributes to higher standards of safety also by introducing automated SHM systems, thereby reducing human interactions during the inspection phase [3].

It has been shown that an effective SHM method could reduce the total maintenance cost compared to traditional NDT approaches by more than 30% for an aircraft fleet [4]. As an example, the life of the F-18 of the Canadian Air Force could be extended by 12 years, by monitoring the operational loads, thus leading to savings of 400 million Canadian dollars

[5]. Therefore, SHM is a major area of interest for the aerospace community, especially considering aging aircraft where the growing maintenance costs, which is estimated at more than $10.4 billion worldwide annually [4].

Among the different approaches of SHM, the guided wave-based strategies are cost effective, fast, repeatable, able to inspect large structures, sensitive to small damage size, and able to detect both surface and internal damage [1]. This technique usually makes use of piezoelectric transducers to generate propagating waves and measures the signature of the echoes that may be influenced by any inhomogeneity (structural feature or defect). Interaction of guided waves with damage can significantly influence their propagation, accompanied by wave scattering effects such as reflection, transmission, and mode conversion. The above is the premise of elastic wave-based damage identification since different locations and severity of damage can cause unique scattering phenomena. Hence ultrasonic guided wave propagation with piezoelectric transducers has been proposed for effective inspection of composite structures [6] and of repaired composites as well as bonded joints [7-9]. When an incipient fundamental symmetric mode (S0) encounters a delamination, a new wave mode, and fundamental shear horizontal (SH) mode, SH0, is generated in addition to the transmitted and reflected S0 waves [10]. From the changes in the amplitude ratio of the reflected waves and the arrival time (in the time domain analysis) of the new mode, delamination length can be used to evaluate the method quantitatively [1-3]. However, sufficient sensitivity to damage-scattered waves depends on the geometrical features, excitation angle and the propagating mode of propagation. It has been demonstrated that the fundamental anti-symmetric mode (A0) is less scattered than the S0 mode for the case of composite skin-stringer assemblies [11, 12]. By monitoring the plane-wave A0 mode in a pitch-and-catch approach at low frequencies, the quality of a joint can be evaluated [11]. Moreover, within-the-bond monitoring of the S0 mode also indicates a significant change of directivity, and a general increase of 60% of the scattered amplitude, which is observed in all directions [12]. Previous SHM studies demonstrated that cracks and notches can exert strong directionality on wave propagation in metallic structures [13-15], so the location of sensors becomes a crucial concern. Few studies have considered the effect of the crack and inclusion on wave scattering in composites. Only one numerical study combined the finite element and finite strip method for scattering analysis of elastic waves in anisotropic plates [16].

In order to investigate the influence of a delamination or impact on guided wave propagation, the widely used approach is to simulate the damage by inserting one or two Teflon tapes of controlled dimensions and locations. This method is common in NDT when calibrating the sensitivity or analyzing the through-the-thickness response to high frequency longitudinal waves, but the validity of the approach for low order guided waves has not been verified yet. However, many of the SHM approaches for efficient interlaminar delamination detection in a CFRP using guided waves propose the use of the A0 mode below 300 kHz [6, 12, 17-20]. Those studies are limited to a 2-D consideration of the problem and understanding of the 3-D behaviour (i.e. scattering behaviour) seems to be a research gap. However, few studies have investigated the influence of hole diameter to wavelength aspect ratios, different stacking sequences [21, 22], delamination size and location [22] on wave scattering characteristics, guided wave scattering comparison of real damage with an artificial defect is not investigated so far. In other words, the influence of different types of damage (artificial, real) on the scattering behaviour of guided waves requires detailed attention. Therefore, an empirical study benefiting from the competitive advantages of a 3-D scattered-based approach, comparing wave interaction with real damage and artificial delamination seems to be crucial.

This paper experimentally scrutinizes the scattering (including reflection and transmission) of anti-symmetric guided waves through composite plates that contain the artificial and real damage. Four quasi-isotropic CFRP samples were manufactured using an identical material with the same stacking sequence layup. For two of the samples, a Teflon tape positioned at different places through-the-thickness is used to mimic an artificial delamination as classically used for bulk wave inspection in contact or immersion tank. Two impact levels of 10 Joules and 15 Joules are applied on two other samples following an ASTM standard [23]. The anti-symmetric guided waves are generated by a co-localized piezoceramic device at three different angles, namely 180°, 135°, and 90°. The non-contact measurement of the in-plane and out-of-plane velocity is performed using a 3-D laser Doppler vibrometer (3D- LDV) over a circular grid. Using the circular scanning points, and by estimating the amplitude ratio of the reflected, transmitted and diffracted waves to the incident wave, the three coefficients representing the behaviour of the guided waves are extracted. The novelty of the approach resides in the comparison of the damage-scattered wave components with respect to damage type, excitation angles, frequency and mode of propagation in order to derive SHM design guidelines, justifying the guided wave method's ability for defect detection.

3.4 Structure description

The structures of interest in this paper are four 30 x 30 cm CFRP test coupons which are composed of 16 plies of unidirectional prepreg tapes (HEXPLY 8552) with quasi-isotropic layup $[0/90/\text{-}45/45]_{2s.}$ The thickness of each lamina is 0.192 mm. Since each individual part is made using 16 plies, the thickness of the sample becomes 3.07 mm. All the coupons are laid up, vacuum bagged simultaneously and cured in an autoclave. The cure cycle for this material starts with applying full vacuum and 103.4 kPa pressures, heating at 3–5°C /minutes to 107°C, and then holding at 107°C, for 30 minutes. After that, pressure is raised, the vent is open to vacuum when the pressure reaches 206.8 kPa, and the pressure finally ramps up to 586 kPa. The temperature cycle follows an increase in the temperature to 176.6°C at 3–5° /minute, holding at 176.6°C for 120 ±10 minutes and eventually cooling the samples at 2–5°C /minute to 65.5°C.

Although the disbond should ideally be initiated by interlaminar cracking to model real Fatigue Damage (FD), here, a circular disbond (with 25 mm diameter) is positioned between the 3^{rd} and 4^{th} layers for the first coupon, and between the 8^{th} and 9^{th} layers (mid-plane) for the second sample by introducing two pieces of Teflon tape (Airtech Teflease MG2R). For the case of Accidental Damage (AD), two coupons are impacted at energy levels of 10 Joules and 15 Joules, using a drop-weight impact system following standards [23]. A summary of the four damaged samples is shown in Table 3.1. For the 3 mm thick specimen manufactured out of CFRP, the 10 J energy impact test is employed as a case that causes barely visible impact damage (BVID) representing half the standardized impact energy following ASTM D7136 /D7136M-15 Standard, while the 15 J impact represents more severe and noticeable damage. Note that the design parameters, including the material, lay-up and damage levels are selected based on a project between industrial and academic researchers, namely the CRIAQ DPHM 501 project, where design parameters and damage levels have been identified, extracted and filtered for their relevance from an extensive list of aerospace structures of interest [24].

Ultrasound scans by immersion have been performed using a Zetec Topaz 32/128 PR and a 64-element IMASONIC probe at 10 MHz. A linear scanning method at 0° with an active aperture of 12 elements (7.2 mm) is used. The probe is mounted on a 2D table in order to perform B- and C-Scan of the structures. The size (diameter) of damage for the pre-inserted delamination are 25 mm, while for the 10 J and 15 J impacts, the sizes measured by C-Scan are 28 mm and 32 mm respectively. The locations of the Teflon positioned between the 3rd and 4th layers, and the mid-plane are also confirmed by B-scan (see Table 3.1).The B-Scan representation in Table 3.1 shows that some fibre breakage is observed at different thicknesses in the case of impacts, but the damage is local such that no fibres are broken around the targeted zone. As classically observed, a typical “double-helix” pattern is also observed, such that trapezoidal delaminations are wrapped in a conical shaped envelope increasing from the impacted side to the free side of the impacted plate.

Table 3.1. Composite samples with delamination and impact

Sample	Type of defect	Diameter	C-Scan	B-Scan
#1	Teflon between the 3rd and 4th plies	25 mm	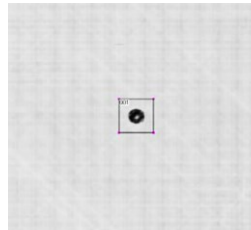	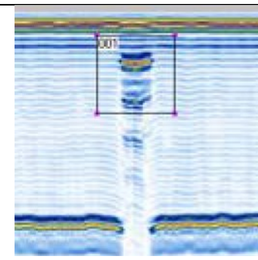
#2	Teflon between the 8th and 9th plies	25 mm	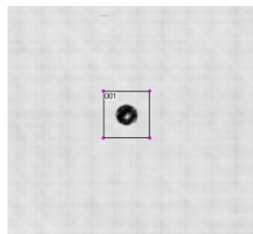	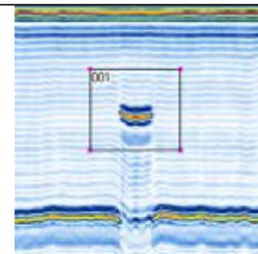
#3	10 Joules impact	28 mm	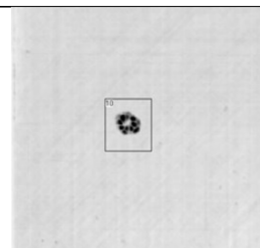	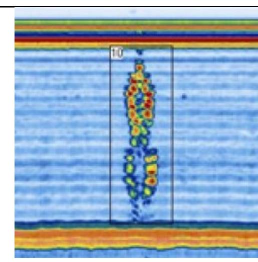
#4	15 Joules impact	32 mm	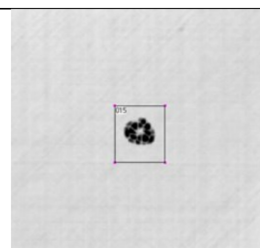	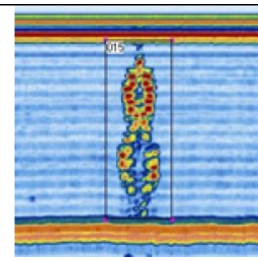

3.5 Experimental methodology

In this research, a scattered-based approach, benefiting the forward (i.e. pitch-and-catch) and backward (i.e. pulse-echo) scattering waveforms, is used to improve the configuration of actuator-sensor pair-based method for efficient inspection of composite structures. Therefore, the diffraction pattern, i.e. wave scattering level at different orientations, including reflection and transmission levels, around the damaged region can be determined to help to understand the 3-D behaviour of guided wave interaction with the defect and allows deriving guidelines for SHM system design.

3.5.1 Guided wave generation and sensing

In order to characterize the guided wave behaviour through the damaged samples, a calibrated and repeatable device capable of generating a specific guided wave mode is required. For this purpose, plane wave generation was chosen in order to allow focusing the energy on the selected area and avoiding geometrical spread induced by circular transducers. The designed device illustrated in Fig. 3.1 consists of two co-localized rectangular piezoceramics (50 x 5 x 0.45 mm^3) maintained and aligned on both sides of the structure using high strength magnets and coupled to the host structure using shear-coupling gel [25]. The dimensions are chosen in order to focus the energy within a 10-degree angle for wavenumbers above 250 rad/m following the model presented in the literature [26].

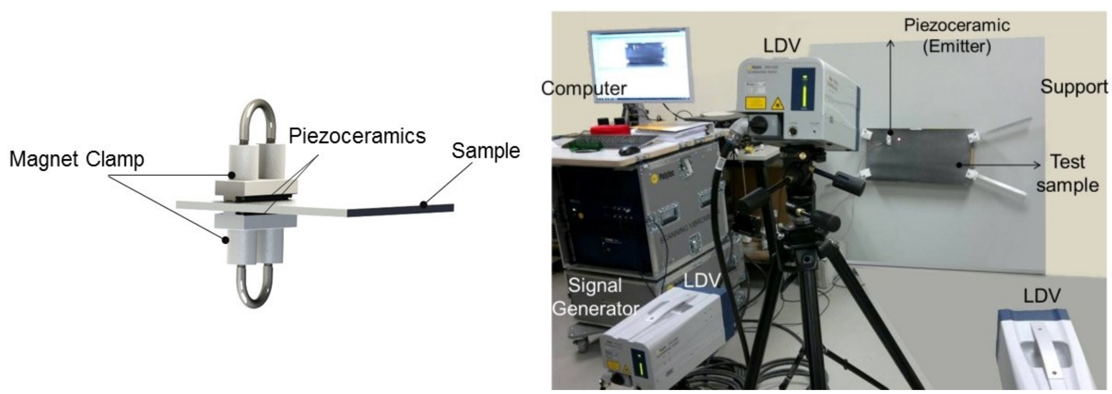

Figure 3.1. Illustration of the piezoceramic element and excitation clamp (left) and the experimental setup (right)

The two actuators can be driven in- and out-of-phase in order to generate symmetric or anti-symmetric modes, respectively. However, due to slight misalignment or tilt, this strategy requires optimization [27] in order to be efficient experimentally. For this purpose, the two piezoceramics are activated individually, and the mode selection is achieved in post-processing by adjusting amplitude and phase of both actuator signals in order to minimize the magnitude of the unwanted mode [12]. The transfer functions between the piezoceramic voltage and the measured 3-D velocity field using a 3-D LDV (PSV-500, Polytec GmbH) are measured in the frequency domain. For this purpose, continuous pseudo-random excitation is used and amplified using a NOVO UAP-8400 voltage amplifier. Measurement of the transfer function is performed using 200 frequency steps between 0 and 500 kHz and averaged 100 times over time frames of 0.4 ms in order to increase the Signal-to-Noise Ratio (SNR). The use of a continuous regime allows working in the bandwidth of interest with a single measurement and benefits from efficient averaging of the phasor in the frequency domain. However, the main drawback is that time-domain information such as wave-packet separation cannot be performed, and consequently, the back-wall reflection needs to be cancelled out using absorbing paste. The propagation characteristics are extracted using spatial Fourier transform [28]. The space between two adjacent points is set to 0.5 mm, ensuring at least five scanning points per minimal wavelength for frequencies below 500 kHz.

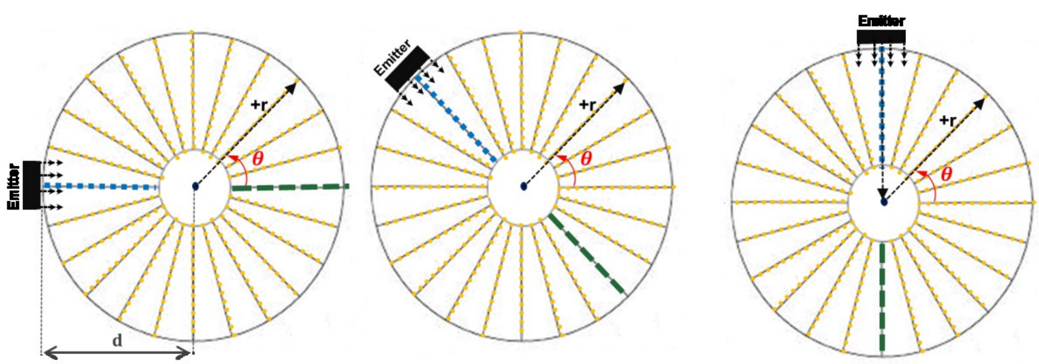

Figure 3.2. Schematic representation of the scanning grid. Reflection (square blue), transmission (rectangular green) and diffraction (circle yellow) scanning points for 180° (left) 135° (middle) and 90° (right) excitation

In order to evaluate the effect of damage on guided wave behaviour at different orientations, a 360° circular scanning grid, consisting of 24 lines (with 15° separation between two adjacent lines), each including 202 scanning points for a total radius of r=100 mm, is defined in the targeted zone (see Fig. 3.2). The centre of the circle is located right in the centre of the plates (centre of the delamination or impact) and incident angles of 180°, 135° and 90° are employed (see Fig. 3.2). A spacing of 20 mm between the measurement points and the damage is ensured in order to avoid measurement of evanescent waves.

3.6 Theoretical considerations, results, and discussion

The propagation of guided waves in thin structures is determined by the knowledge of the complex wavenumber $k\,(\omega,\theta) = k_R + j\,k_I$ associated with each propagating mode at angular frequency ω and angle θ. The real part k_R of the wavenumber k represents the propagation term of the wavenumber and is related to the wavelength λ by the relation: $k_R = 2\pi/\lambda$. The wave attenuation coefficient is defined by the imaginary part k_I of the wavenumber and is classically expressed in Nepers per metre (Np/m). It is responsible for an exponential decrease of the in-plane and out-of-plane displacement field due to material damping. Under the plane wave assumption, the expression of any component of the displacement field $u(r,\omega,\theta)$ in the frequency domain can be derived for a given divergent mode propagating from the centre in the $+r$ direction (scattered wave):

$$u(r,\omega,\theta) = U_s(\omega,\theta)\; e^{-k_I(\omega,\theta).r} \quad e^{jk_R(\omega,\theta).r} \tag{3-1-a}$$

Similarly for a convergent plane wave to the centre in the $-r$ direction (incident wave):

$$u(r,\omega,\theta) = U_i(\omega,\theta)\; e^{+k_I(\omega,\theta).r} \quad e^{-jk_R(\omega,\theta).r} \tag{3-1-b}$$

where $U_s(\omega,\theta)$ and $U_i(\omega,\theta)$ represents the complex amplitudes of the scattered and incident wave respectively. Plane wave propagation is assumed for ease of interpretation. Indeed, a geometrical spread could be introduced by considering a cylindrical propagation for the diffracted field, but in the case of perfect transmission or reflection, the associated coefficients would differ from 1. Moreover, this would only introduce a $1/\sqrt{kr}$ in Eq. 3-1-a that would depend on frequency but would not modify the conclusions of the study. Consequently, a simple plane wave model is considered for both incident and diffracted fields. To extract the amplitude and real part of the wavenumber, the method used is to perform a two-dimensional Fourier transform [28] and measure the amplitude associated with each mode. Damping quantity is highly sensitive to noise measurement, radiation condition (plane wave or cylindrical), multimodal propagation, mode conversion phenomena and material anisotropy [12]. By the use of plane wave excitation, the attenuation with respect to the propagation distance only depends on the material damping and not on the geometrical spread of the wave. Although a high level of damping and noise (low SNR) is observed below 100 kHz for anti-symmetric mode, it is less affected by the damping than the symmetric mode [12], since its energy level is higher [12, 13]. Therefore only the first anti-symmetric mode (A0) is employed and its results are presented in this paper.

3.6.1 Reflection and transmission

The reflection $R(\omega)$ and transmission $T(\omega)$ coefficients are defined by the following amplitude ratios:

$$R(\ \omega) = \frac{U_r(\theta_{inc}, \omega)}{U_i(\theta_{inc}, \omega)}\ \mathrm{e}^{-\mathrm{k_I}(\theta_{inc})\mathrm{d}} \tag{3-2}$$

$$T(\omega) = \frac{U_t(\theta_{inc} + \pi, \omega)}{U_i(\theta_{inc}, \omega)}\ \mathrm{e}^{-\mathrm{k_I}(\theta_{inc})\mathrm{d}} \tag{3-3}$$

where θ_{inc} denotes the incidence angle (180°, 135° and 90°), $U_r(\omega, \theta)$ and $U_t(\omega, \theta)$ represents the amplitudes of the reflected and transmitted waves, respectively. In Eq. (3-2) and Eq. (3-3), the $\mathrm{e}^{-\mathrm{k_I}(\theta_{inc})\mathrm{d}}$ term allows compensating the attenuation of the incident wave along the distance (d) from the emitter to the centre of the measurement grid (See Fig. 3.2) for the three excitation angles.

After performing the post-processing described above on the raw data captured by 3D-LDV, the reflection, and transmission of A0 mode for both the damaged samples are obtained and presented in Figs 3.3 and 3.4, respectively, when the guided waves are excited at 180°, 135° and 90°. Mode conversion is not observed in the present case and is thus not presented for clarity. Due to low SNR for frequencies below 50 kHz for A0, the results are only presented in a limited bandwidth for which the SNR is guaranteed to be above 10 dB.

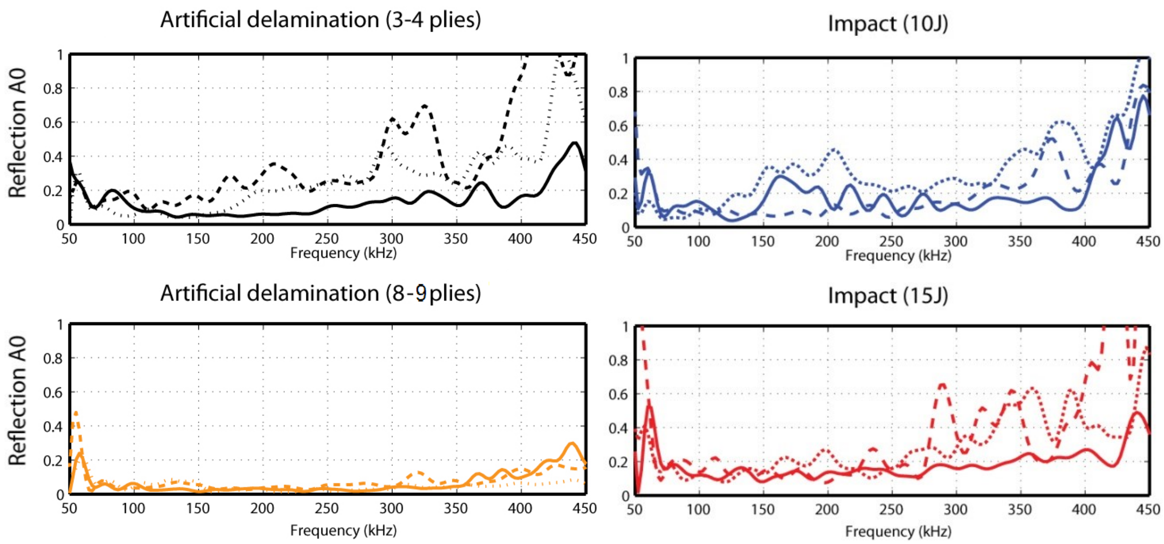

Figure 3.3. Reflection coefficients of the A0 mode for the four damaged samples, excitation angle of 180° (dashed lines), 135° (solid lines) and 90°(dotted lines)

The reflection coefficient versus frequency for the four different damaged samples at three excitation angles is illustrated in Fig. 3.3. The first thing to note is that the mid-plane Teflon-tape delamination reflects the least energy, around 5%, although at a high frequency range (above 400 kHz) its reflection level reaches up to 25%. The overall reflection behaviours of the guided wave for the other three samples are similar to each other. A marginal difference observed among them, noting more reflected energy at higher frequencies. The incidence angle has little effect on the reflection coefficient since a quasi-isotropic layup is used in the present study. The maximum reflection mostly corresponds to the 15 J impacted sample as it reflects significant energy (around 30%) between 250 kHz and 350 kHz frequency bandwidth at 180° excitation, whereas the 10 J impacted sample shows lower amounts of echo noticeably. The difference between the 10 J and the 15 J impacts is insignificant unless one examines frequencies between 150 kHz and 250 kHz.

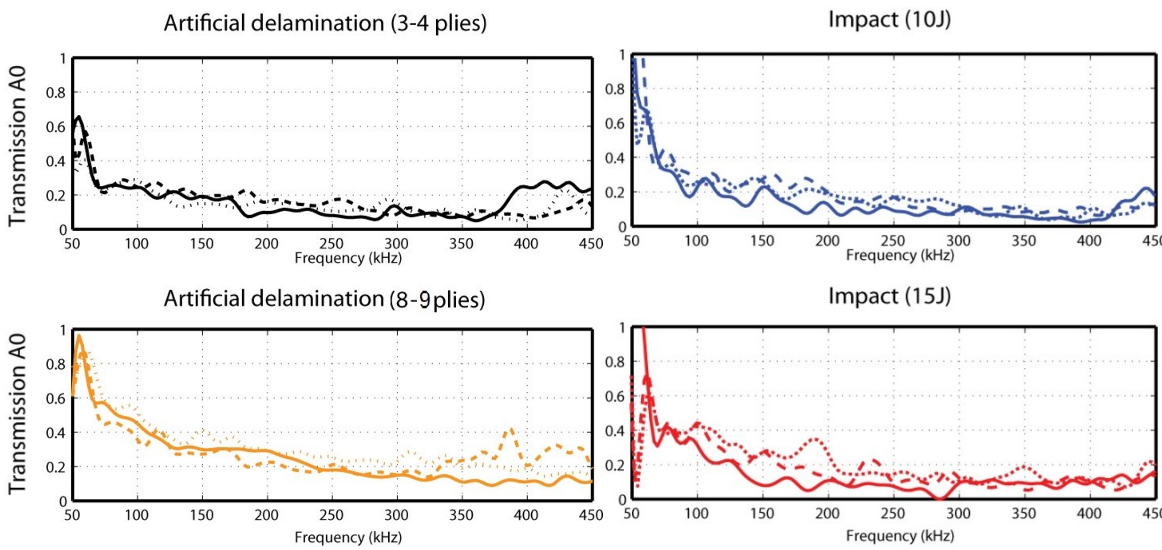

Figure 3.4. Transmission coefficients of the A0 mode for the four damaged samples, excitation angle of 180° (dashed lines), 135° (solid lines) and 90° (dotted lines)

Fig. 3.4 provides a plot of the transmission coefficients by the damage types at frequencies between 50 and 450 kHz. While the minimum reflection is induced by the mid-plane delamination (Fig. 3.3), the transmission level through mid-plane Teflon is larger than for other defects, for the same reason that was mentioned before. Comparing Figs 3.3 and 3.4, it appears that while the reflection versus frequency is an upward trend (i.e. reflection increases with increasing frequency), the transmission is downward, such that at high frequency, less energy is transmitted. This is due to the fact that the resin and viscoelastic properties of the composite attenuate the energy of the waves at higher frequencies [12]. However, the damage also plays a crucial role in dissipating energy, by introducing standing waves in the delaminated area.

From the reflection and transmission results, it can be concluded that the non mid-plane delamination can simulate low-level energy impact (BVID), whereas the mid-plane positioned Teflon cannot. It is also important to note that that the incidence angle has little effect, so that by employing the pitch-and-catch (transmission) and the pulse-echo (reflection) configurations, both techniques are suitable for impact and delamination detection.

3.6.2 Scattering

The scattering effect is very useful when considering imaging processes such as Delay-and-Sum [29], Inverse methods [30], Time-reversal [31], or Correlation-based [32], for which the scattering at a potential damage is used for localization. Instead of using a pitch-and-catch approach, this method allows for using a sparse array of transducers. However, the frequency and mode must be chosen carefully in order to make sure that the damage sensitivity is ensured. The normalized scattering or diffraction coefficient $S(\omega)$ is introduced as the following amplitude ratios:

$$S(\theta,\omega) = \frac{U_s(\theta,\omega)}{U_i(\theta_{inc},\omega)} \sqrt{\frac{k_R(\theta)}{k_R(\theta_{inc})}}\, \mathrm{e}^{-\mathrm{k_I}(\theta_{inc})\mathrm{d}} \tag{5}$$

In the definition of the scattering coefficient, the term $\sqrt{\frac{k_R(\theta)}{k_R(\theta_{inc})}}$ is introduced in order to compensate for the anisotropy of the structure. Indeed in the case of isotropic structures, this term equals 1, but allows representing the dependency of the scattering with respect to the wavenumber, assuming that a cylindrical diffraction of the incident wave is observed at the centre of the measurement grid.

The main objective is to investigate if any of the different defects generate similar scattering behaviour, such that a Teflon-tape delamination can possibly represent a real damage zone. It should be noted that the detectable size of damage often depends on the wavelength, which is related to the excitation frequency and host structure properties. The wave propagation approach (including acoustic, guided and also electromagnetic waves) quantitatively evaluates the damage that is at least half of the size of its wavelength [33]. A high frequency wave (i.e., small wavelength) is always preferred so as to have the capacity to detect small sized damage [1]; however, it has its own challenges regarding low energy due to attenuation of materials.

The diffraction patterns for the first anti-symmetric mode excited at three incident angles are presented in Figs 3.5, 3.6 and 3.7 for three frequency ranges, namely:

- 50 kHz, for which the incident wavelength is approximately the defect size (low frequency or diffraction behaviour),
- 200 kHz for which the incident wavelength equals one third of the defect size (middle frequency or transmission behaviour),
- 350 kHz for which the incident wavelength equals one sixth of the defect size (high frequency or reflection behaviour).

The first set of results in Fig. 3.5 representing the low frequency range shows that the mid-plane Teflon-tape's scattering behaviour is quite different from the three other damage types. The low energy impact (e.g. 10J) diffraction pattern akin to the 3^{rd}-4^{th} layered positioned Teflon-delamination is observed when the wavelength is relatively similar to the defect size. The order of amplitude also confirms that in a low-frequency range, the strong energy of guided waves is scattered at angles different from reflection or transmission. Thus a diffraction regime is observed and can be easily used for damage imaging using a piezoceramic array.

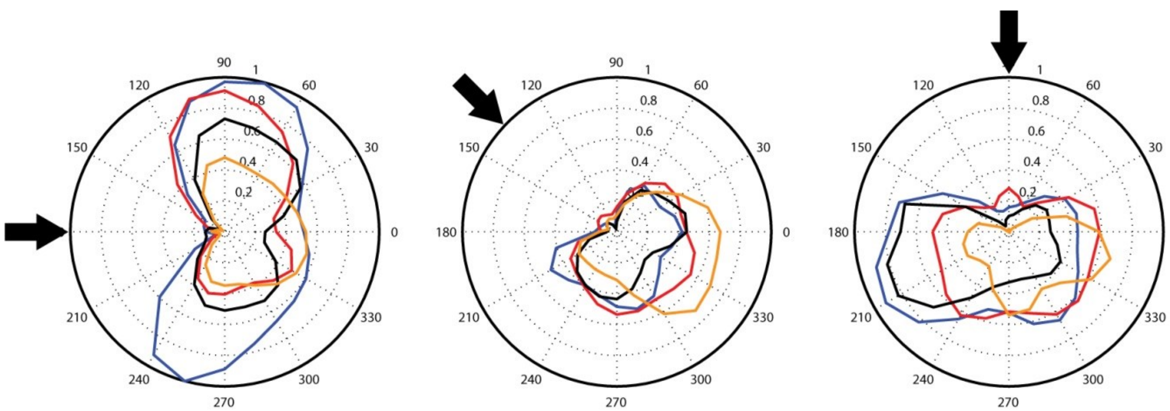

Figure 3.5. Diffraction pattern of the A0 mode excited at 50 kHz, 180° (left), 135° (middle), and 90°(right) for the four damaged plates: Teflon 3, 4 (black), Teflon 8, 9 (yellow), 10 J (blue), and 15 J (red)

Looking at the diffraction patterns at 200 kHz and 350 kHz (Figs 3.6, 3.7), less scattering is observed, and the wave is more transmitted or reflected in the incident directions. Moreover, the level of reflected and transmitted energies is reduced by 60% compared to at 50 kHz. Again, the mid-plane delamination acts differently while the non-mid-plane delamination and low energy impact level have similar directivity patterns at both frequencies.

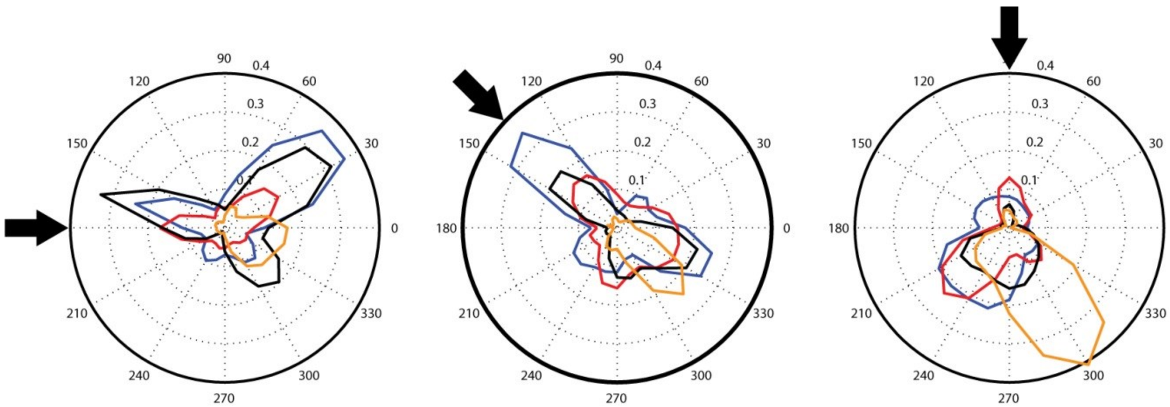

Figure 3.6. Diffraction pattern of the A0 mode excited at 200 kHz, 180° (left), 135° (middle), and 90° (left) for the four damaged samples: Teflon 3, 4 (black), Teflon 8, 9 (yellow), 10 J (blue), and 15 J (red)

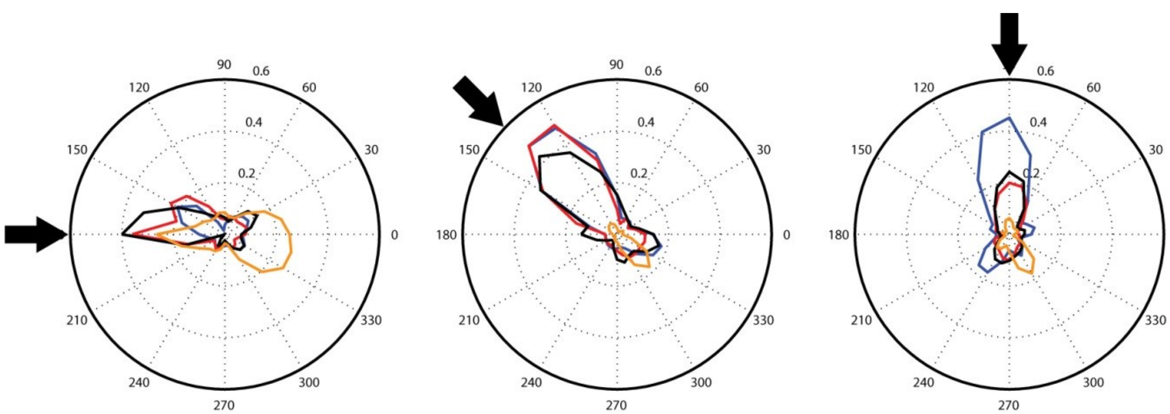

Figure 3.7. Diffraction pattern of the A0 mode excited at 350 kHz, 180° (left), 135° (middle), and 90° (right) for the four damaged samples: Teflon 3, 4 (black), Teflon 8, 9 (yellow), 10 J (blue), and 15 J (red)

While in a low frequency range (around 50 kHz), the transmission side of the directivity pattern was dominant, an apparent balance between reflection and transmission sides of distributed energy is noticed around the mid-frequency of excitation (200 kHz). However, Fig. 3.7 indicates that at a higher frequency (350 kHz), no significant energy is transmitted through the defects, and all the energy is attenuated due to standing wave behaviour or reflected, which confirms the upward reflection and downward transmission trends versus frequency. This confirms that pitch-and-catch and pulse-echo configurations are valid when the wavelength is smaller than half the damage size.

To conclude, the scattering results show that the mid-plane delamination causes an entirely different diffraction pattern while the non-mid-plane delamination and low energy impact level have similar directivity patterns. In a low frequency range, the strong energy is scattered at angles different from reflection or transmission whereas at higher frequencies, less diffraction is observed, and the wave is more transmitted or reflected in the incident directions.

3.7 Conclusion

A guided wave propagation strategy is proposed for inspection of composite structures incorporating artificial and real damage. Four structures made of quasi-isotropic unidirectional CFRP with inserted Teflon tape delamination and impact damage are studied. The anti-symmetric mode of guided wave is generated by piezoceramics, and an LDV is employed to capture the signals. The reflection, transmission and scattering behaviour of the plane guided waves are studied as a function of frequency and the defect type, damage level, and excitation angle. The excitation frequency attributed to the different wavelengths play a crucial role in the reflection, transmission, and scattering behaviour. It is concluded that non-mid-plane artificial delamination can accurately represent real impact, particularly BVID damage. Based on the experimental observations, guidelines for the design of an efficient SHM system can be derived:

1) The reflection increases with respect to frequency for both Teflon-type delamination and real impact damage, while the transmission decreases with respect to frequency.

   In the case of quasi-isotropic structures, the incidence angle has little influence on the wave behaviour in the pitch-and-catch (transmission) and pulse-echo (reflection) configurations.

2) The mid-plane Teflon-tape scattering behaviour is completely different from a real impact. However, the low energy (10 J) impact's diffraction pattern akin to the non mid-plane Teflon-type delamination is observed.

Future work will aim at determining the optimal configuration for artificial damage using Teflon tape in order to mimic as closely as possible the effect of realistic damage such as delamination, impacts, fibre breakage and weaving on guided waves scattering. Attention should be paid to combinations of multiple artificial delaminations of varying sizes based on C-Scan observations.

3.8 Acknowledgments

The research is supported by the Natural Sciences and Engineering Research Council of Canada (NSERC) through the framework of the Consortium for Research and Innovation in Aerospace in Québec (CRIAQ) DPHM 501 project as well as Bombardier Aerospace and L-3 MAS.

3.9 References

[1] Su, Z., and Ye, L. Identification of Damage Using Lamb Waves, From Fundamentals to Applications, Berlin: Springer-Verlag GmbH & Co., 2009.

[2] Standard Guide for Nondestructive Testing of Polymer Matrix Composites Used in Aerospace Applications, ASTM E2533 - 09, DOI: 10.1520/E2533-09.

[3] Rose, J. Ultrasonic Guided Waves in Solid Media, Cambridge University Press, New York, 2014.

[4] Chang, F. –K., Introduction to health monitoring: context, problems, solutions. 1st European Pre-workshop on Structural Health Monitoring, July 9, 2002; Paris, France.

[5] Caron, Y., Richard, Y., CF-188 Fatigue Life Management Program, NATO publication RTO-MP-7, AC/323 (AVT) TP/4, Paper 4,1998.

[6] Su, Z., Ye, L., Lu, Y. Guided Lamb waves for identification of damage in composite structures: A review, *Journal of Sound and Vibration* 2006; 295: 753-780.

[7] Diamanti, K., Soutis, C., Hodgkinson, J.M. Non-destructive inspection of sandwich and repaired composite laminated structures, *Composites Science and Technology* 2005; 65: 2059-2067.

[8] Sherafat, M.H., Quaegebeur, N., Lessard, L., Hubert, P., Masson P. Finite element modeling of Lamb wave propagation in composite stepped joints, *Journal of Reinforced Plastic and Composites* 2016; 35 (10): 796-806.

[9] Matt, H., Bartoli, I., Lanza di Scalea, F. Ultrasonic guided wave monitoring of composite wing skin-to-spar bonded joints in aerospace structures, *Journal of the Acoustical Society of America* 2005; 118: 2240-2253.

[10] Su, Z., Yang, C., Pan, N., Ye, L., Zhou, L.M. Assessment of delamination in composite beams using shear horizontal (SH) wave mode, *Composites Science and Technology* 2007; 67: 244-251.

[11] Sherafat. M.H., Guitel, R., Quaegebeur, N., Lessard, L., Hubert, P., Masson, P. Guided wave scattering behaviour in composite bonded assemblies, *Composite Structures* 2016;136: 696-705.

[12] Sherafat, M.H., Guitel, R., Quaegebeur, N., Hubert, P., Lessard, L., Masson, P. Structural Health Monitoring of a Composite Skin-Stringer Assembly using Within-the-bond Strategy of Guided Wave Propagation. *Materials and Design* 2016; 90: 787-794.

[13] Alleyne, D.N., Cawley, P. The interaction of Lamb waves with defects, IEEE. Transactions on Ultrasonics, Ferroelectrics and Frequency Control 1992; 39(3): 381-397

[14] Jin J, Quek ST and Wang Q. Design of interdigital transducers for crack detection in plates, *Ultrasonics* 2005; 43: 481-493.

[15] Tua, P.S., Quek, S.T., Wang, Q. Detection of cracks in plates using piezo-actuated Lamb waves, *Smart Materials and Structures* 2004; 13: 643-660.

[16] Liu, G.R. A combined finite element-strip element method for analyzing elastic wave scattering by cracks and inclusions in laminates, *Computational Mechanics*, 2002; 28: 76-81.

[17] Guo, N., Cawley, P. The interaction of Lamb waves with delaminations in composite laminates. *Journal of the Acoustical Society of America*, 1993; 94: 2240-2246.

[18] Quaegebeur, N., Micheau. P., Masson, P., Maslouhi, A. Structural health monitoring strategy for detection of interlaminar delamination in composite plates, *Smart Materials and Structures* 2010; 19 (8): 5-14.

[19] Basri, R., Chiu, W.K. Numerical analysis on the interaction of guided Lamb waves with a local elastic stiffness reduction in quasi-isotropic composite plate structures, *Composite Structures* 2004, 66: 87-99.

[20] Veidt, M., Ng, C.T. Influence of stacking sequence on scattering characteristics of the fundamental anti-symmetric Lamb wave at through holes in composite laminates, *Journal of the Acoustical Society of America*, 2011; 129(3): 1280-1287.

[21] Ng, C.T., Veidt, M., Rose, L.R.F., Wang, C.H. Analytical and finite element prediction of Lamb wave scattering at delaminations in quasi-isotropic composite laminates, *Journal of Sound and Vibration* 2012; 331(22): 4870-4883.

[22] Ng, C.T., Veidt, M. Scattering of the fundamental anti-symmetric Lamb wave at delaminations in composite laminates, *Journal of the Acoustical Society of America* 2011; 129(3):1288-1296.

[23] Standard Test Method for Measuring the Damage Resistance of a Fiber-Reinforced Polymer Matrix Composite to a Drop-Weight Impact Event, ASTM D7136 / D7136M – 15.

[24] Ostiguy, P.C., Sherafat, M.H., Franca, D.R., Bouslama, N., Quaegebeur, N., Maslouhi, A., Lessard, L., Hubert, P., Viens, M., Mofakhami, M.R., Hajjar, Z., Masson P. Selection of structural features for the systematic study of guided wave propagation and interaction with damage, International Workshop on Structural Health Monitoring 2015, Sept. 2015.

[25] Guitel, R., Quaegebeur, N., Micheau, P., Masson P. Clamped piezoelectric movable transducer for robust and selective guided wave mode generation, CanSmart/SMN Workshop, July 15, 2015, Vancouver, BC.

[26] Francesco, L.S., Matt, H., Ivan, B. The response of rectangular piezoelectric sensors to Rayleigh and Lamb ultrasonic waves, *Journal of the Acoustical Society of America* 2007; 121, 175-187.

[27] Ostiguy, P.C., Quaegebeur, N., Masson, P. Assessment of the excitelet algorithm for in-situ mechanical characterization of orthotropic structures, SPIE Smart Structures and Materials/NDE, 2012: 83480N.

[28] Alleyne, N.D., Cawley, P. A 2-Dimensional Fourier transform method for the quantitative measurement of Lamb modes, *Ultrasonics Symposium*1990; 1143-1146.

[29] Sharif-Khodaei, Z., Aliabadi, M.H. Assessment of delay-and-sum algorithms for damage detection in aluminum and composite plates, *Smart Materials and Structures* 2014; 23, 2-27.

[30] Staszewski, W.J., Pierce, S.G., Worden, K., Culshaw, B.Wavelet signal processing for enhanced Lamb wave defect detection in composite plates using optical fiber detection, *Optical Engineering* 1997; 36(7): 1877-1888.

[31] Sohn, H., Park, H.W., Law, K.H., Farrar, C.R. Combination of a time reversal process and a consecutive outlier analysis for baseline-free damage diagnosis, *Journal of Intelligent Material Systems and Structures* 2007; 18: 335-346.

[32] Wang, D., Ye, L., Su, Z., Lu, Y., Li, F, Meng, G. Probabilistic damage identification based on correlation analysis using guided wave signals in Aluminum Plates, *Structural Health Monitoring* 2010; 9(2): 133-144.

[33] Lee, B.C., Staszewski, W.J. Modelling of Lamb waves for damage detection in metallic structures: part II - wave interactions with damage, *Smart Materials and Structures* 2003; 12: 815-824.

CHAPTER 4. SECOND MANUSCRIPT

4.1 Preface

In the previous chapter, the interaction of the guided wave propagation with the defects in the simple composite plates was investigated. The strategy of reflection, transmission, and scattering of the ultrasonic waves under the plane wave generation and measured velocity field using an LDV was effectively applied. It worked properly, and the results were convincing. However, the wave behaviour in the composite assemblies is more complicated because of the presence of adhesive and the joint edges. This chapter focuses on applying the technique to a composite skin-stringer assembly using the within-the-bond line strategy. The components of reflected, transmitted, and scattered wave signals around the targeted zone are derived and analyzed, to detect disbond between the skin panel and the stringer.

Structural Health Monitoring of a Composite Skin-Stringer Assembly using Within-the-bond Strategy of Guided Wave Propagation*

* Materials & Design 2016; 90: 787-794

Mohammad H. Sherafat, Pascal Hubert, Larry Lessard
Department of Mechanical Engineering, McGill University, Macdonald Engineering Building, 817 Sherbrooke West, Montreal, QC, Canada, H3A 0C3

Robin Guitel, Nicolas Quaegebeur, Patrice Masson
GAUS, Department of Mechanical Engineering, Université de Sherbrooke, Sherbrooke, QC, Canada, J1K 2R1

4.2 Abstract

The objective of this paper is to investigate the within-the-bond guided wave propagation in a composite skin-stringer joint. The structure of interest is composed of three carbon fibre reinforced polymer (CFRP) plates bonded together by adhesive film. This bonded joint is prone to disbond when submitted to extreme loads or fatigue. Therefore, two bonding conditions are investigated, namely undamaged and damaged (with disbond). The artificial disbond is introduced into the joint using a circular Teflon tape during manufacturing. Two co-localized slender rectangular piezoceramics are used to generate plane guided waves within-the-bond lines and non-contact measurement is performed using a 3-D laser Doppler vibrometer (LDV) to extract the required information for evaluation of the bonding conditions. The results include reflection, transmission and also scattering of the guided waves at the joint as a function of frequency, propagating mode and presence of artificial damage. It was found that the amplitude of the reflection, transmission coefficients and directivity patterns of scattered waves are affected by the presence of damage, such that Structural Health Monitoring (SHM) design guidelines can be derived for efficient damage detection in the composite assemblies using a within-the-bond inspection strategy.

Keywords: Structural health monitoring (SHM), Composite joints, Guided wave propagation, Damage detection, Skin-stringer assembly

4.3 Introduction

Composite skin-stiffener assemblies are extensively employed in Principle Structural Elements (PSE) of aerospace structures (i.e. aircraft wings, control surfaces and fuselage skins). This structural feature mostly consists of either co-cured or adhesively bonded stringers at regular intervals. The bonded composite joints are also being increasingly used to extend the operational life in aerospace and maritime industries as well as in civil infrastructure [1]. The major advantages of adhesive bonding include higher fatigue resistance, light weight, ability to join thin and dissimilar components, proper sealing, lower manufacturing costs, and good vibration and damping properties [2]. However, the joint area is known as a zone of potential weakness, because of the load transferring phenomena taking place that may induce possible disbonds. Moreover, the adhesive is prone to degradation over time, harsh environment or improper installation, resulting in local disbond or porosity.

These types of damage can significantly jeopardize the performance and safety of a structure with little-advanced warning, and since they cannot be easily detected by visual inspection, Non-Destructive Testing (NDT) methods are being employed for detailed inspection of the structures. Conventional NDT approaches have attained maturity in engineering applications during the last decades, but since they are usually conducted at regular scheduled intervals during the part's lifetime, they cannot provide descriptive information about structural integrity in a real-time manner. Moreover, most of the existing NDT methods require extremely time-consuming point-by-point inspection. Structural Health Monitoring (SHM) has been proposed as an improved and retrofitted version of traditional NDT for continuous inspection of the structural features including composite joints to evaluate health and integrity of the assemblies. SHM systems replace scheduled maintenance with condition-based maintenance, thus saving the cost of unnecessary maintenance as well as improving the level of safety through the consideration of working conditions updates [3]. It has been shown that an effective SHM could reduce the total maintenance cost compared to traditional NDT approaches by more than 30% for an aircraft fleet [4]. Among the different approaches of SHM, ultrasonic guided (Lamb) wave propagation with piezoelectric transducers has been proposed for effective monitoring of composite structures [5] since it is quick, repeatable, sensitive to small-sized damage and cost-effective [3]. Guided wave propagation has been successfully employed in the past for damage detection in repaired composites and bonded joints as well [6-10].

Previous studies demonstrate that two strategies can be employed for inspection of bonded joints using guided waves [9], namely "across-the-bond" and "within-the-bond". The "across-the-bond" method has been mostly employed in previous studies for inspection of metallic assemblies [11, 12]. With this method, the degree of disbond in adhesive joints can be estimated by measuring the attenuation level of the A0 mode [13]. The second approach examined in the literature is the "within-the-bond" method by which the bond-line is used as a waveguide hence the influence of complex geometrical features on wave behaviour is minimized [14]. It has been shown that using this approach, a primary anti-symmetric mode (A0) below a frequency of 200 kHz is a good candidate for effective inspection of hybrid bonded structures [15]. Within-the-bond inspection allows detecting damage by monitoring changes in the phase velocity of the anti-symmetric mode [16], in the wavenumber versus frequency [17] using spatial Fourier transformation or also by monitoring the attenuation level of guided waves [18]. A study including the effect of joint geometry has been presented [9] using a within-the-bond approach in the pitch-and-catch configuration. Measurement of the RMS signal amplitude exhibits a strong sensitivity to the bonding condition, such that attenuation of the A1 and S0 modes appears as a potential candidate for bond inspection within-the-bond [15]. Although several studies have investigated Lamb wave scattering due to a hole and rivet in metallic structures [19, 20], the scattering of guided waves through a composite adhesive bonded joint has not been addressed so far.

In this paper, using the reflection, transmission, and scattering of guided waves, the state of integrity of a composite skin-to-stringer is studied. The main idea is to define the inspection characteristics in terms of mode, frequency and transducer location (reflection, transmission or scattering) for a within-the-bond strategy, for which the excitation is performed along the joint. For this purpose, the whole assembly is manufactured and instrumented in order to include the complex geometry, bondlines' reflection, and joint edge scattering. The guided waves are generated by a co-localized piezoceramic device, and non-contact measurement of the in-plane and out-of-plane velocity is performed using a 3-D Laser Doppler Vibrometer (3D- LDV) over a circular grid of points. Using the circular scanning grid, and by estimating the amplitude ratio of the reflected, transmitted and scattered waves to the incident wave, the behaviour of the guided waves is investigated. By comparing the sensitivity of the scattering with respect to bonding condition, frequency and mode of propagation, SHM design guidelines are extracted justifying the guided wave method's ability for disbond detection.

4.4 Structure description

Composite bonded joints are selected as a simplified representative of hybrid or composite assemblies, co-cured stiffened panels or repairs in the aerospace industry. The structure of interest in this paper is a skin-stringer bonded joint commonly used in aircraft structures. The material used is an out-of-autoclave plain weave prepreg (CYCOM 5320) with the same properties in the warp and weft directions. The layup is $[0/45/90/-45]_s$, where each ply represents a woven layer, and the 0-degree direction is the warp direction. The assembly is composed of three quasi-isotropic panels bonded together using Cytec FM® 300-2M adhesive. The elastic material properties of the material used in this research are given in Table 4.1.

Table 4.1. Material properties from manufacturers of woven CFRP (CYCOM 5320) and adhesive film (Cytec FM-300-2)

Material	**$E_{11} = E_{22}$ (GPa)**	**E_{33} (GPa)**	**$\upsilon_{12} = \upsilon_{13} = \upsilon_{23}$**	**$G_{12} = G_{13} = G_{23}$ (GPa)**	**ρ (kg/m^3)**
CFRP	64.6	14	0.042	4.13	1300
Adhesive	1.0	1.0	0.3	0.38	1420

The skin dimensions are 12″ x 36″ (304 mm x 914 mm) and the two stringers are 3″ x 12″ each (76 mm x304 mm) bonded using the adhesive as depicted in Fig. 4.1. The thickness of each lamina is 0.0834″ (0.212 mm). Since each individual part is made of 8 plies, the thickness of stringers and skin become 0.067″ (1.7 mm) each, and that of the stiffened region of the skin is 0.1343″ (3.409 mm), which includes the thickness of the adhesive, 0.0035″ (0.09 mm). A circular disbond (with 25.4mm diameter) is introduced into the joint using two pieces of Teflon tape, as a reliable way to model a defect of a known initial size. However, the disbond should ideally be an interlaminar crack to model a real case. In a "co-bonding" strategy, the skin is cured, and the stringer is laminated onto the skin (with the help of the adhesive) and then cured; while in a "secondary bonding" strategy, both parts are cured separately and then glued together using an adhesive. In this study, the three components of the assembly are laid up, vacuumed bagged simultaneously and cured in one step using the "co-curing" strategy.

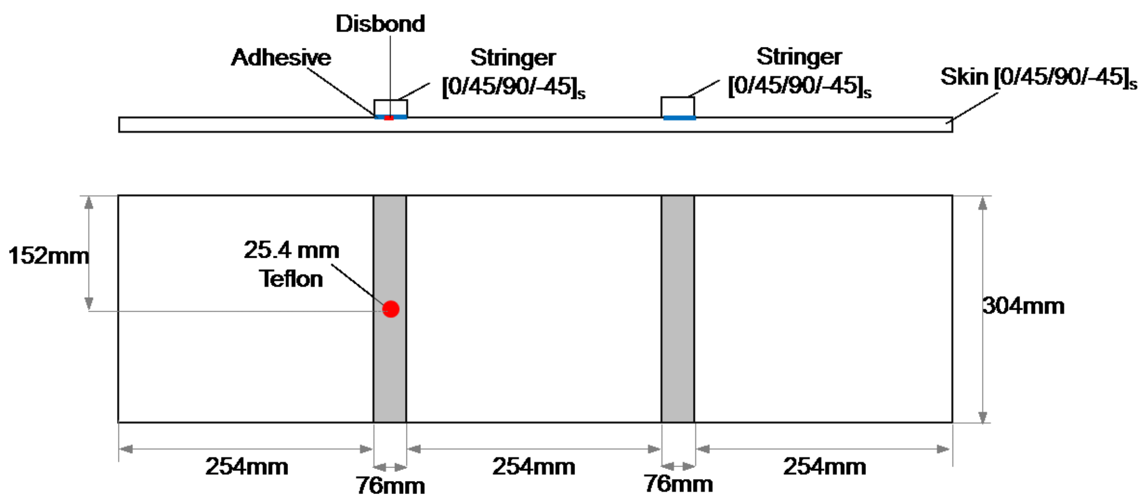

Figure 4.1. Schematic view of the skin-stringer bonded joint configuration; undamaged (right) and damaged joint (left)

4.5 Experimental methodology

Two basic configurations are usually employed in guided wave techniques for damage detection: "pulse-echo" and "pitch-and-catch". In the former, both transmitter and receiver are located on the same side of the targeted zone, and the sensor receives the echoed wave signals from the defect or structural feature; therefore, the sensitivity is mainly governed by the magnitude of the wave back-scattered (reflected) from the damage. In the latter method, waves are emitted from an actuator to travel across the inspection area, while a sensor on the other side of the area captures the wave signal propagated through the inspection area. Hence the sensitivity of the latter configuration is governed by the magnitude of the forward-scattering (transmitted) wave signal across the inspection area. Such configurations cannot locate the defects unless a sparse network of transducers is used to offer multiple forward-scattering and backward-scattering wave signals [3]. In this research, an LDV and a "scattered-based" approach, benefiting the forward and backward scattering waveforms, are used as tools to improve the configuration of actuator-sensor pair-based method for efficient inspection of composite skin-stringer assemblies. Therefore, the diffraction pattern, i.e. wave scattering level at different orientations, including reflection and transmission levels, around the joint can be determined to help understand guided wave interaction with disbond and allows deriving guidelines for SHM system design.

4.5.1 Guided wave generation and sensing

In order to characterize the guided wave behaviour through the pristine and disbond joints, a calibrated and repeatable device capable of generating a specific guided wave mode is required. For this purpose, plane wave generation was chosen in order to allow focusing the energy on the selected area and avoiding geometrical spread induced by finite size transducers. The designed device illustrated in Fig. 4.2 (a) consists of two co-localized rectangular piezoceramics (50 x 5 x 0.45mm) maintained and aligned on both sides of the structure using high strength magnets and coupled to the host structure using dedicated gel. The dimensions are chosen in order to focus the energy within a 10-degree angle for wavenumbers above 250 rad/m following the model presented in [25]. The two actuators can be driven in- and out-of-phase in order to generate symmetric or anti-symmetric modes, respectively. However, due to slight misalignment or tilt, this strategy requires optimization in order to be efficient experimentally. For this purpose, the two piezoceramics are activated simultaneously, and the mode selection is achieved in post-processing by adjusting amplitude and phase of both actuator signals in order to minimize the amplitude of the unwanted mode.

The transfer functions between the piezoceramic voltage and the measured 3-D velocity field using a 3-D LDV (PSV-500, Polytec GmbH) are measured in the frequency domain (see Fig. 4.2 (b)). For this purpose, continuous pseudo-random excitation is used and amplified using a NOVO UAP-8400 voltage amplifier. Measurement of the transfer function is performed using 200 frequency steps between 0 and 500 kHz and averaged 100 times over time frames of 0.4 ms in order to increase the Signal-to-Noise Ratio (SNR). The use of a continuous regime allows working in the bandwidth of interest with a single measurement and benefits from efficient averaging of the phasor in the frequency domain. However, the main drawback is that time-domain information such as wave-packet separation cannot be performed, such that back-wall reflection will be observed. The propagation characteristics are extracted using spatial Fourier transform as described in [21]. The space between two adjacent points is set to 0.5mm, ensuring at least five scanning points per minimal wavelength for frequencies below 500 kHz.

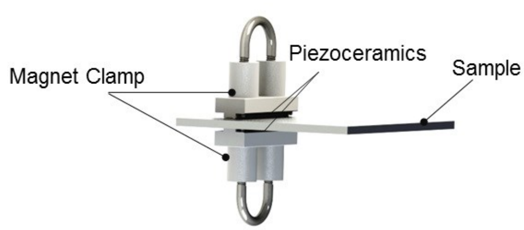

(a)

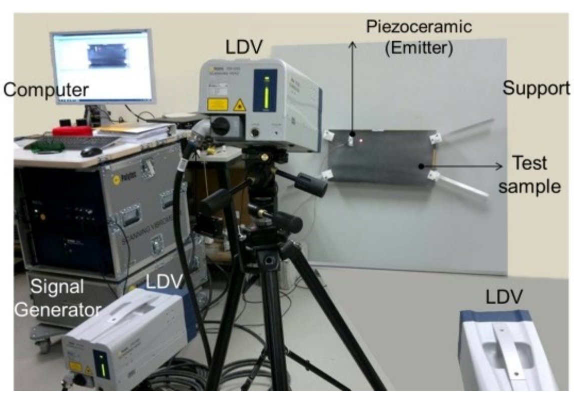

(b)

Figure 4.2. Illustration of the piezoceramic element and excitation clamp (a) and the experimental set up (b)

In order to evaluate the effect of disbond on guided wave behaviour at different orientations, a 360° circular scanning grid, consisting of 24 lines (with 15° variation between two adjacent lines), each including 202 scanning points for a total radius of r=100 mm, is defined in the targeted zone (see Fig. 4.3). The centre of the circle is located right in the centre of the joint or disbond in the undamaged and damaged joint respectively, and the excitation incident angle of 90° within-the-bond is employed (see Fig. 4.3).

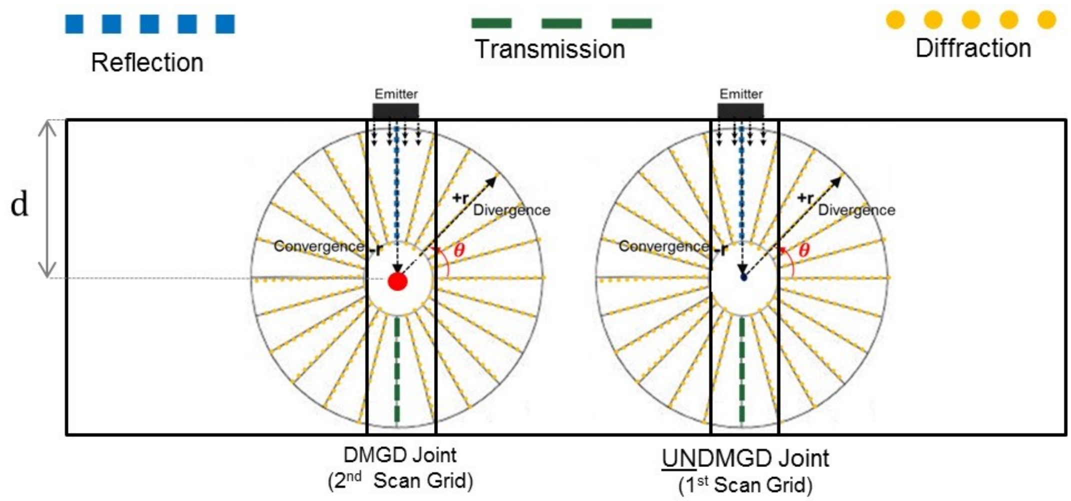

Figure 4.3. Scanning grid of the undamaged joint (first scan grid) and the damaged joint (second scan grid). Reflection (square blue), transmission (rectangular green) and diffraction (circle yellow) scanning points

4.6 Theoretical considerations, results, and discussion

4.6.1 Wavenumber extraction

The propagation of guided waves in thin structures is determined by the knowledge of the complex wavenumber $k\,(\omega,\theta) = k_R + j\,k_I$ associated with each propagating mode at angular frequency ω and angle θ. The real part k_R of the wavenumber k represents the propagation term of the wavenumber and is related to the wavelength λ by the relation: $k_R = 2\pi/\lambda$. The wave attenuation coefficient is defined by the imaginary part k_I of the wavenumber and is classically expressed in Nepers per metre (Np/m). It is responsible for an exponential decrease of the in-plane and out-of-plane displacement field due to material damping. Under the plane wave assumption, the expression of any component of the displacement field $u(r,\omega,\theta)$ in the frequency domain can be derived for a given divergent mode propagating from the centre in the $+r$ direction (scattered waves):

$$u(r,\omega,\theta) = U_s(\omega,\theta)\, e^{-k_I(\omega,\theta).r} \quad e^{jk_R(\omega,\theta).r} \tag{4-1-a}$$

And similarly for a convergent plane wave to the centre in the $-r$ direction (incident wave):

$$u(r,\omega,\theta) = U_i(\omega,\theta)\, e^{+k_I(\omega,\theta).r} \quad e^{-jk_R(\omega,\theta).r} \tag{4-1-b}$$

where $U_s(\omega,\theta)$ and $U_i(\omega,\theta)$ represents the complex amplitudes of the scattered and incidents wave respectively. A plane wave propagation is assumed for ease of interpretation. Indeed, a geometrical spread could be introduced by considering a cylindrical propagation for the diffracted field, but in the case of perfect transmission or reflection, the associated coefficients would differ from 1. Moreover, this would only introduce a $1/\sqrt{kr}$ in Eq. 4-1a that would depend on frequency but would not modify the conclusions of the study. Consequently, a simple plane wave model is considered for both incident and diffracted fields. To extract the amplitude and real part of the wavenumber, the method used is to perform a two-dimensional Fourier transform [21] and measure the amplitude associated with each mode. Fig. 4.4 presents the Wavenumber / Frequency representation along the reflected path defined in Fig. 4.3 for an incident S0 mode (both actuator in-phase) and A0 mode (both actuators out of phase). Theoretical predictions of the dispersion curves in the joint direction are superimposed and a good agreement between predictions and measured propagating modes are observed. In this figure, it appears that the selective mode generation is performed between 50 and 350 kHz for A0 mode and between 175 and 400 kHz for S0 mode. Out of these regions, the single mode excitation is no longer valid, such that the mode sensitivity of the damage cannot be correctly characterized. For instance, at 400 kHz, S0 mode is also excited when only A0 mode is desired and the presence of A1 mode, whose cut-off frequency is about 400 kHz, deteriorates the mode selectivity of the co-localized excitation device. It must also be noted that the S0 mode is more prone to noise since its generated energy is less than A0 mode.

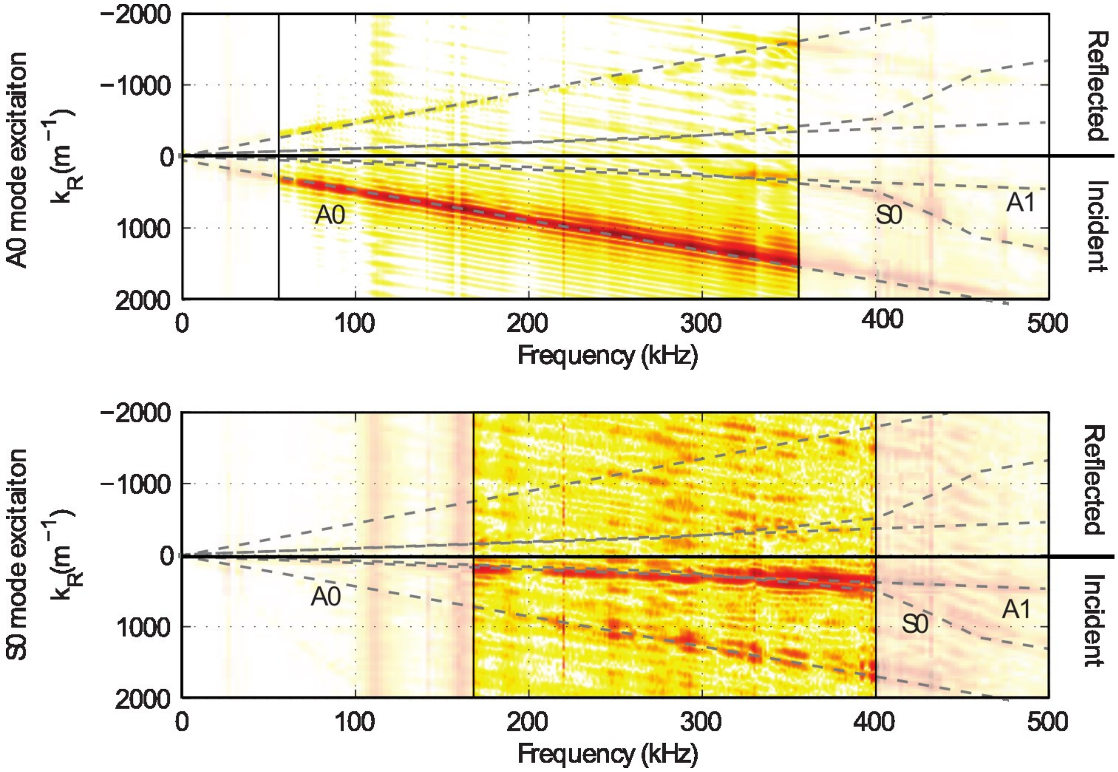

Figure 4.4. Frequency/wavenumber representation of the measured signals in the reflected path (see Fig. 4.3). The positive wavenumber domain corresponds to the incident field while the negative wavenumbers represent the reflected field.

4.6.2 Damping extraction

Damping estimation is less trivial than real wavenumber extraction. In theory, the imaginary part could be estimated via the extent of the peaks in the wavenumber domain. However, this quantity is highly sensitive to noise measurement, radiation condition (plane wave or cylindrical), and multimodal propagation.

In this paper, the use of plane wave excitation is preferred since the attenuation with respect to the propagation distance only depends on the material damping and not on the geometrical spread of the wave, as mentioned in Section 4.5.1. The advantage of plane wave excitation is thus that it allows precise extraction of the imaginary part of the wavenumber while requiring only one measurement per angle(θ). For the case of isotropic structures, this coefficient is independent of angle and only dependent on frequency, while for anisotropic structures, curved panels or non-annealed metallic sheets, the dependency with respect to angle must be considered. In this research, the damping of the bonded zone is evaluated when the guided waves are excited only at θ_{inc}= 90 $^{\circ}$ using an optimization process [22] in order to find the optimal complex wavenumber that approximate the measured out-of-plane velocity field using Eq.(4-1). Extraction of the normalized damping coefficient is then performed by computing the ratio between imaginary and real parts of the wavenumber as a function of angle and frequency:

$$\eta\,(\omega,\theta)=k_I\,(\omega,\theta)/k_R\,(\omega,\theta) \tag{4-2}$$

Fig. 4.5 represents the damping coefficient of first two fundamental modes in the two bonded joints. As mentioned before, it is highly sensitive to noise, mode conversion phenomena, and anisotropy. However, it appears that A0 mode is less affected by the damping than S0 mode, and as mentioned in Section 4.6.1, due to the fact that its energy level is lower than S0 mode. A minimum of the attenuation is observed between 125 kHz to 275 kHz for anti-symmetric mode, allowing defining SHM guidelines based on optimal frequency ranges and mode selection in section 4.6.3.

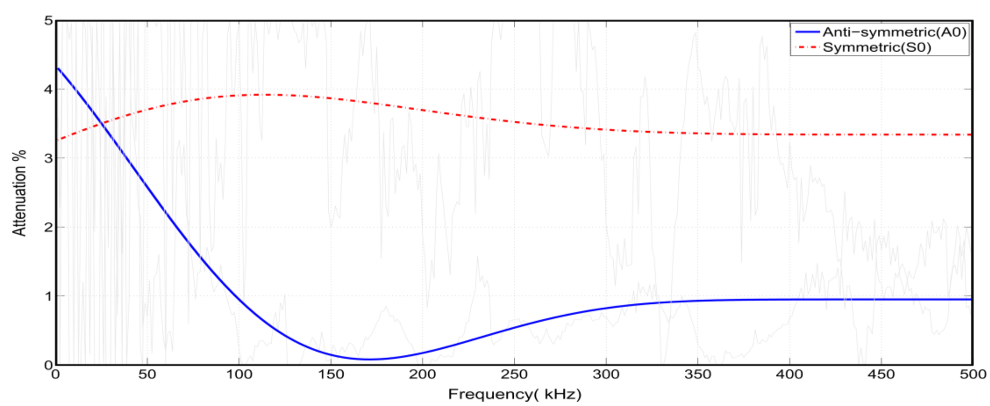

Figure 4.5. Damping coefficient η of the A0 (blue) and S0 (red) modes in the bond line direction for the undamaged joint as a function of mode and frequency. The attenuation curves are obtained after smoothing of the raw estimated parameters

4.6.3 Reflection and transmission

The reflection $R(\omega)$ and transmission $T(\omega)$ coefficients are defined as the following amplitude ratios:

$$R(\omega) = \frac{U_r(\theta_{inc}, \omega)}{U_i(\theta_{inc}, \omega)} \, \mathrm{e}^{-\mathrm{k_I}(\theta_{inc})\mathrm{d}} \tag{4-3}$$

$$T(\omega) = \frac{U_t(-\theta_{inc}, \omega)}{U_i(\theta_{inc}, \omega)} \, \mathrm{e}^{-\mathrm{k_I}(\theta_{inc})\mathrm{d}} \tag{4-4}$$

where θ_{inc} denotes the incidence angle (90° in the present case), $U_r(\omega, \theta)$ and $U_t(\omega, \theta)$ represents the amplitudes of the reflected and transmitted waves respectively. In Eqs. (4-3 and 4-4), the $\mathrm{e}^{-\mathrm{k_I}(\theta_{inc})\mathrm{d}}$ term allows compensating the attenuation of the incident wave along the distance (d) from the emitter to the centre of the measurement grid (See Fig. 4.3).

After performing the post-processing described above on the raw data captured by 3D-LDV, the reflection, and transmission of A0 and S0 modes for both the undamaged (UNDMGD) and damaged (DMGD) joints are obtained and presented in Figs 4.6 and 4.7. Mode conversion is inexistent in the present case and is thus not presented for clarity. Due to low SNR for frequencies below 50 kHz for A0 and 150 kHz for S0, the results are only presented in a limited bandwidth for which the SNR is guaranteed above 10 dB.

In Fig. 4.6, it appears that, even in the undamaged case, a strong reflection can be observed for both A0 and S0 modes. This is due to the bondlines' reflection from the stringer's edges that induces an increase of the reflection coefficient below 200 kHz for A0 mode and an average reflection of 25% for S0 mode. However, since this back-wall reflection is also present in the presence of the damage, the comparison between both bonding scenarios allows deriving guidelines for the proper damage detection in pulse-echo (reflection) mode. In Fig. 4.6, the reflection behaviour of the two modes is different, and one can see that the S0 mode is generally more reflected than A0 mode. Indeed, below 350 kHz, few A0 mode reflection (less than 5%) can be observed independently on the damage presence, such that A0 does not appear as a good candidate considering an inspection task in pulse-echo for frequencies below 350 kHz. Concerning S0 mode, a strong echo (90% reflection) is observed at 230 kHz in the absence of disbond. This corresponds to a wavelength of approximately 25 mm. In the presence of the disbond, this peak is shifted around 200 kHz. However, due to the complex behaviour of the S0 reflection coefficient, it does not appear as a good candidate neither in pulse-echo mode.

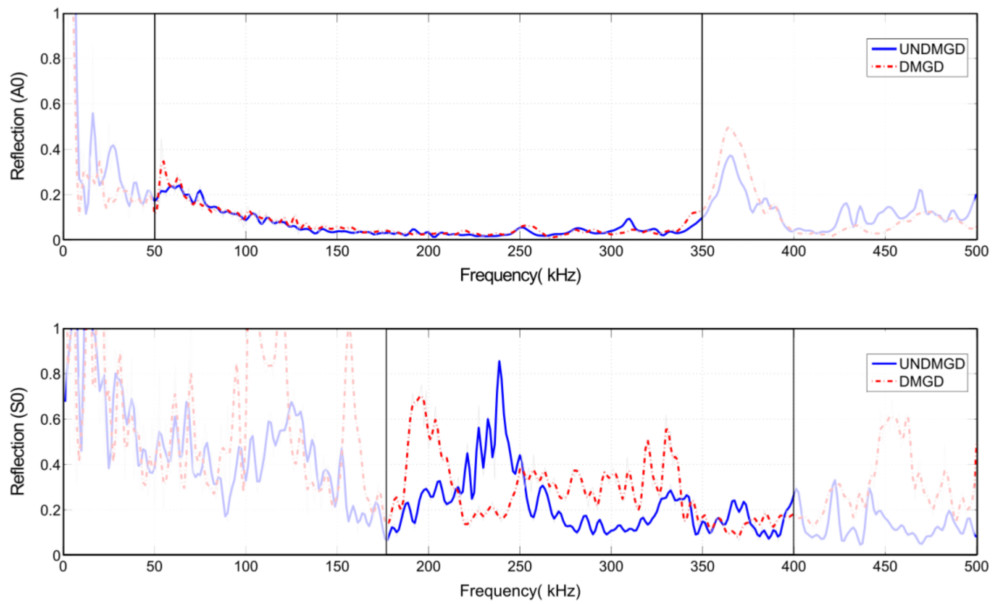

Figure 4.6. Reflection coefficients of A0 (top) and S0 (bottom) mode for both undamaged (solid blue) and damaged (dashed red) lines

From the transmission results (Fig. 4.7) it is noticed that depending on the in-phase or out-of-phase excitation of the guided waves, the level of transmitted of energy through the joint varies. Since the A0 mode is more dependent on the out-of-plane displacement of the particles, its transmission coefficient is generally smaller than S0 mode. This is due to the fact that the resin and viscoelastic property of the adhesive material attenuate the energy of the waves at higher frequencies [10, 23]. Moreover, the behaviour of the guided wave in transmission illustrates that the difference between the undamaged and damaged level is more noticeable when A0 mode is excited in the joint (Fig. 4.7-top), and an increase of

10% of the transmission is observed in the presence of the damage, confirming that the fundamental anti-symmetric mode (A0) is more sensitive to disbond damage than the S0 mode [24]. This can be attributed to the fact that in the presence of the disbond, the guided wave travels through the disbonded part of the joint and is thus not affected by the damping of the adhesive tape.

Therefore, the pitch-catch configuration (transmission approach), where guided waves are excited out-of-phase (A0 mode) can be an appropriate SHM methodology in the frequency range between 50 and 350 kHz. A damage index such as RMS energy of peak amplitude should thus be effective in a pitch-and-catch configuration for which a dense meshing of transducers would be required on the bondline.

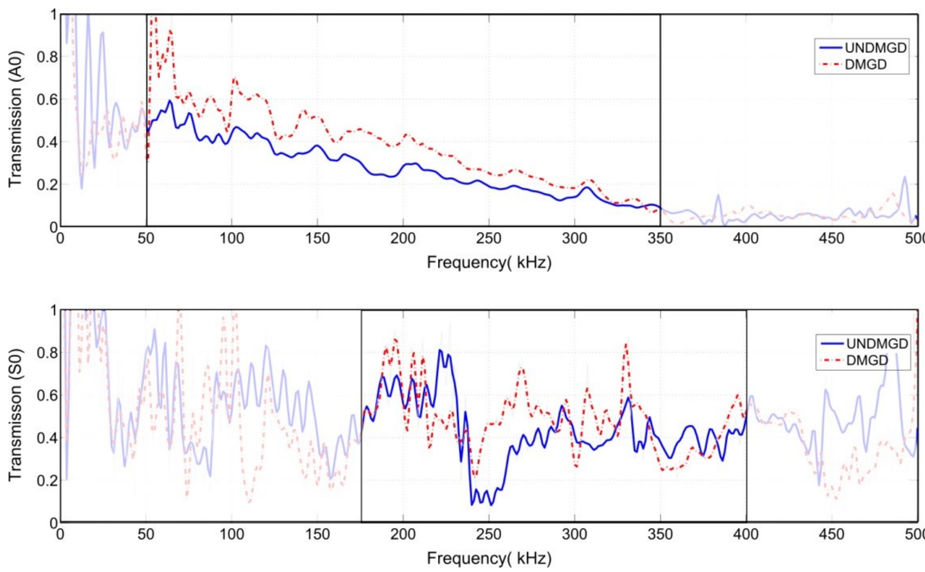

Figure 4.7. Transmission coefficients of A0 (top) and S0 (bottom) mode for both undamaged (solid blue) and damaged (dashed red) lines

4.6.4 Scattering at the disbond

The scattering effect is very useful when considering imaging processes such as Delay-and-Sum or Excitelet, for which the reflection at a potential damage is used for localization. Instead of using a pitch-and-catch approach, this method thus allows for using a sparse array of transducers. However, the frequency and mode must be chosen carefully in order to make sure that the damage sensitivity is ensured.

The normalized scattering or diffraction coefficient $S(\omega)$ is introduced as the following amplitude ratios:

$$S(\theta, \omega) = \frac{U_s(\theta, \omega)}{U_i(\theta_{inc}, \omega)} \sqrt{\frac{k_R(\theta)}{k_R(\theta_{inc})}}\, \mathrm{e}^{-\mathrm{k_I}(\theta_{inc})\mathrm{d}} \tag{4-5}$$

In the definition of the scattering coefficient, the term $\sqrt{\frac{k_R(\theta)}{k_R(\theta_{inc})}}$ is introduced in order to compensate for the anisotropy of the structure. Indeed in the case of isotropic structures, this term equals 1 but allows representing the dependency of the scattering with respect to the wavenumber, assuming that a cylindrical diffraction of the incident wave is observed at the centre of the measurement grid.

The diffraction patterns of two fundamental modes are plotted in Fig. 4.8 at 200 kHz and 300 kHz. The results show that the A0 mode is very directional (less scattered), considering the fact that the excitation is also a plane wave. On the other hand, the S0 mode is more diffracted at low frequencies; however, it also behaves as a directional plane-wave-like at higher frequencies. This observation could be attributed to the fact that the stringer edges (the bond-lines) tend to create a waveguide as the frequency increases (and the wavelength decreases) [14] minimizing the leaking the energy of guided waves in other directions for the A0 mode as well as S0 mode at high frequencies.

In the presence of damage, no significant change of A0 mode scattering is observed, except an increase of transmission, as noted in the previous section (4.6.3). Thus, this mode does not appear as a good candidate for damage imaging based on guided wave reflection and scattering at the damage. However, concerning the S0 mode, a significant change of directivity is observed, and a general increase of 60% of the scattered amplitude is observed for all the directions. Thus, a change in the radiation pattern for S0 mode of the joint is and could be used for damage imaging since disbond causes wave scattering behaviour.

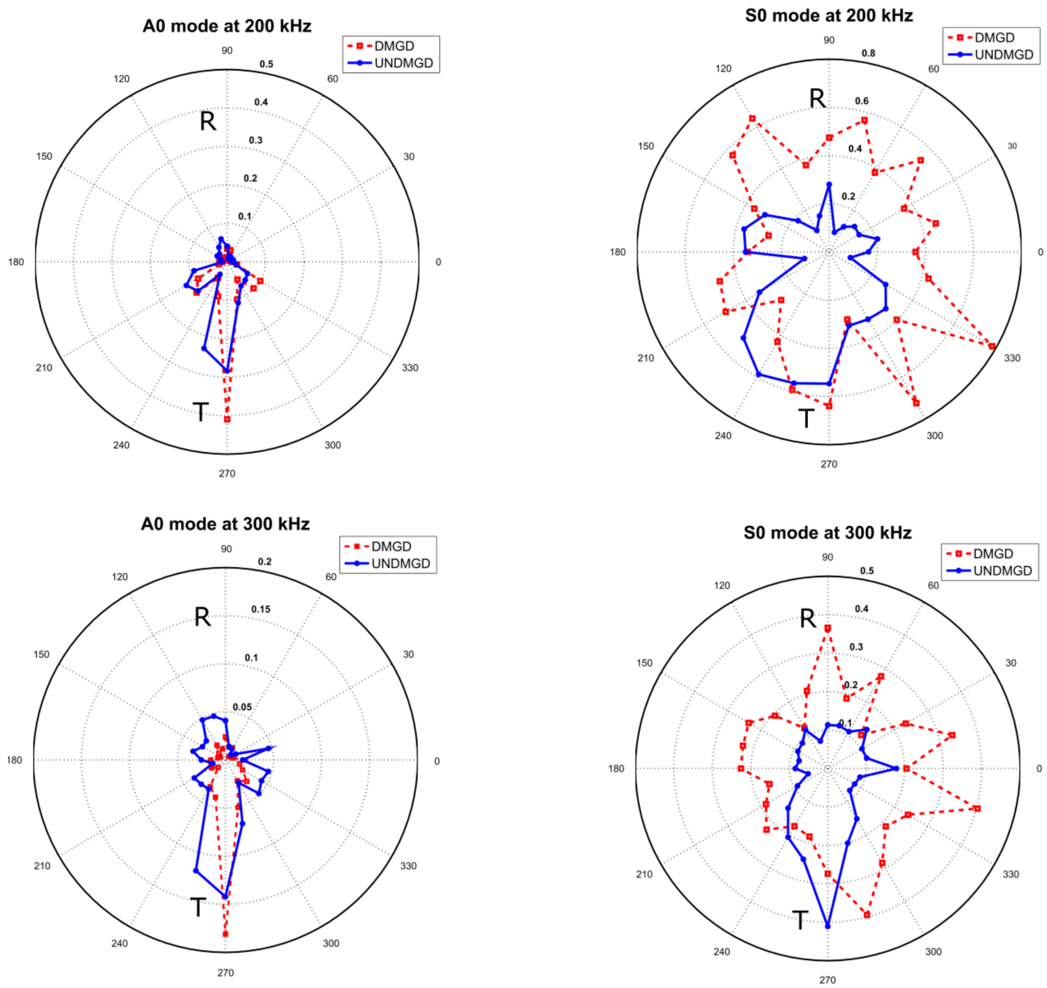

Figure 4.8. The effect of excitation frequency and propagating mode on the scattering behaviour: diffraction pattern of the A0 (left) and S0 modes (right) for the undamaged (solid blue) and the damaged joint (dashed red)

4.7 Conclusion

A strategy of using within-the-bond propagation of guided waves is proposed for inspection of composite joints. The structure is one skin-stringer panel made of quasi-isotropic CFRP plates bonded together with an adhesive film. Two bonded joint conditions have been investigated for the joint: undamaged and damaged (with inserted Teflon tape as a disbond). The guided wave is generated by piezoceramics and LDV is employed to capture the A0 and S0 mode signals. The reflection, transmission and scattering behaviour of the plane guided waves are studied as a function of mode, frequency and the quality of the joint. The excitation frequency and propagation mode both play a crucial role in the reflection, transmission, and scattering behaviour. Based on the experimental observations, guidelines for the design of an efficient SHM system can be derived. In a pitch-and-catch configuration, the A0 mode is highly sensitive to the damage for frequencies below 350 kHz and a decrease of 10% of the transmission is observed. In a pulse-echo configuration, the S0 mode around 200 kHz could be used for monitoring an echo induced by the presence of a disbond. For damage imaging based on the scattering of the wave at the disbond, S0 mode appears as the best candidate below 350 kHz since an increase of 60 % of the scattered field is observed in the presence of a disbond, modifying the radiation pattern of the joint. Thus, the comparison with a baseline measurement should allow detection and localization of the disbond.

4.8 Acknowledgments

This research was supported by the Natural Sciences and Engineering Research Council of Canada (NSERC) through the framework of the Consortium for Research and Innovation in Aerospace in Québec (CRIAQ) DPHM 501 project as well as Bombardier Aerospace and L-3 MAS.

4.9 References

[1] Chiu, W.K., Koh, Y.L., Galea, S.C., Rajic N. Smart structure application in bonded repairs, *Composite Structures* 2000; 50: 433-444.

[2] Samaratunga, D., Jha, R., Gopalakrishnan, S. Wave propagation analysis in adhesively bonded composite joints using the wavelet spectral finite element method, *Composite Structures* 2015; 122: 271-283.

[3] Su, Z., Ye, L. Identification of damage using Lamb waves, From fundamentals to applications. Berlin: Springer-Verlag GmbH & Co., 2009.

[4] Chang, F.-K., Introduction to health monitoring: context, problems, solutions. 1st European Pre-workshop on Structural Health Monitoring, July 9, 2002; Paris, France.

[5] Su Z., Ye L., Lu Y. Guided Lamb waves for identification of damage in composite structures: A review, *Journal of Sound and Vibration* 2006; 295: 753-780.

[6] Diamanti, K., Soutis, C., Hodgkinson, J.M. Non-destructive inspection of sandwich and repaired composite laminated structures, *Composite Science and Technology* 2005; 65:2059-2067.

[7] Diamanti, K., Soutis, C. Structural health monitoring techniques for aircraft composites structures, *Progress in Aerospace Sciences* 2010; 46:342-52.

[8] Pavlopoulou, S., Soutis, C., Manson, G. Non-destructive inspection of adhesively bonded patch repairs using Lamb waves, *Plastics, Rubber and Composites* 2012; 41:61-8.

[9] Matt, H., Bartoli, I., Lanza di Scalea, F. Ultrasonic guided wave monitoring of composite wing skin-to-spar bonded joints in aerospace structures, *Journal of the Acoustical Society of America* 2005; 118: 2240-53.

[10] Sherafat, M. H., Quaegebeur, N., Lessard, L., Hubert, P., Masson, P. Guided wave propagation through composite bonded joints, 7th European Workshop on Structural Health Monitoring; July 2014; Nantes, France.

[11] Lowe, M.J.S., Challis, R.E., Chan, C.W. The transmission of Lamb waves across adhesively bonded lap joints, *Journal of the Acoustical Society of America* 2000; 107: 1333-46.

[12] Lowe, M.J.S., Cawley, P. The applicability of plate wave techniques for the inspection of adhesive and diffusion bonded joints, *Journal of Nondestructive Evaluation*, 1994; 13(4), 185-200.

[13] Lanza di Scalea, F., Rizzo, P. Propagation of ultrasonic guided waves in lap-shear adhesive joints: case of incident A0 Lamb wave, *Journal of the Acoustical Society of America*; 115:146-57.

[14] Seifried, R., Jacobs, L.J., Qu, J. Propagation of guided waves in adhesive bonded components, NDT&E International 2002; 35:317-28.

[15] Quaegebeur, N., Micheau, P., Masson, P. Castaings, M. Methodology for optimal configuration in structural health monitoring of composite bonded joints. Smart Mater Struct 2012; 21:105001-11.

[16] Kundu, T., Maji, A., Ghosh, T., Maslov, K. Detection of kissing disbonds by Lamb waves, *Ultrasonics* 1998; 35:573-80.

[17] Heller, K., Jacobs, L.J., Qu, J. Characterization of adhesive bond properties using Lamb waves, *NDT&E International* 2000; 33:555-563.

[18] Nagy, P.B., Adler, L. Nondestructive evaluation of adhesive joints by guided waves, *Journal of Applied Physics* 1989; 66:4658–63.

[19] Hinders, M.K., Lamb wave scattering from rivets. *Review of Progress in Quantitative Nondestructive Evaluation* 1996; 15: 209-216.

[20] Mckeon, J.C.P, Hinders, M. K. Lamb wave scattering from a through hole, *Journal of Sound and Vibration* 1999; 224(5): 843-862.

[21] Alleyne, N.D., Cawley, P. A 2-Dimensional Fourier transform method for the quantitative measurement of Lamb modes, *Ultrasonics Symposium*1990:1143-1146.

[22] Ostiguy, P.C., Quaegebeur, N., Masson, P. Assessment of the excitelet algorithm for in-situ mechanical characterization of orthotropic structures, SPIE Smart Structures and Materials/NDE, 2012:83480N

[23] Sherafat, M. H., Guitel, R., Quaegebeur, N., Lessard, L., Hubert, P., Masson, P. Characterization of guided waves propagation in a composite skin-stringer assembly. 10th International Workshop on Structural Health Monitoring 2015, Sept 2015; Stanford, CA, USA.

[24] Soutis, C., Ihn, J.B. Design, analysis, and SHM of bonded composite repair and substructure2009, Encyclopaedia of Structural Health Monitoring, Chapter11, 1-17.

[25] Francesco, L.S., Matt, H., Ivan, B. The response of rectangular piezoelectric sensors to Rayleigh and Lamb ultrasonic waves, *Journal of the Acoustical Society of America* 2007; 121, 175-187.

CHAPTER 5. THIRD MANUSCRIPT

5.1 Preface

In the previous chapter, the interaction of guided wave propagation with disbond in the skin-stringer panel was investigated using within-the-bond strategy. The objective of this chapter is to incorporate an across-the-bond strategy to scrutinize the effects of excitation angle, frequency, and mode selection and disbond on the diffraction pattern of the guided wave propagation.

Guided Wave Scattering Behaviour in Composite Bonded Assemblies*

* Composite Structures 2016; 136: 696-705

Mohammad H. Sherafat, Larry Lessard, Pascal Hubert

Department of Mechanical Engineering, McGill University, Macdonald Engineering Building, 817 Sherbrooke West, Montreal, QC, Canada, H3A 0C3

Robin Guitel, Nicolas Quaegebeur, Patrice Masson

GAUS, Department of Mechanical Engineering, Université de Sherbrooke, Sherbrooke, QC, Canada, J1K 2R1

5.2 Abstract

Composite bonded joints are prone to disbond when submitted to fatigue or extreme loads. The objective of this paper is to evaluate the integrity of a composite skin-stringer joint using the scattering behaviour of the Lamb waves. The structure of interest is composed of three carbon fibre reinforced polymer (CFRP) plates bonded together by adhesive film as a typical representative of skin-stringer assembly. Two different bonding conditions are investigated for the joint: undamaged and damaged (with disbond). A circular disbond is introduced into the joint using Teflon tape during manufacturing. Two co-localized rectangular piezoceramics are used to generate plane guided waves at 180° and 135° incidence. A non-contact measurement is performed using a 3-D Laser Doppler Vibrometer (LDV) to extract the required information for evaluation of bonding condition. The results present the different scattered field of the guided waves at the joint as a function of frequency, mode, excitation angle and presence of artificial damage. It was found that the amplitude and directivity patterns of scattered fields are affected by the presence of damage, such that SHM design guidelines can be derived for efficient damage detection in the composite skin-stringer bonded joints.

Keywords: Guided wave propagation, Adhesive bonded joint, Disbond, Non-Destructive Testing (NDT), Structural Health Monitoring (SHM)

5.3 Introduction

Stiffened-skin composite structures have been intensively used in aerospace structures as a noteworthy design choice for aircraft control surfaces like flaps, aileron and even rudder and elevator skins. These structures mostly consist of either co-cured or adhesively bonded stringers at regular intervals. Composite bonded joints are also found in patch repairs to restore structural integrity. Experimental studies indicate that an adhesively bonded joint can restore the strength of the repaired structure up to 80% of the original undamaged laminate strength [1]. The joint area is known as a zone of potential weakness, because of the load transferring phenomena taking place and causing possible disbond. Moreover, joints are prone to degradation of the adhesive over time, harsh environment or improper installation resulting in local disbond or porosity. These types of damage can significantly jeopardize the performance and safety of a structure with little advanced warning, and since they cannot be easily detected by visual inspection, Non-Destructive Testing (NDT) methods are being employed for detailed inspection of the structures.

Over the last 50 years, NDT techniques have attained maturity in engineering applications, playing a crucial role in the assessment of the integrity and durability of composite structures. Conventional NDT approaches are usually conducted at regular scheduled intervals during the lifetime and cannot provide descriptive information about structural integrity. Moreover, almost all of the existing NDT methods require extremely time-consuming point by point inspection. Structural Health Monitoring (SHM) as an improved and retrofitted version of traditional NDT has been proposed for continuous inspection of the structural features including composite joint to evaluate health and integrity of the joints in a real-time manner. SHM systems aim at replacing scheduled maintenance with as-needed (condition-based) maintenance, thus saving the cost of unnecessary maintenance as well as improving the level of safety through the consideration of working conditions updates [2]. It has been shown that an effective SHM could reduce the total maintenance cost compared to traditional NDI approaches by more than 30% for an aircraft fleet [3]. Among the different approaches of SHM, ultrasonic guided (Lamb) wave propagation with piezoelectric transducers has been proposed for effective monitoring of composite structures [4] since it is quick, repeatable, sensitive to small-sized damages and cost-effective [2]. Guided waves can propagate in symmetrical or anti-symmetrical modes with respect to the neutral axis of the plate. Symmetric modes have a more radial in-plane displacement of particles, whereas anti-symmetric modes mostly have out-of-plane displacement. Therefore, a symmetric mode often indicates thickness bulging and contracting while an anti-symmetric mode presents constant-thickness bending. Guided wave propagation has been successfully employed in the past for damage detection in repaired composites and bonded joints as well [5-9].

Previous studies demonstrate that two strategies can be employed for inspection of bonded joints using guided waves [8], namely “within-the-bond” and “across-the-bond”. The first approach examined in the literature is the “within-the-bond” method by which bond-lines is used as a waveguide hence the influence of complex geometrical features on wave behaviour is minimized [10]. It has been shown that using this approach, a primary anti-symmetric mode (A0) below 200 kHz frequency range is a good candidate for effective inspection of hybrid bonded structures [11]. The “across-the-bond” method is the second strategy which has been mostly employed in previous studies for inspection of metallic assemblies [12, 13]. With this method, the degree of disbond in adhesive joints can be estimated by measuring the attenuation level of the A0 mode [14]. Although there are several studies, which investigated the Lamb wave scattering from the hole and rivet in metallic structures [15, 16] the scattering of guided waves through the composite adhesive bonded joint has not been addressed in detail yet.

In this paper, the integrity state of a composite skin to stringer is studied by characterizing the scattered guided waves field through a bonded joint. The guided waves are generated by a co-localized piezoceramic device, and non-contact measurement of the in-plane and out-of plane velocity is performed using a 3-D Laser Doppler Vibrometer (3D- LDV) over a circular grid of points. For a given frequency and mode, by comparing the sensitivity of the scattering field with respect to bonding condition, SHM design guidelines are extracted justifying the guided wave method’s ability for disbond detection.

5.4 Structure description

Composite bonded joints are usually selected as a typical candidate of hybrid or composite assemblies, co-cured stiffened panels or repairs in the aerospace industry. The structure of interest is selected based on a project between industrial and academic researchers, namely (CRIAQ) DPHM 501, where structural features and design parameters have been identified, extracted and filtered for their relevance from an extensive list of aerospace structures of interest [17]. Based on the reduced list, the structure presented in this paper is chosen as a classic representative composite assembly commonly used in aircraft structures. It is composed of three quasi-isotropic $[0/45/90/-45]_s$ panels made of out-of-autoclave woven prepreg (CYCOM 5320). The elastic material properties of the material used in the paper are given in Table 5.1.

Table 5.1. Material properties from manufacturers of woven CFRP (CYCOM 5320) and adhesive film (Cytec FM-300-2)

Material	$E_{11} = E_{22}$ (GPa)	E_{33} (GPa)	$\upsilon_{12} = \upsilon_{13} = \upsilon_{23}$	$G_{12} = G_{13} = G_{23}$ (GPa)	ρ (kg/m^3)
CFRP	64.6	14	0.042	4.13	1300
Adhesive	1.0	1.0	0.3	0.38	1420

However, the disbond should ideally be an interlaminar crack to model a real case, a circular (diameter of 25.4mm) disbond is introduced into the joint using Teflon tape. Two pieces of inserted Teflon tape can simulate the disbond between the skin and the stringer, and is a reliable way to model a defect of a known initial size. The skin dimension is 304 mm x 914 mm and the two stringers are 76 mm x 304 mm each bonded using Cytec FM® 300-2M as depicted in Fig. 5.1. The thickness of each lamina is 0.212 mm. Since each individual part is made of 8 plies, the thickness of stringers and skin worked out to 1.7 mm each and that of the stiffened region of the skin to 3.40 mm including the thickness of adhesive 0.09 mm. In a “co-bonding” strategy, the skin is cured, and the stringer is laminated onto the skin (with the help of the adhesive) and then cured; while in a “secondary bonding” strategy, both parts are cured separately and then glued together using an adhesive. In this study, the three components of the assembly are laid up, vacuumed bagged simultaneously and cured in one step using the “co-curing” strategy.

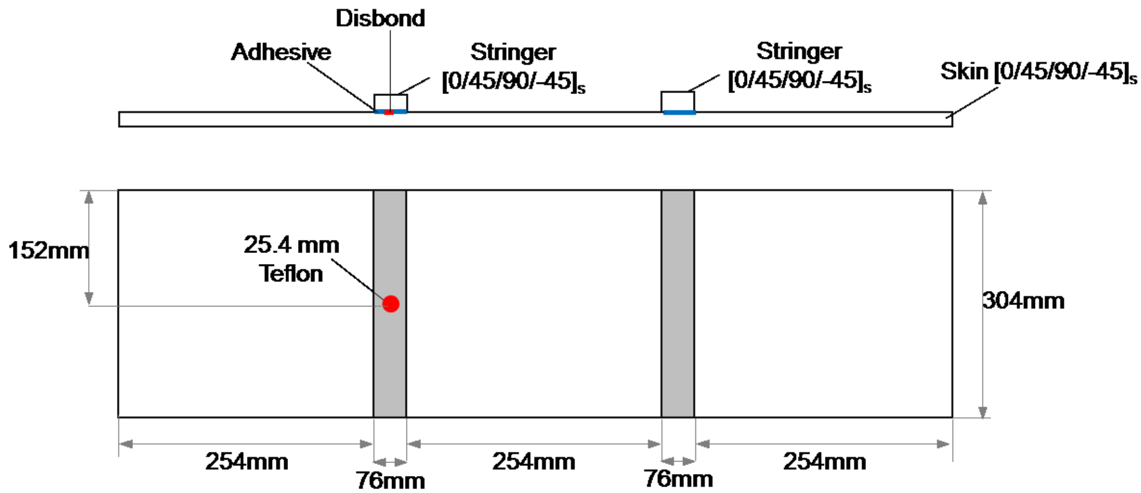

Figure 5.1. Schematic view of the skin-stringer bonded joint configuration; undamaged (right) and damaged joint (left)

5.5 Experimental methodology

Two basic configurations are usually employed in guided wave techniques for damage detection: “pulse-echo” and “pitch-and-catch”. In the former, both transmitter and receiver are located on the same side of the targeted zone, and the sensor receives the echoed wave signals from the defect or structural feature; therefore, the sensitivity is mainly governed by the magnitude of the wave back-scattered from the damage. In the latter method, waves are emitted from an actuator to travel across the inspection area, while a sensor on the other side of the area captures the wave signal propagated through the inspection area. Hence the sensitivity of the latter configuration is governed by the magnitude of the forward-scattering wave signal across the inspection area. Such configurations cannot locate the defects unless a sparse network of transducers is used to offer multiple forward-scattering and backward-scattering wave signals [3]. In this research, an LDV and a “scattered-based” approach, benefiting the forward and backward scattering waveforms, are used as tools to improve the configuration of actuator-sensor pair-based method for efficient inspection of composite skin-stringer assemblies. Therefore, the diffraction pattern, i.e. wave scattering level at different orientations around the joint can be determined to help understand guided wave interaction with disbond and allows deriving guidelines for SHM system design.

5.5.1 Guided wave generation and sensing

In order to characterize the scattering of the guided waves through the pristine and disbond cases, a calibrated and repeatable device capable of generating a specific guided wave mode is required. For this purpose, plane wave generation was chosen in order to allow focusing the energy on the selected area and avoiding geometrical spread induced by finite size transducers. The designed device illustrated in Fig. 5.2 consists of two co-localized rectangular piezoceramics (50 x 5 x 0.45mm) maintained on both sides of the structure using high strength magnets. The two actuators can be driven in- and out-of phase in order to generate symmetric or anti-symmetric modes respectively. However, due to slight misalignment or tilt, this strategy requires optimization in order to be efficient experimentally. For this purpose, the mode selection is achieved in post-processing by adjusting amplitude and phase of both actuator signals in order to minimize the amplitude of the unwanted mode.

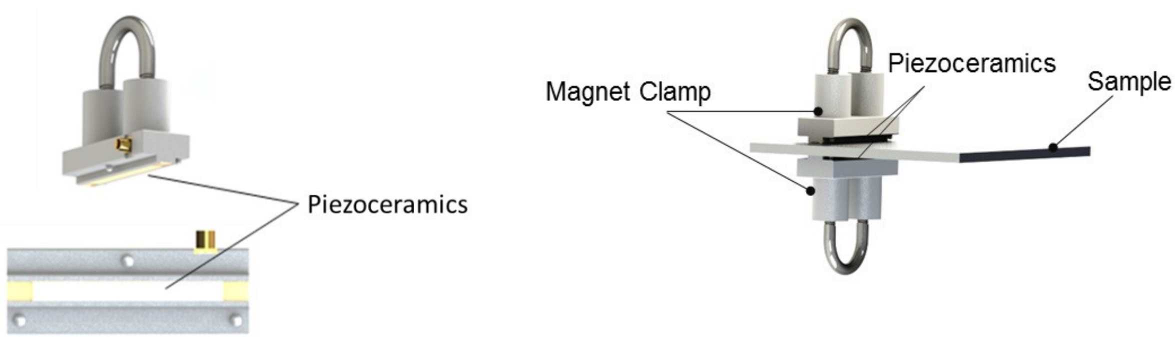

(a) (b)

Figure 5.2. Illustration of the piezoceramics element (a) and excitation clamp (b).

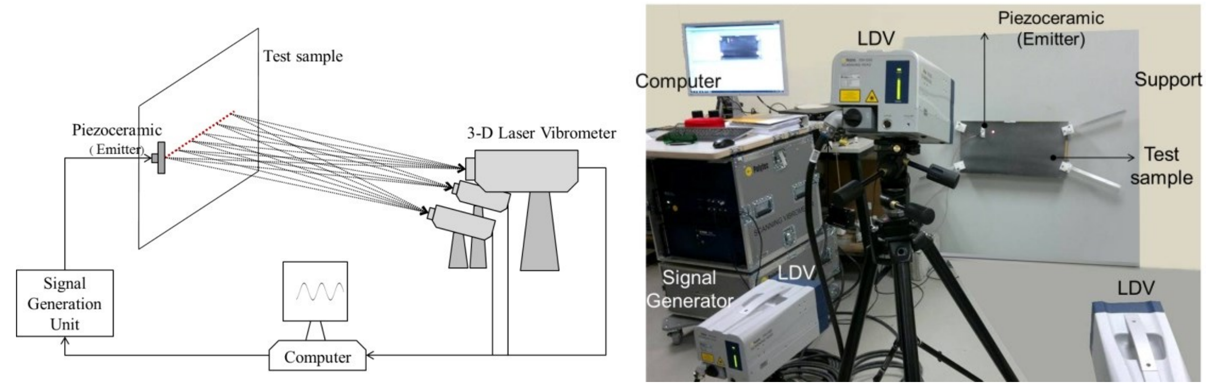

(a) (b)

Figure 5.3. Schematic (a) and actual (b) illustration of the experimental setup

Pseudo-random excitation signals are used below 500 kHz and amplified using a NOVO UAP-8400 voltage amplifier. Non-contact measurement of the in-plane and out-of-plane velocity is performed using a 3-D LDV (PSV - 400, Polytec GmbH), as presented in Fig. 5.3. The transfer functions between the input voltage and the measured 3-D velocity field are measured using 100 averages for increasing the Signal to Noise Ratio (SNR). The propagation characteristics are extracted using spatial Fourier transform as described in [18]. The space between two adjacent points is set at about 0.5mm, ensuring at least 5 points per minimal wavelength for frequencies below 500 kHz.

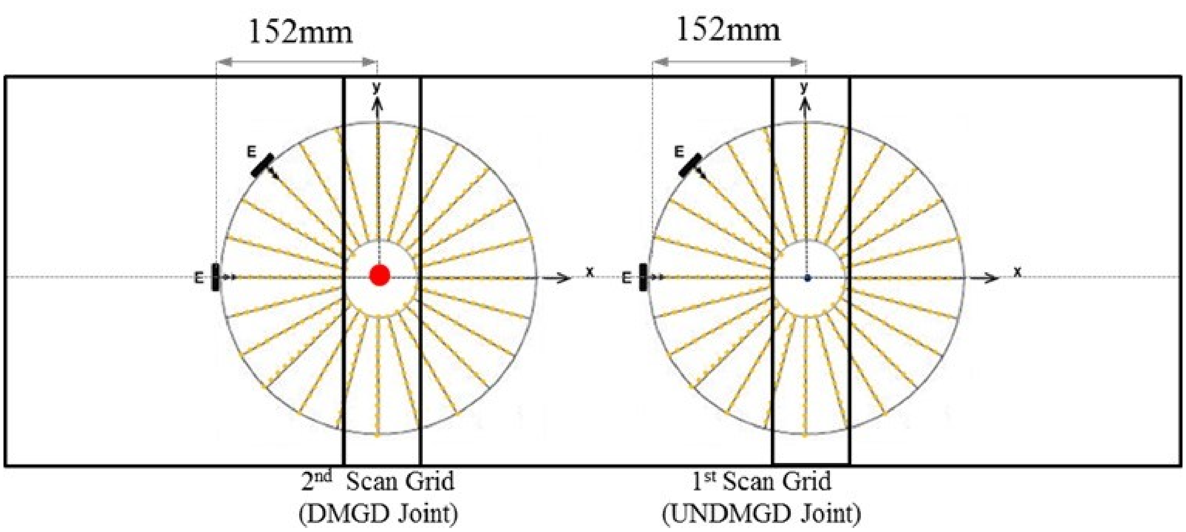

Figure 5.4. Scanning grid of the undamaged joint (first scan grid) and the damaged joint (second scan grid)

In order to evaluate the effect of disbond on guided wave behaviour in different orientations, a 360-degree circular scanning grid, consisting of 48 lines (with 7.5° variation between two adjacent lines), each including 202 scanning points is defined in the targeted zone (see Fig. 5.4). The centre of the circle is located right in the centre of the joint or disbond in the undamaged and damaged joint respectively. Two excitation incident angles of 180° (see Fig. 5.5) and 135° (see Fig. 5.6) are employed to investigate the effect of excitation orientation as well. For both damage and undamaged cases, the displacement field decomposition in the frequency domain of any quantity:

$$\begin{aligned} u(r,\theta_{inc},\theta_{diff},\omega) &= u_{inc}(r,\theta_{inc},\omega) + u_{diff}(r,\theta_{inc},\theta_{diff},\omega) \\ &= U_{inc}(\theta_{inc},\omega)e^{-jk(\theta_{inc},\omega)\,r} + U_{diff}(\theta_{inc},\theta_{diff},\omega)e^{-jk(\theta_{diff},\omega)\,r} \end{aligned} \tag{5-1}$$

Where k, ω are the wavenumber of the propagating wave and angular frequency respectively. θ_{inc} is the angle of the incident wave, θ_{diff} the angle of the diffracted waveform. To extract the wavenumber, the method used is to perform a two-dimensional Fourier transform [18] in order to obtain the complex amplitude $U_{diff}$and U_{inc} of the diffracted and incident fields as a function of wavenumber and frequency. Estimation of the attenuation coefficient k_i cannot be obtained by the same method due to its imprecision, but an optimization process is used instead as proposed in [19]. The scattering (diffraction) level is defined as the following amplitude ratios:

$$Scattering\ \text{Coefficient}(\theta_{inc},\theta_{diff},\omega) = U_{diff}(\theta_{diff},\omega)/U_{inc}(\theta_{inc},\omega) \tag{5.2}$$

After performing the signal processing described above on the raw data captured by 3D-LDV, the diffraction pattern of symmetric and anti-symmetric modes for both the undamaged (UNDMGD) and damaged (DMGD) joints are obtained.

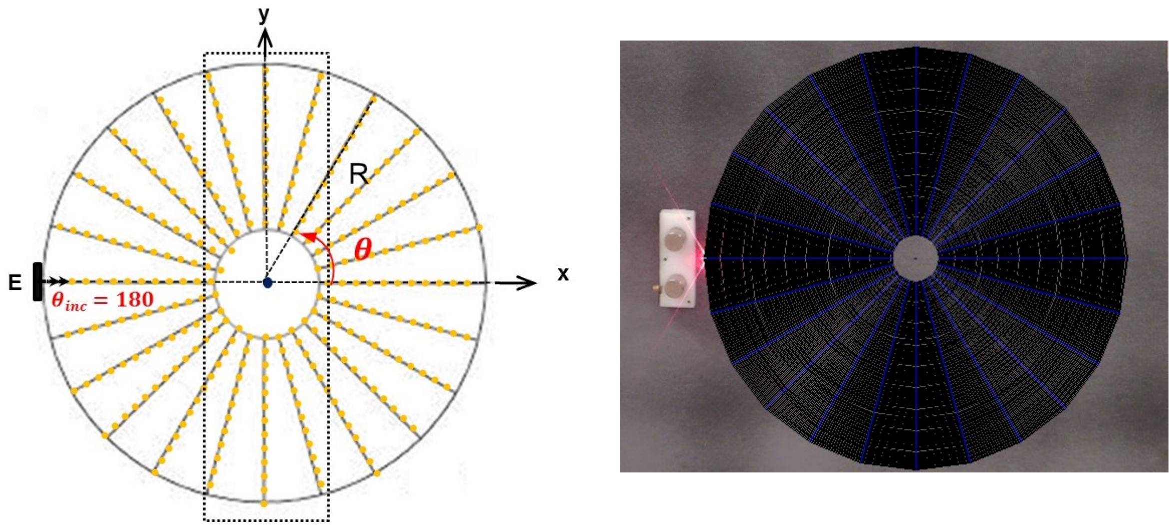

(a) (b)

Figure 5.5. Schematic view (a) and actual representation (b) of the scanning grid details for 180° excitation incident angle

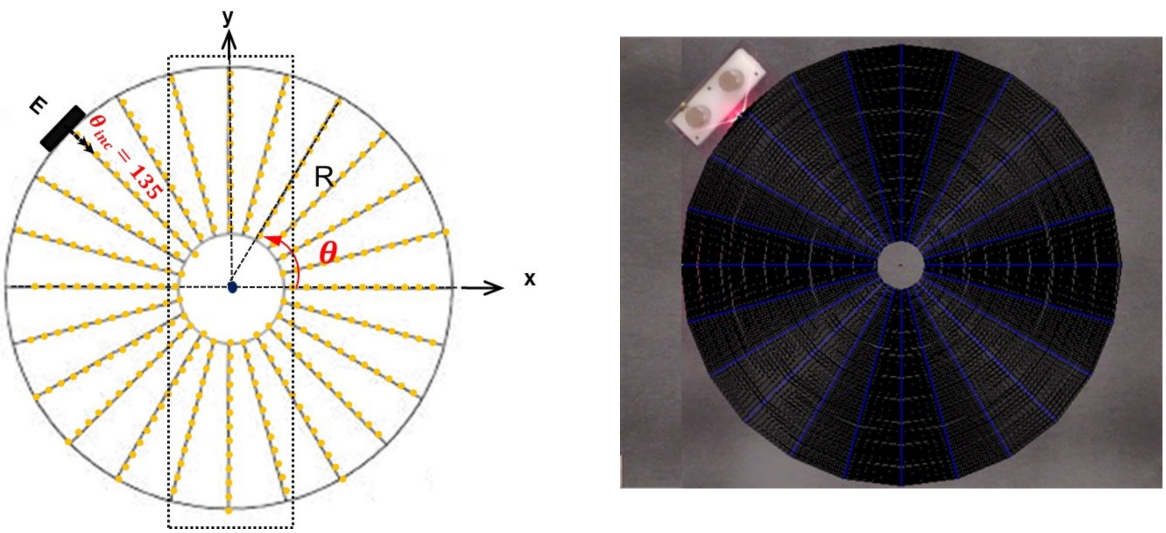

(a) (b)

Figure 5.6. Schematic view (a) and actual representation (b) of the scanning grid details for 135° excitation incident angle

5.6 Result and discussion

5.6.1 Influence of the mode and frequency of guided wave on scattering

The selection of the appropriate Lamb wave mode and frequency to detect damages efficiently is a challenging task due to its dispersive nature. This is further complicated due to the propagation into the anisotropic material and complex structural features. To find out which Lamb wave mode is the best candidate for effective monitoring of the composite bonded joint, the angular scattering coefficients of the first two fundamental modes, anti-symmetric (A0) and symmetric (S0) are plotted in Fig. 5.7 for two bonding conditions at five different frequencies (i.e. 100 kHz, 200 kHz, 300 kHz, 400 kHz, 500 kHz). However, in the case of the S0 mode, the 100 kHz pattern is not shown due to low SNR in the measurements for frequencies below 150 kHz.

Regarding the propagating mode, the results illustrate that the A0 mode is more directional (less scattered) rather than the S0 mode. In other words, the S0 is more diffracted in all the directions around the joint specifically at low frequencies; however, at higher frequencies, the S0 mode tends to become directional as well. Comparing the scattering coefficients of the two modes also indicates that the scattering level of the A0 mode is slightly smaller than the S0 mode for a full range of frequencies. This may be due to the fact that the A0 mode is more attenuated upon encountering the adhesive, as observed in previous studies [9]. For the effect of the excitation frequency, Fig. 5.7 also illustrates that the effect of attenuation due to damping of the adhesive and epoxy increases with respect to the frequency, such that the level of scattering coefficient of both modes decreases at higher frequencies.

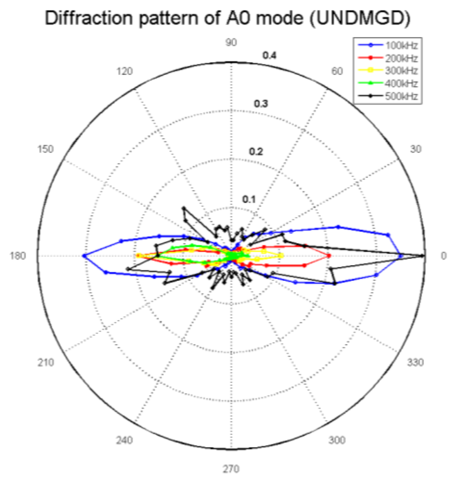

a

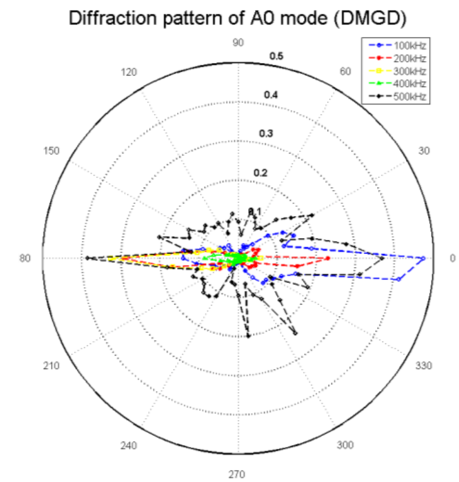

c

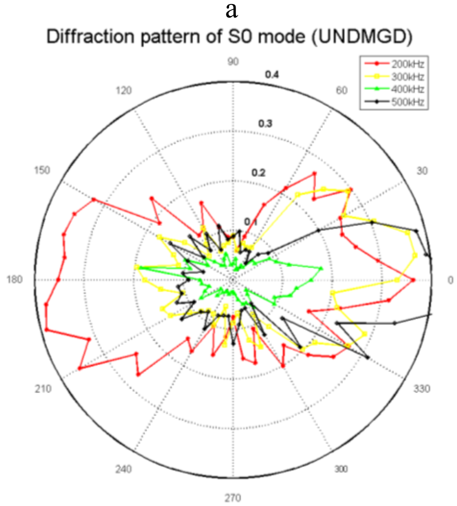

b

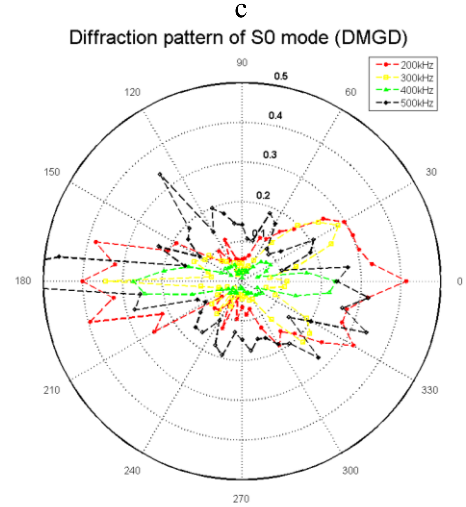

d

Figure 5.7. The effect of excitation frequency on the scattering behaviour: Diffraction pattern of the A0 (top) and S0 modes (bottom) for the undamaged (left) and the damaged joint (right) for an incident wave oriented at 180°

5.6.2 The effect of the excitation orientation of guided waves on scattering

The comparison of the diffraction patterns of the S0 mode at 180° and 135° incident angles at different frequencies is plotted in Fig. 8. The frequency of 150 kHz is a representative of the low frequency range while 300 kHz and 500 kHz represent the range of mid and high frequency ranges respectively. From the results, one can see that at almost all the frequencies, when waves are excited at 135° , the joint absorbs the energy of the wave much more than at 180° excitation. As mentioned in Section 5.6.1, the S0 mode behaviour at higher frequencies (above 300 kHz) tends to become more directional and less scattered, therefore the plane wave is rotated by 45°, when guided waves are excited at 135° rather than 180° (Fig. 5.8(c), Fig. 5.8(f)).

The diffraction patterns when the A0 mode is excited at different angles are plotted in Fig. 5.9. The presented results indicate that A0 mode scattering behaviour is less affected by the orientation of excitation. Even though the energy dissipation through the joint at 135° (in comparison with 180 °) is still observed, the major influence of the excitation angle is the 45° rotation of the transmission and specular reflection. In this case also at high frequencies (above 400 kHz), the A0 mode tends to become more scattered and less directional (Fig. 5.9(c), Fig. 5.9(f)).

Overall, the excitation at 135° exhibits less energy and less amplitude in comparison with 180°. Although the adhesive is an isotropic layer and stacking sequence is $[0/90/-45/45]_{2s}$, when the guided waves are excited at 135°, the absorption by the joint is larger than at 180° excitation for both modes at the low frequency range. Hence, despite the fact that the in-plane isotropy (regarding the mechanical properties) is obtained by quasi-isotropic lay-up, the excitation orientation of guided waves impacted the level of scattering coefficients through the joint.

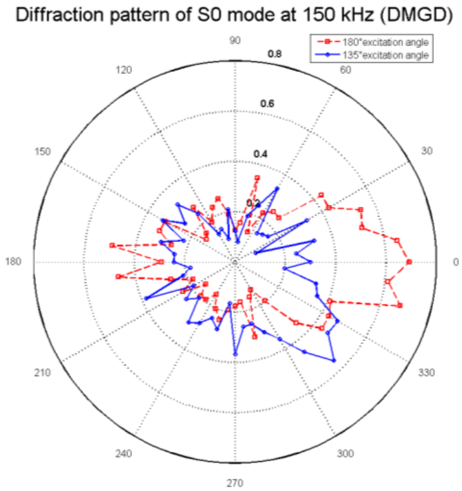

a

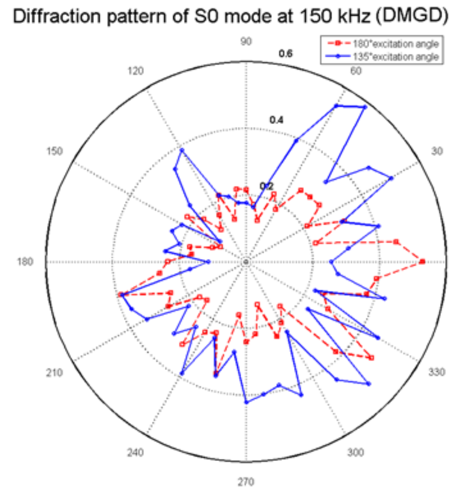

d

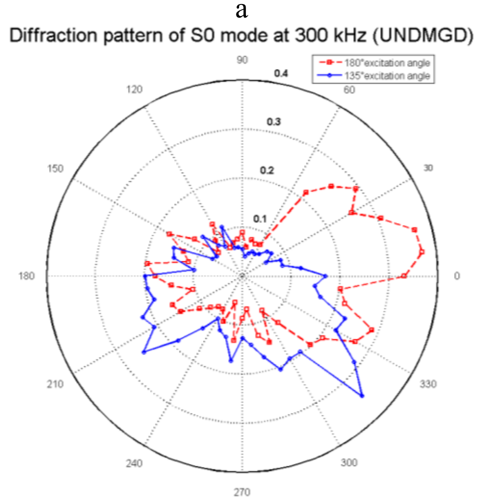

b

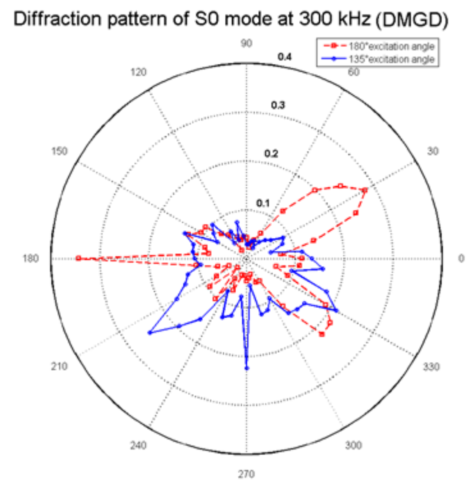

e

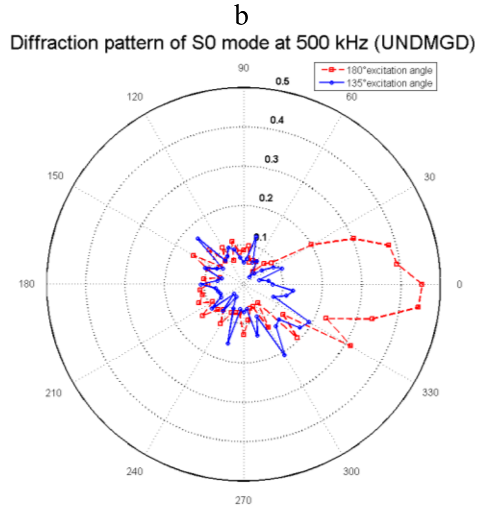

c

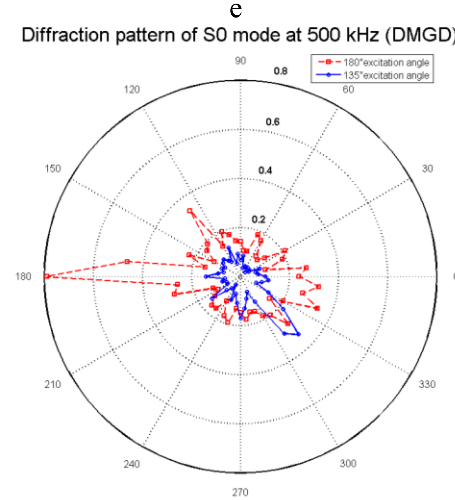

f

Figure 5.8. Diffraction pattern of the S0 mode at 150 kHz (top) 300 kHz (middle) and 500 kHz (bottom) for 180° and 135 ° excitation incident angles for the undamaged (left) and damaged joint (right)

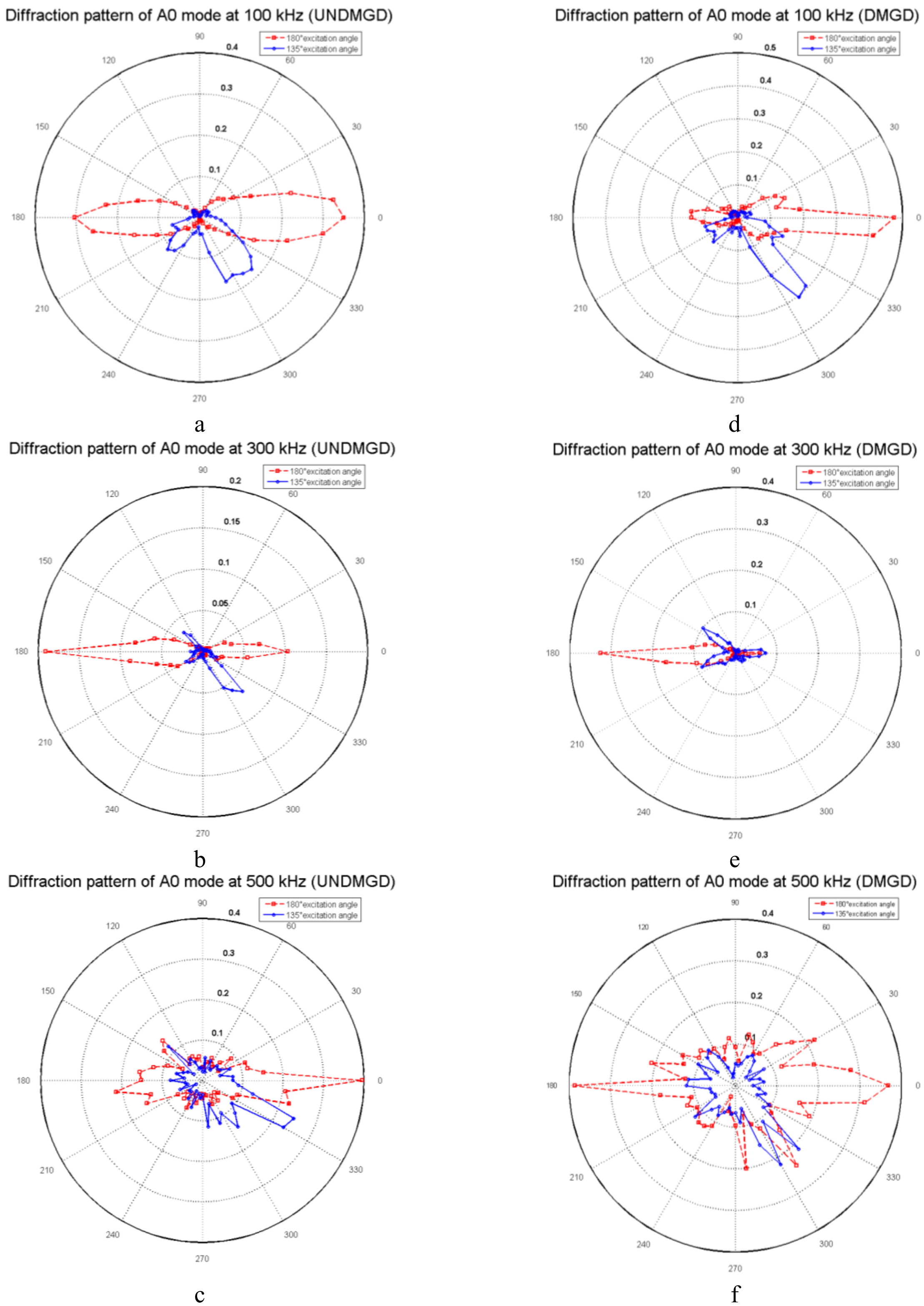

Figure 5.9. Diffraction pattern of the A0 mode at 100 kHz (top) 300 kHz (middle) and 500 kHz (bottom) for 180° and 135 ° excitation incident angles for the undamaged (left) and damaged joint (right)

5.6.3 The effect of disbond on scattering

As explained in section 5.4, the two joints are manufactured with identical materials and configuration, except for the presence of the Teflon tape in the damaged case. However, as previously mentioned, it is known that Teflon is not a perfect representative of the interlaminar crack or delamination. The literature [4] widely uses Teflon as an artificial disbond. Therefore, the effect of disbond on the wave scattering can be distinctively investigated. Fig. 5.10 represents the difference between the undamaged and damaged scattering coefficients with respect to the angle of the measurement for a 180° incident angle.

$$Difference = |\, Scattering\ (UNDMGD) - Scattering\ (DMGD)\, | \tag{5-3}$$

The best candidates of the frequency, mode and angle of measurement can be selected for effective disbond detection using diffraction patterns. Note that for the A0 and S0 modes, at a frequency of 100 kHz and 150 kHz respectively, the average difference between the baseline and damaged scattering coefficients is larger than for other frequencies. This low frequency range also guarantees the acceptable level of wave energy as explained in Section 5.6.1. In contrast, the higher frequencies ensure smaller wavelength, such that maximum sensitivity to the damage size can be achieved. Hence, a compromise between low frequency (higher level of wave energy) and higher frequencies (shorter wavelength, detecting smaller damages) needs to be taken out depending on the critical damage size.

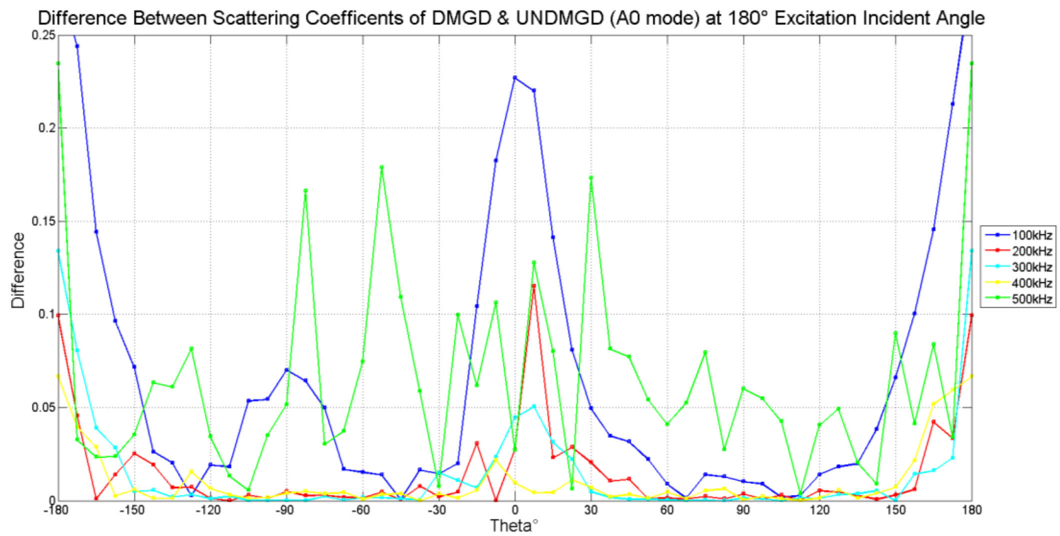

(a)

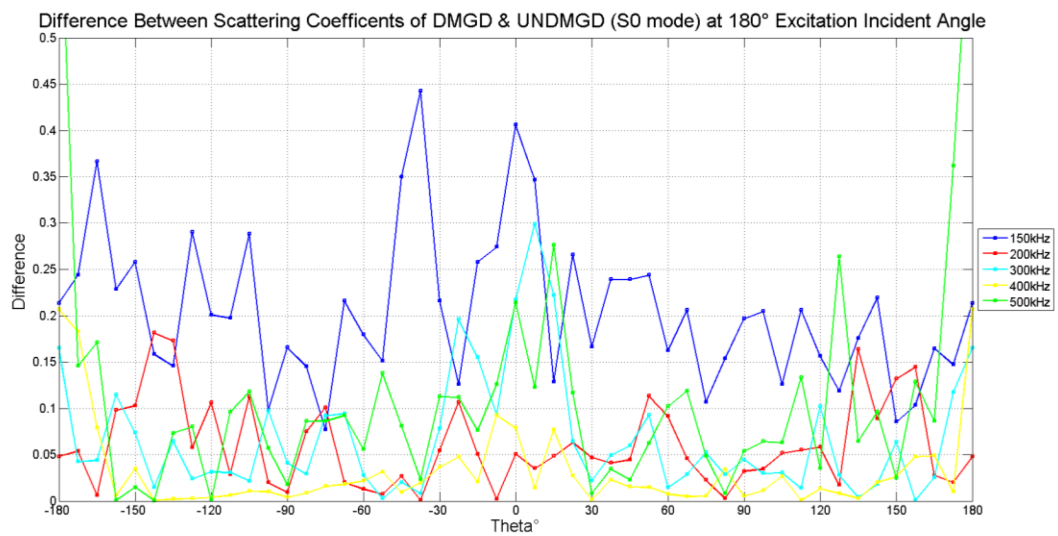

(b)

Figure 5.10. The sensitivity of the scattering field to the disbond: the difference between the undamaged and damaged scattering coefficients at every 50 kHz for 180° excitation angle

Since the A0 mode is more directional, the difference between the undamaged and damaged scattering coefficients, around 0° is more visible while for the S0 mode this difference can be noticed for almost all the orientations. Another advantage of using the A0 mode is that small wavelength comparable to the disbond size can be generated [11]. In the presence of damage, a 20% change of A0 mode scattering amplitude is observed in Fig.

5.11(a), specifically at the transmission side; while a larger radiation difference (around 30%) for S0 mode is shown in Fig. 5.11(b). The symmetric mode could be used for damage imaging based on scattering since the disbond causes wave scattering behaviour.

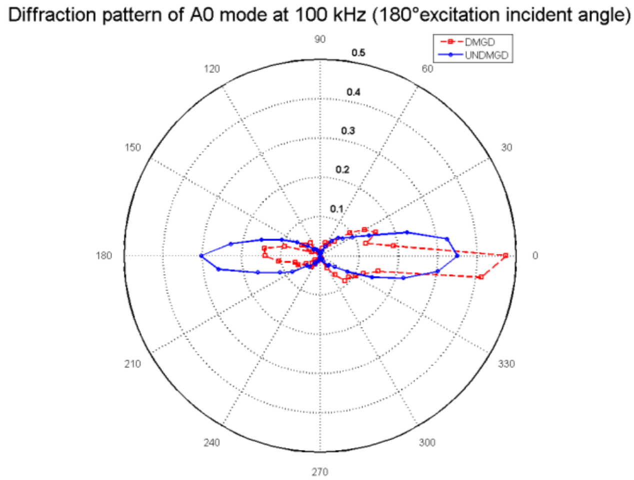

(a)

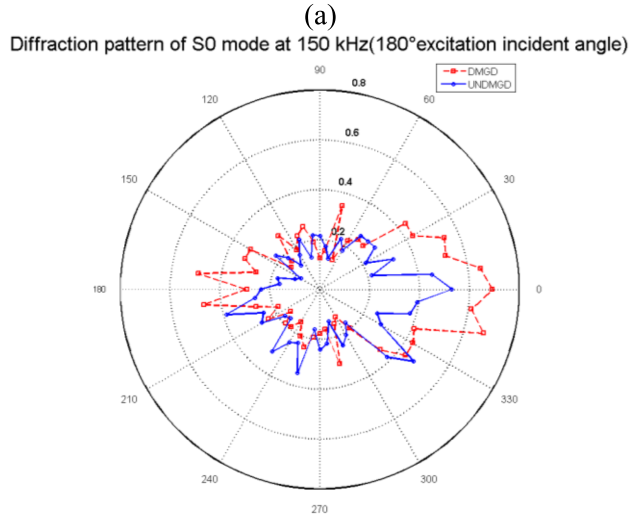

(b)

Figure 5.11. The effect of the disbond on the scattering behaviour: Diffraction pattern of the A0 mode (left) and S0 mode (right) for 180° excitation

From the presented results and above mentioned explanation, the mode and frequency selection as well as the incidence angle play a crucial role in disbond detection capabilities. Therefore, SHM guidelines for effective monitoring of a skin-stringer joint using guided wave excitation across the bond-line can be summarized below:

1) The A0 mode is more directional while the S0 is more scattered in all the orientations.
2) The S0 mode has a larger amplitude than the A0 mode since the out-of-plane motion of particles is more attenuated upon encountering the adhesive.
3) Excitation of guided waves at the low frequency range (below 150 kHz) ensures that the energy of diffracted waves is strong enough to be used for inspection.
4) In the case of the symmetric mode, guided wave behaviour changes with respect to the incidence angle. The adhesive absorbs the energy of the waves at 135° excitation more than at 180° excitation.
5) The anti-symmetric mode scattering is less affected by the orientation of the excitation, therefore; the plane wave orientation is rotated by 45° which is the result of altering the excitation from 180° to 135°.
6) Monitoring the assembly in anti-symmetric excitation around the orientation of the excitation (0°, 180°) at 100 kHz helps to investigate the quality of joint while for the symmetric excitation since the waves are scattered, more sensors need to be employed around the targeted zone at 150 kHz.
7) For damage imaging, the S0 mode appears to be the right candidate at around 150 kHz since an increase of 30% of the scattering coefficient is observed in the presence of a disbond.

5.7 Conclusion

An ultrasonic technique using guided wave scattering is proposed for inspection of composite assembly in this paper. The structure is a skin-stringer panel made of quasi-isotropic CFRP plates bonded together with an adhesive film. Two bonded joint conditions have been investigated for the joint: undamaged and damaged (with inserted Teflon tape as a disbond). The guided wave is generated by piezoceramics and LDV is used to capture the A0 and S0 mode propagation. The level of scattering through the adhesive and disbond is measured by normalizing the amplitude of scattered waves in different orientations by the amplitude of the incident wave in the frequency-wavenumber domain. The results determine the sensitivity of the scattering pattern around the joint to the disbond, mode and frequency and orientation of generated plane waves. Selection of the optimal mode and frequency range for inspection based on scattering analysis proposed some guidelines. Both adhesive and disbond attenuate the level of energy at higher frequencies. The A0 mode shows a more directional behaviour while S0 is more refracted, specifically at low frequencies. However, the optimum frequency range, propagating mode, and excitation angle is usually dependent on the geometrical features and defect size; a plane wave generation at 180° in pitch-catch and pulse-echo configurations based on scattering coefficients of the A0 and S0 modes at 100 kHz and 150 kHz is proposed respectively as an effective disbond detection.

5.8 Acknowledgments

This research was supported by the Natural Sciences and Engineering Research Council of Canada (NSERC) through the framework of the Consortium for Research and Innovation in Aerospace in Québec (CRIAQ) DPHM 501 project as well as Bombardier Aerospace and L-3 MAS.

5.9 References

[1] Soutis, C., Hu, F.Z. Design and performance of bonded patch repairs of composite structures, *Proceedings of the Institution of Mechanical Engineers, Part G: Journal of Aerospace Engineering* 1997; 211:263-71.

[2] Su, Z., Ye, L. Identification of Damage Using Lamb Waves, From Fundamentals to Applications. Berlin: Springer-Verlag GmbH & Co., 2009

[3] Chang, F.-K. Introduction to health monitoring: context, problems, solutions. 1st European Pre-workshop on Structural Health Monitoring, July 9, 2002; Paris, France.

[4] Su, Z., Ye, L., Lu, Y. Guided Lamb waves for identification of damage in composite structures: A review, *Journal of Sound and Vibration* 2006; 295: 753-780

[5] Diamanti, K., Soutis, C., Hodgkinson, J.M. Non-destructive inspection of sandwich and repaired composite laminated structures, *Composites Science and Technology* 2005; 65: 2059-67.

[6] Diamanti, K., Soutis, C. Structural health monitoring techniques for aircraft composites structures, *Journal of Aerospace Engineering* 2010; 46:342-52.

[7] Pavlopoulou, S., Soutis, C., Manson, G. Non-destructive inspection of adhesively bonded patch repairs using Lamb waves, *Plastics, Rubber and Composites* 2012; 41:61-68.

[8] Matt, H., Bartoli, I. Lanza di Scalea, F. Ultrasonic guided wave monitoring of composite wing skin-to-spar bonded joints in aerospace structures. *Journal of Aerospace Engineering* 2005; 118: 2240-53.

[9] Sherafat, M.H., Quaegebeur, N., Lessard, L., Hubert, P., Masson, P. Guided wave propagation through composite bonded joints, 7th European Workshop on Structural Health Monitoring; July 2014; Nantes, France.

[10] Seifried, R., Jacobs, L.J., Qu, J., Propagation of guided waves in adhesive bonded components, *NDT&E International* 2002; 35:317-28.

[11] Quaegebeur N, Micheau P, Masson P and Castaings M. Methodology for optimal configuration in structural health monitoring of composite bonded joints, *Smart Materials and Structures* 2012; 21:105001-11.

[12] Lowe, M.J.S, Challis R.E., Chan, C.W. The transmission of Lamb waves across adhesively bonded lap joints, *Journal of the Acoustical Society of America* 2000; 107: 1333-46.

[13] Lowe, M.J.S, Cawley, P. The applicability of plate wave techniques for the inspection of adhesive and diffusion bonded joints, *Journal of Nondestructive Evaluation* 1994;13 (4), 185-200.

[14] Scalea F.L.D, Rizzo, P. Propagation of ultrasonic guided waves in lap-shear adhesive joints: case of incident A0 Lamb wave, *Journal of the Acoustical Society of America* 2004; 115:146-57

[15] Hinders, M.K. Lamb wave scattering from rivets, Review of Progress in *Quantitative Nondestructive Evaluation* 1996;15: 209-216.

[16] Mckeon, J.C.P, Hinders, M.K. Lamb wave scattering from a through hole, *Journal of Sound and Vibration* 1999; 224 (5): 843-862

[17] Ostiguy, P.C., Sherafat, M.H., Franca, D.R., Bouslama, N., Quaegebeur, N., Maslouhi, A., Lessard, L., Hubert, P., Viens, M., Mofakhami, M.R., Hajjar, Z., Masson P. Selection of

structural features for the systematic study of guided wave propagation and interaction with damage; International Workshop on Structural Health Monitoring 2015, Sept. 2015, Stanford, USA

[18] Alleyne, N.D., Cawley, P. A 2-Dimensional Fourier transform method for the quantitative measurement of Lamb modes, *Ultrasonics Symposium* 1990:1143-1146

[19] Ostiguy, P.C., Quaegebeur, N., Masson, P. Assessment of the excitelet algorithm for in-situ mechanical characterization of orthotropic structures, SPIE83480N, 2012, doi:10.1117/12.914842.

CHAPTER 6. FOURTH MANUSCRIPT

6.1 Preface

In the fourth and fifth chapters, the integrity of a skin-stringer panel was evaluated using within-the-bond and across-the-bond line strategies. The next level of complexity is the composite stepped joint, as a general representative of a scarf repair. The objective is to evaluate the effect of the steps of the patch and adhesive on the wave behaviour to detect a possible disbond. A numerical analysis is performed using a Finite Element Method (FEM) and then validated by the experimental assessment method explained in chapters 3, 4 and 5.

Finite Element Modelling of Lamb Wave Propagation in Composite Stepped Joints*

* Journal of Reinforced Plastics and Composites 2016; 35(10): 796-806

Mohammad H. Sherafat, Pascal Hubert, Larry Lessard

Department of Mechanical Engineering, McGill University, Macdonald Engineering Building, 817 Sherbrooke West, Montreal, QC, Canada, H3A 0C3

Nicolas Quaegebeur, Patrice Masson

GAUS, Department of Mechanical Engineering, Université de Sherbrooke, Sherbrooke, QC, Canada, J1K 2R1

6.2 Abstract

The objective of this research is to evaluate the integrity of a composite bonded joint by simulating Lamb wave propagation using Finite Element (FE) methods. The structure of interest is composed of two stepped carbon fibre reinforced polymer (CFRP) plates bonded together by an adhesive film. Two different bonding conditions are examined for the joint: undamaged and damaged (with disbond). In the finite element model, an anti-symmetric guided wave is excited by imposing an out-of-plane displacement on the surfaces and a spatial Fourier Transform is performed before and after the bond-line for extraction of reflection and transmission coefficients. For validation, experiments are also conducted using two co-localized rectangular piezoceramics for plane wave generation. A 3-D laser Doppler vibrometer (LDV) is employed for non-contact measurement of the in-plane and out-of-plane velocity. The results confirm the reflections from the steps' edges, and it is found that the level of reflection and transmission of the guided wave mode is different for undamaged and damaged joints. The anti-symmetric mode in the pulse-echo configuration seems to be an efficient mode and strategy for disbond detection in composite repairs. The results verify that guided wave propagation is very effective for disbond detection in composite bonded joints and scarf repairs.

Keywords: Adhesive joints, Composite scarf repair, Disbond, Finite element analysis (FEA), Non-destructive testing (NDT), Structural health monitoring (SHM)

6.3 Introduction

Adhesive bonding of composite structural elements is intensively used in the aerospace industry to restore structural integrity in repair or assembled sub-structures. Experimental studies indicate that an adhesively bonded joint can restore the strength of the repaired structure up to 80% of the original undamaged laminate strength [1]. However, this structural feature is prone to degradation of the adhesive over time, improper installation or disbonding when submitted to fatigue or extreme loads that cannot be observed using a visual inspection when the disbond is in the middle of the laminate. These types of damage can significantly jeopardize the performance and safety of a structure with little advanced warning, and since they cannot be easily detected by visual inspection, non-destructive inspection (NDI) methods are being employed for detailed inspection of the structures. Over the last 50 years, NDI techniques have attained maturity in engineering applications, playing a significant role in the assessment of the integrity and durability of the structures. Conventional NDI approaches are usually conducted at regular scheduled intervals during the lifetime of assets and cannot provide descriptive information about structural integrity. Structural health monitoring (SHM) as an updated and retrofitted version of traditional NDI is proposed for continuous inspection of the structural features including composite joints to evaluate health and integrity of the joints in a real-time manner. SHM systems replace scheduled maintenance with as-needed maintenance, thus saving the cost of unnecessary maintenance as well as improving the level of safety through the consideration of working condition updates [2]. It has been shown that an effective SHM can reduce the total maintenance cost compared to traditional NDI approaches by more than 30% for an aircraft fleet [3].

Among the different approaches of SHM, guided (Lamb) wave propagation with piezoelectric transducers has been proposed for effective monitoring of composites [4-6] since it is quick, repeatable, sensitive to under-sized damages and cost-effective [2].

Several numerical modelling methods of Lamb waves have been employed for SHM application. Boundary element [7, 8] and finite element methods are well established for an understanding of wave propagation in metallic and composite plates [9-13]. The interaction of Lamb waves with delamination of different sizes at various locations along the structure is studied using 3-D finite element (FE) analysis [14]. Previous studies show that two strategies can be employed for inspection of bonded joints [15]. The first approach examined in the literature is the "within-the-bond" method which allows using bond lines as a waveguide resulting in minimization of the influence of complex geometrical features on wave behaviour [16]. It has been shown that using this approach, a primary anti-symmetric mode (A0) below 200 kHz frequency range is a good candidate for effective inspection of composite-to-metallic bonded structures [17]. The "across-the-bond" method is the second strategy which has been employed in previous studies for damage detection in simple and complex metallic assemblies [18]. With this method, the degree of disbond in adhesive joints can be estimated by measuring the attenuation level of the A0 mode [19]. The anti-symmetric (A0) mode and A-scan approach were also developed for a cross-ply 8-layer composite plate with delamination. It has been documented that when the delamination is placed at different locations through the thickness, multiple reflections from the delamination edges occur. When A0 is the incident wave, large reflected waves can be seen when the delamination is located near the surface, while reflected waves are small for a delamination located around the mid-plane [20]. Lamb wave propagation has been used in the past for damage detection in composite joints and repairs [21-25]. It has been shown that the change in the behaviour of wave propagation was observed at the boundary of impacted regions in scarf repairs using elastic-wave visualization [22]. The performance of both external and scarf bonded repair applied to impacted CFRP laminates was assessed under uniaxial tensile loading. A set of data extracted from 225 kHz Lamb wave excitation served as the baseline for characterization of loading stage [22], but the wave interaction mechanism upon encountering the steps was not studied in detail.

In this paper, the "across-the-bond" strategy using anti-symmetric mode excitation is used to examine two scarf-jointed carbon fibre reinforced polymer (CFRP) samples as a general representative of a repair patch or a composite assembly. The objective is to evaluate the effect of adhesive and steps on wave behaviour to detect possible disbond in the stepped joint, which is a common defect feature found in scarf repairs. A two-dimensional Finite Element Analysis (FEA) is first developed for the structure, and ultrasonic guided waves are generated by imposing displacements on the top and bottom surfaces of the plate. Experimental validation of propagation characteristics is performed, using a laser Doppler vibrometer (LDV), in the joint region in order to justify the selection of mode, frequency and inspection configuration for disbond detection in a composite scarf joint.

6.4 Numerical Modeling

6.4.1 Finite element modeling

In order to determine guided wave behaviour through the composite bonded structure, numerical simulations are carried out by commercial finite element (FE) software, COMSOL 4.3a. The structure of interest is selected based on a project between industrial and academic researchers, namely the CRIAQ DPHM 501 project, where structural features and design parameters have been identified, extracted and filtered for their relevance from an extensive list of aerospace structures of interest [26, 27]. A two-dimensional section of the whole structure considered in the experiment section is modelled to save computational time. Geometry and detailed description of the joint are shown in Fig. 6.1. A two-dimensional problem is defined using plane-strain assumptions [28-30] representative of an infinite medium along the z-direction. Newport woven CFRP and adhesive film with material properties described in Table 6.1 have been used.

Table 6.1. Material properties of woven CFRP (Newport NB 321 3K) and adhesive film [17]

Material	E_{11} (GPa)	E_{22} (GPa)	υ_{12}	G_{12} (GPa)	ρ (kg/m^3)
CFRP	64.12	8.2	0.3	4.13	1200
Adhesive	1.0	1.0	0.3	0.38	1420

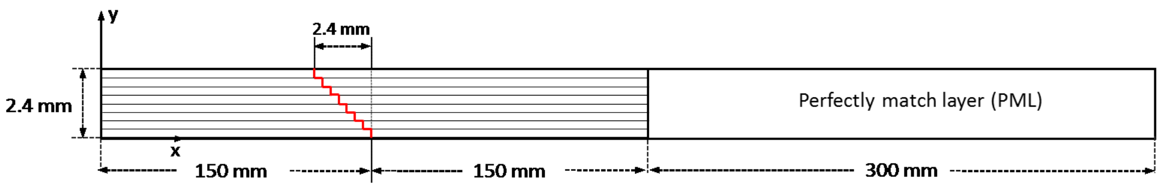

(a)

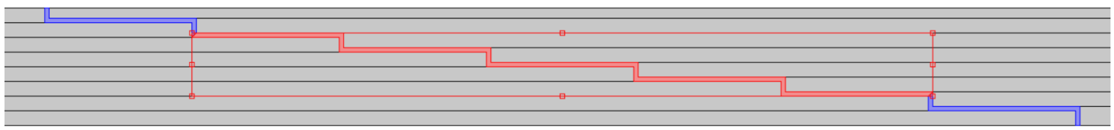

(b)

Figure 6.1. Definition of the geometry of the structure (a), and detailed presentation of the undamaged (blue) and damaged (red) steps (b) used for 2-D FEM modelling of the scarf bonded joint

Since each lamina is plain weave material, eight layers of plies are used for making a quasi-isotropic layup $[0/90/45/-45]_{2s}$. In the FE model, no damping was incorporated in the composite [28-30] for simplicity, while a 10% loss factor is introduced to the adhesive. The thickness of the adhesive, the thickness of each ply and the laminate thickness is 0.09 mm, 0.3 mm and 2.4 mm, respectively. In the joint region, each ply is stepped by 3 mm resulting in a scarf length of 21 mm as shown in Fig. 6.1. The two stepped samples with a length of 150 mm are attached using adhesive film. No contact elements are used for simulating the disbond [28, 29], such that a portion of the adhesive is removed and replaced using a combination of increasing of Young's modulus and loss factor of the adhesive layer by a factor of 3, as proposed in the literature [17]. Therefore, 2-D plane strain triangular elements, which have a length of 0.25 mm are used for their ability to conform to irregular areas. This length is chosen based on several convergence studies to make sure that enough elements (at least six elements) are used per wavelength. Eight nodes elements (four corners, four mid-side nodes) allow predicting 2-D vibrations with two translation degrees-of-freedom at each node. Local mesh refinement (see Fig. 6.2) has been implemented around the steps for both joints. A Perfectly Matched Layer (PML) is attached to the right-end of the structure to prevent unwanted reflect waves from the edge.

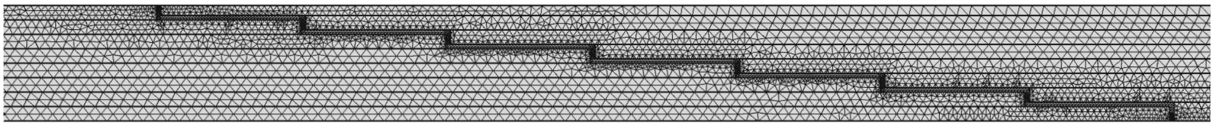

Figure 6.2. Mesh refinement representation around the steps

6.4.2 Excitation of guided waves

Single frequency excitation of ultrasonic guided waves is considered for frequencies below 500 kHz. The low frequency range (below 500 kHz) can be used as the less dispersive region [2] to ensure that only the low order modes (A0, S0, and SH0) are propagating in the structure. Note that a point-node excitation at the upper and lower sides of the laminate is employed to introduce the excitation in the form of displacement.

Based on the literature, it must be noted that the S0 mode is more prone to noise since its generated energy is generally less than the A0 mode [17]. Whereas the anti-symmetric mode is less affected by noise and is stronger than the S0 mode in terms of amplitude; indicating that it is more efficient in pitch-and-catch and pulse-echo approaches [23, 24]. Moreover, looking at the dispersion curves in Fig. 6.3, in the curves corresponding to the perfect bonded case and in the damaged case (considering that the guided waves propagate in the upper and lower parts of the joint), it is observed that only the A0 mode is affected by the change of bonding condition, such that the sensitivity of the S0 mode to the damage should be low.

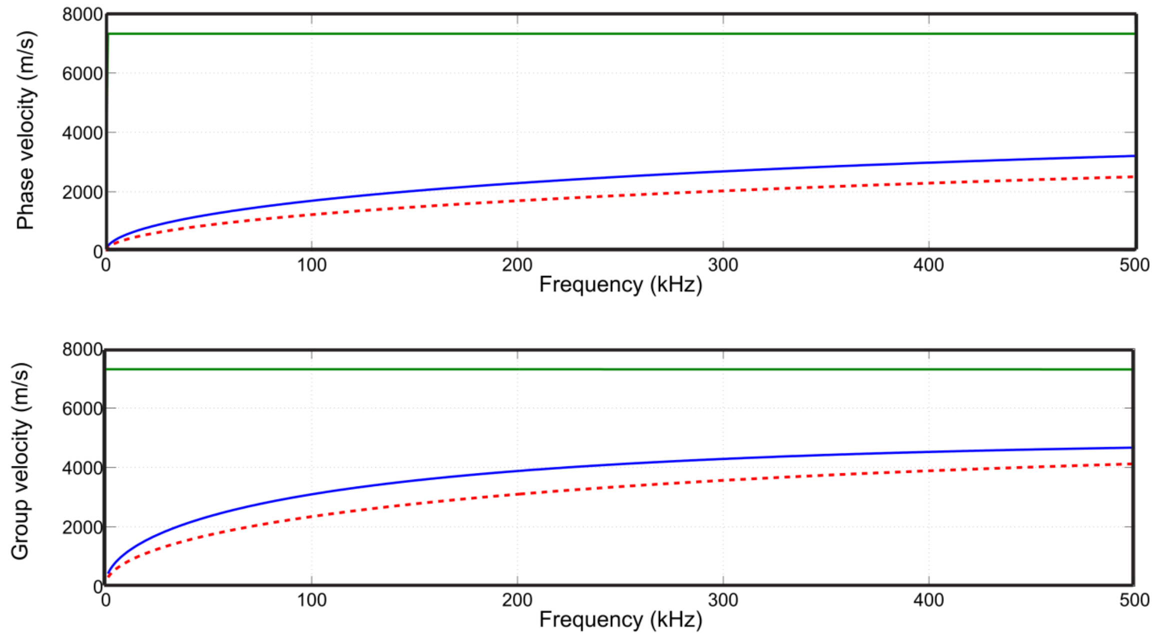

Figure 6.3. Dispersion curve for the composite scarf joint, green line (S0 mode), solid blue line (A0 mode undamaged) and dashed red line (A0 mode damaged)

Therefore, in the simulation, the A0 mode is excited by applying an out-of-plane displacement in the same direction (out-of-phase excitation) at the top and bottom of the plate at x=0. Two scanning lines before and after the joint are defined on the plate surface with the length of 100mm and with a 1 mm spacing between two adjacent scanning points. To extract the propagation characteristics the in-plane and out-of-plane displacements of the scanning points is captured and then analyzed using spatial Fourier Transform, as described in the following section.

6.5 Numerical results and discussion

6.5.1 Guided wave propagation and characterization

In order to characterize wave propagation in a composite scarf joint, the first simulation is performed on the undamaged structure. To understand how the guided waves interact with the joint, the displacement field decomposition in the frequency domain of any quantity are defined as:

$$u(x,\omega) = U_{inc}(\omega)e^{-jk(\omega)\,x} + U_{refl}(\omega)e^{jk(\omega)\,x} \text{ (reflection side)}$$
$$u(x,\omega) = U_{tran}(\omega)e^{-jk(\omega)\,x} \text{ (transmission side)} \qquad (6\text{-}1)$$

Where u, k, ω are the displacement of the surface, the wavenumber of the propagating wave and angular frequency respectively. To extract the wavenumber, a two-dimensional Fourier transform [31] is performed in order to obtain the complex amplitude U of the incident and reflected/transmitted fields as a function of frequency. Fig. 6.4 presents the wavenumber / frequency representation for the out-of-plane displacement along the reflected path for the case of out-of-phase excitation.

In Fig. 6.4, a considerable amount of A0 mode energy is reflected around 300 kHz in the case of the undamaged scarf, which introduces a peak in the reflection coefficient versus frequency plot in section 3.2. However, in the case of the damaged joint, this energy concentration is no longer visible, defining a potential frequency range of interest.

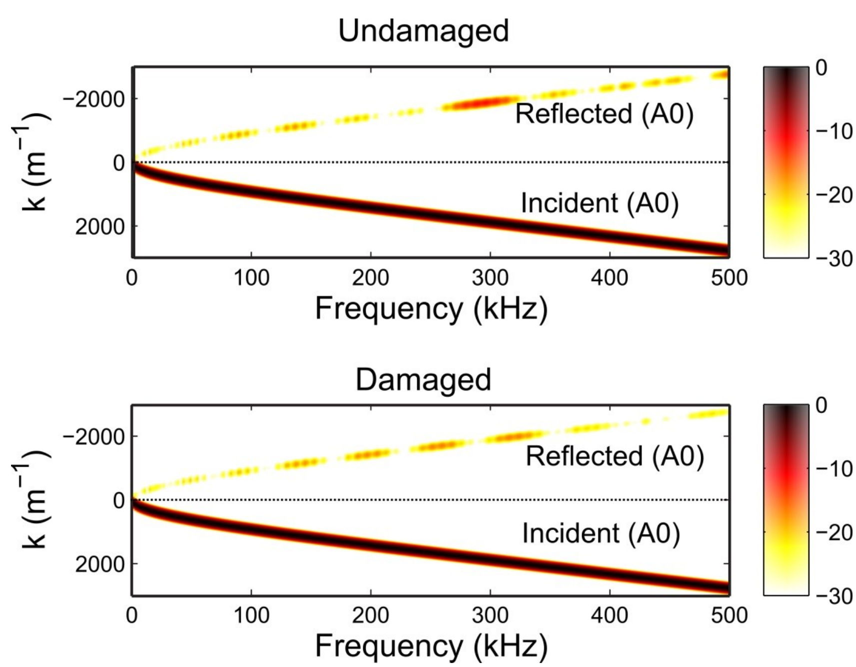

Figure 6.4. Frequency/Wavenumber transform of the out-of-plane displacement for a propagating wave on the reflection side in the undamaged (top) and damaged (bottom) joint

6.5.2 Reflection and transmission coefficients

For effective evaluation of wave travelling behaviour before and after the joint, using Eq. 6-1, two reflection and transmission coefficients are defined as:

$$R(\omega) = \frac{U_{refl}(\omega)}{U_{inc}(\omega)} \tag{6-2}$$

$$T(\omega) = \frac{U_{trans}(\omega)}{U_{inc}(\omega)} \tag{6-3}$$

The two coefficients are plotted versus frequency for both joints in Fig 6.5 for an A0 incident mode.

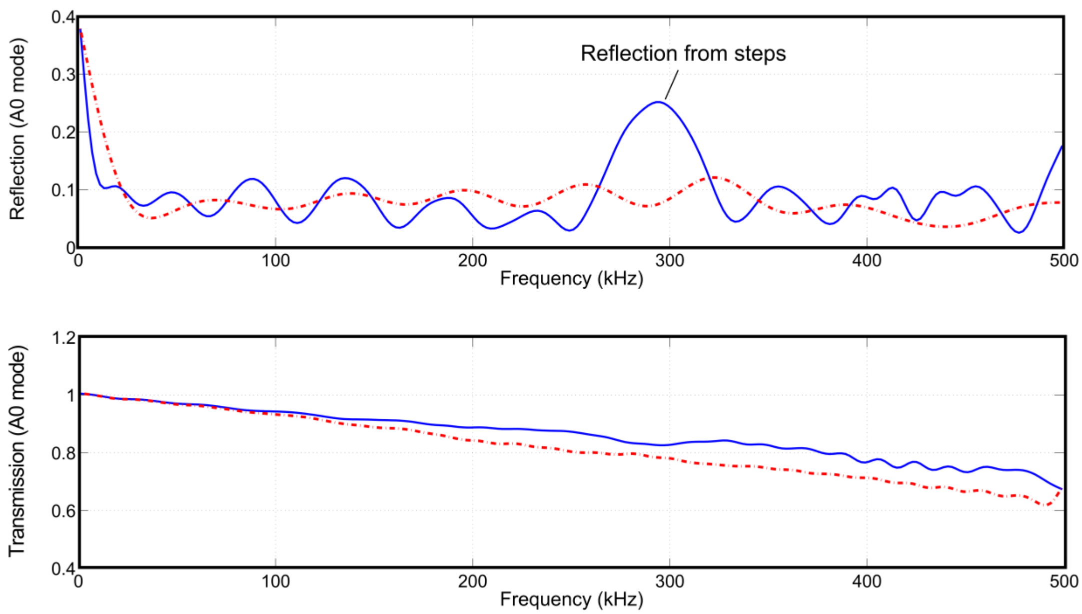

Figure 6.5. Reflection coefficient (top) and transmission coefficient (bottom) of A0 mode for the undamaged (solid-blue) and damaged (dash-red) stepped joint as a function of frequency

As mentioned in the section 5.5.1, a reflection peak at around 300 kHz in the undamaged joint attributed to a wavenumber of approximately 1700 m-1, which corresponds to a wavelength of 3.1 mm. This is approximately the same as the length of increments steps between two adjacent layers. The reflections may thus come from discontinuities [20] and here represent the abrupt change of the stiffness and also the level of impedance between adjacent CFRP and adhesive film layer at local steps. Reflected waves mostly come from the steps near to the surface and the other steps, which are located around mid-plane, are negligible [30]. The phenomenon can be explained by the fact that each step plays a similar role as a small delamination. When the incident A0 wave propagates into the “entrance” of each step it is transmitted towards right, and since the upper and lower regions of the steps do not have the same thickness (except for the middle step), it travels on the upper/lower sides independently and reaches the right edge of the step with different phases and arrival times [20]. This creates a reflection since the incident wave interacts with the steps, and the repetition of such reflections at the exit of each step causes a reflection peak at 300 kHz. In the case of a damaged joint, the peak is no longer observed due to the presence of the disbond since inserted Teflon incorporates more damping and stiffness within the disbonded steps. Thus, a decrease from 25% to 5% (reduction of 80%) of the reflection coefficient is observed, allowing for efficient monitoring of the joint condition. Looking at the evolution of the transmission in Fig 6.5, it appears that a decrease of 10% is observed in the whole frequency range for the damaged case, indicating the fact that disbond attenuates the wave energy on the transmission side. However, this relatively small change of transmission may lead to false diagnostic since noise, environmental changes or transducer degradation may lead to relative changes of the same order of magnitude. Thus, the inspection strategy based on observation of the reflection coefficient of the A0 mode around 300 kHz appears to be the best candidate for proper monitoring of scarf joints.

6.6 Experimental setup

6.6.1 Structural description

For the experimental validation, the structure presented in the numerical is manufactured as a classic representative composite repair. Two stepped panels, with the geometry, material, and layup explained in section 6.4.1, are bonded together using adhesive film. The two panels, with a quasi-isotropic layup $[0/90/-45/45]_{2s}$ made of Newport woven 321 prepreg, are attached using adhesive film: Cytec FM® 300-2M. The scarf angle is about 6 degrees, such that eight layer steps of 3 mm are used in order to form each sample (see Fig. 6.6). A circular disbond (2 cm diameter) is also introduced during manufacturing by inserting two pieces of Teflon tape. In this study, the two components of the structure are laid up, vacuumed bagged simultaneously and cured in one step using the ‘‘co-curing” strategy.

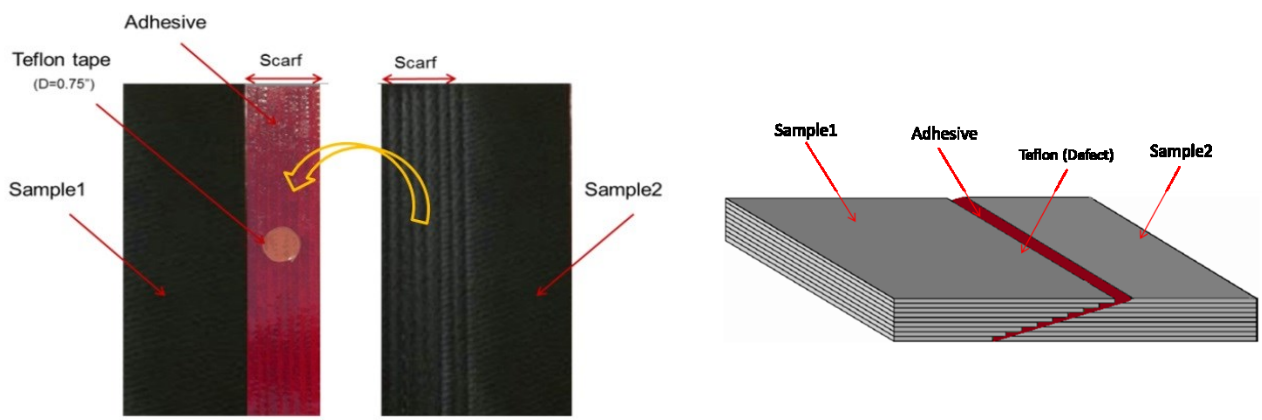

Figure 6.6. Manufacturing of composite scarf joint using two stepped samples

6.6.2 Guided wave generation and sensing

In order to characterize the guided waves through the pristine and disbonded stepped joint, a plane wave generation was chosen in order to collimate the wave on the selected area and avoiding geometrical spread induced by finite size transducers. The designed device illustrated in Fig. 6.7(a) consists of two co-localized rectangular piezoceramics (50 x 5 x 0.45mm) made of PZT-5A, maintained on both sides of the structure using high strength magnets and coupled to the host structure using dedicated shear-coupling gel. Due to a high value of the width-to-length ratio, the generation of a plane wave in front of the actuator is almost guaranteed. The two actuators can be driven in- and out-of-phase in order to generate symmetric or anti-symmetric modes, respectively. However, due to slight misalignment or tilt, this strategy cannot be employed in practical cases. For this purpose, the two piezoceramics are activated separately, and mode separation is achieved in post-processing using an optimization process adjusting the amplitude and phase [32] to minimize the unwanted mode. In this paper, only the first anti-symmetric mode (out-of-phase excitation) is proposed for evaluation of wave behaviour through the joint following the numerical analysis of the joint.

(a)

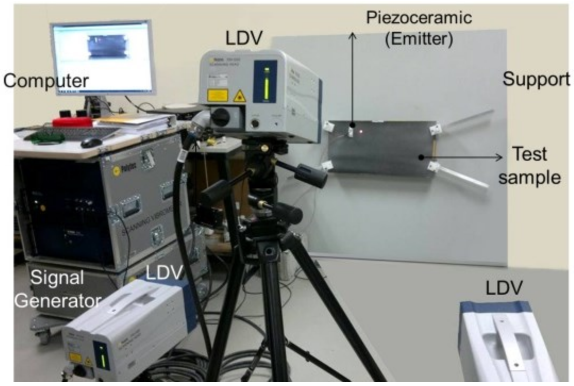

(b)

Figure 6.7. Illustration of the piezoceramics and excitation clamp (a) and the experimental setup (b)

Non-contact measurement of the in-plane and out-of-plane velocity is performed using a 3-D LDV system (PSV-500, Polytec GmbH), as presented in Fig. 6.7(b). The transfer functions below 500 kHz between the input voltage and the measured 3-D velocity field are measured using 100 averages in order to increase the Signal-to-Noise-Ratio (SNR). For this purpose, pseudo-random excitation is used and amplified using a NOVO UAP-8400 voltage amplifier [33]. The propagation characteristics in terms of reflection and transmission coefficients are extracted using spatial Fourier transform [31] over a linear grid of measurement points as presented in Fig. 6.8, allowing separation of the incident and reflected fields. The space between two adjacent points is set to about 0.5mm, ensuring at least 5 points per minimal wavelength for frequencies below 500 kHz. Due to the finite width of the actuator, natural mode selection occurs for specific wavelengths defined by λ = 10 mm and λ = 3 mm, while natural mode rejection appears when the wavelength is λ = 5 mm. However, since the reflection coefficient is computed using spatial Fourier transform, the reflected wave amplitude is normalized by the incident wave amplitude, such that the finite width of the piezoceramics has no influence on the extracted reflection coefficient.

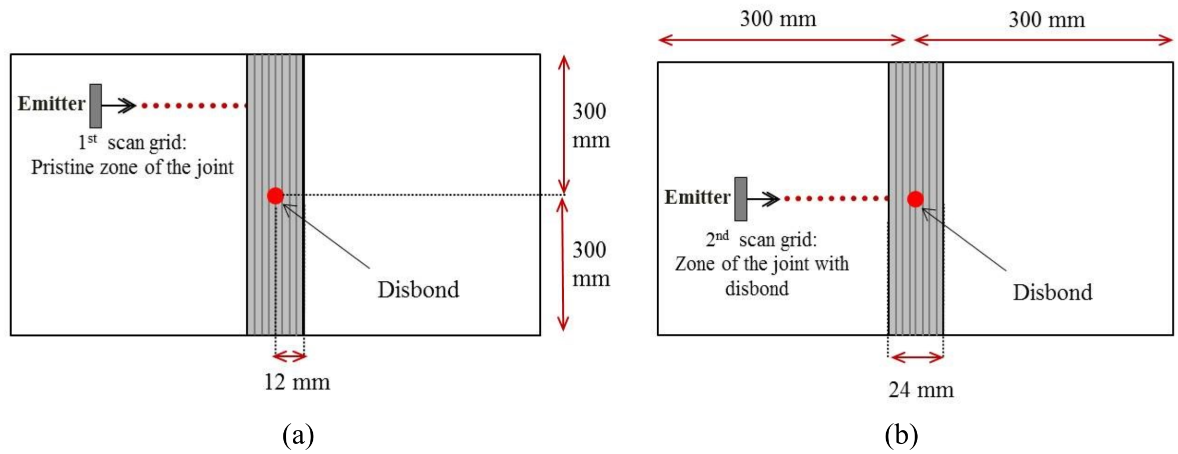

Figure 6.8. Two linear scanning grids, the pristine zone of the joint (a) and zone of the joint with disbond (b)

6.6.3 Experimental results and discussion

The measurements of the transfer function between the actuator voltage and the measured velocity over the three directions are taken over a linear grid of 300 points in simple plate zone (see Fig. 6.8) and the propagation characteristics are extracted using spatial Fourier transform [31].

Fig. 6.9 illustrates the results in terms of frequency/wavenumber (f/k) transform for the two components of the velocity field for a propagation following the x direction when the two co-localized piezoceramics are out-of-phase (anti-symmetrical excitation). In the Fig. 6.9, as expected, A0 mode is naturally amplified when driving the two actuators out-of-phase and is more observed in the z-component of the velocity field (out-of-plane velocity). For evaluation of the reflection coefficients of the guided waves through the joint, Eq. 6.1 and Eq. 6.2 are employed. The reflection coefficient for both the undamaged (UNDMGD) and damaged (DMGD) joints are obtained and presented in Fig. 6.10(top).

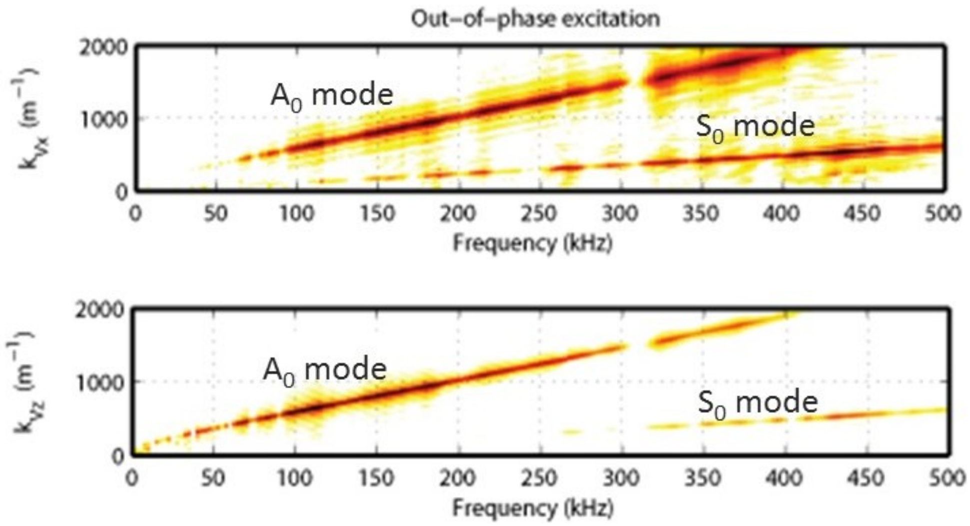

Figure 6.9. Frequency/Wavenumber transform for a propagating wave in the composite plate. Components in the x- (top) and z- direction (bottom) are presented for the case out-of-phase excitation

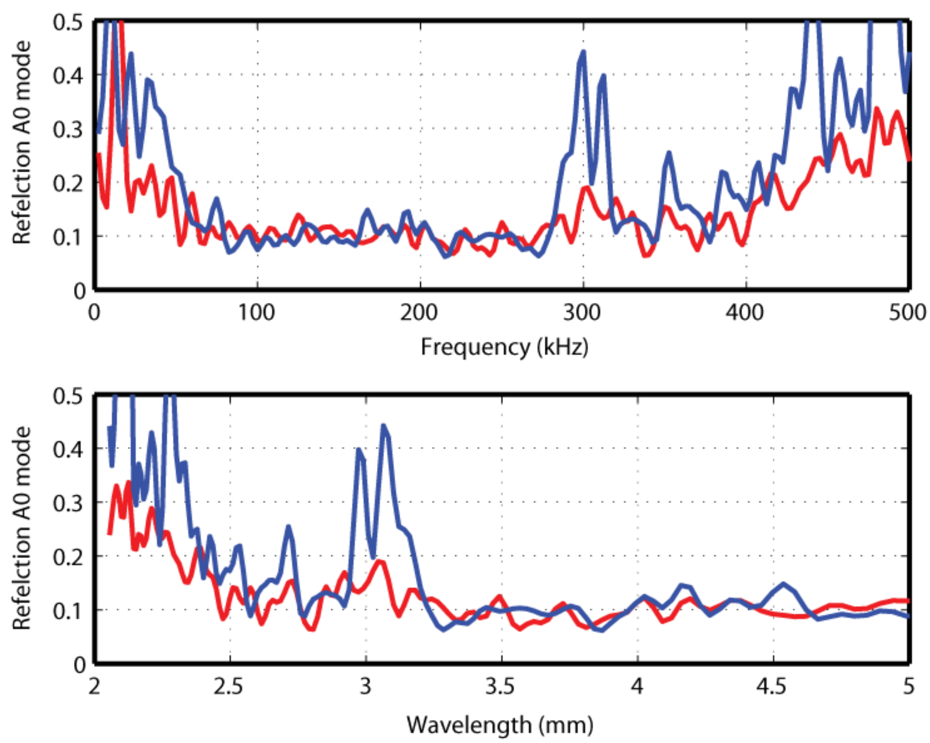

Figure 6.10. Reflection coefficients of A0 mode versus frequency (top) and wavelength (bottom) for the undamaged (blue) and damaged (red) stepped joint

A fairly good agreement between numerical simulation and experimental results is obtained. The results show that a reflection peak at 300 kHz is observed in the case of the undamaged joint which corresponds to what has been explained in the numerical section for the reflection from the steps and disbond edge. This peak corresponds to a wavelength of 3.1 mm (see Fig. 6.10(bottom)), approximately the same as the length of increments steps between two adjacent layers. The absolute level of reflection is about 40% compared to 25% in the numerical study. The discrepancy may be attributed to the modeling of the Teflon tape as representative of the disbond. For the damaged joint, the level of the reflection peak at 300 kHz is not captured due to the absence of standing waves at the scarf, such that a decrease of 60% of the reflection is observed compared to the undamaged case.

For confirmation, a seven cycle harmonic excitation with a central frequency of 300 kHz is applied to the structure and A-scan is performed using LDV measurement of the out-of-plane velocity at one point before the joint edge at a distance of 25 mm. The normalized echoed signal in the time domain is presented in Fig. 6.11.

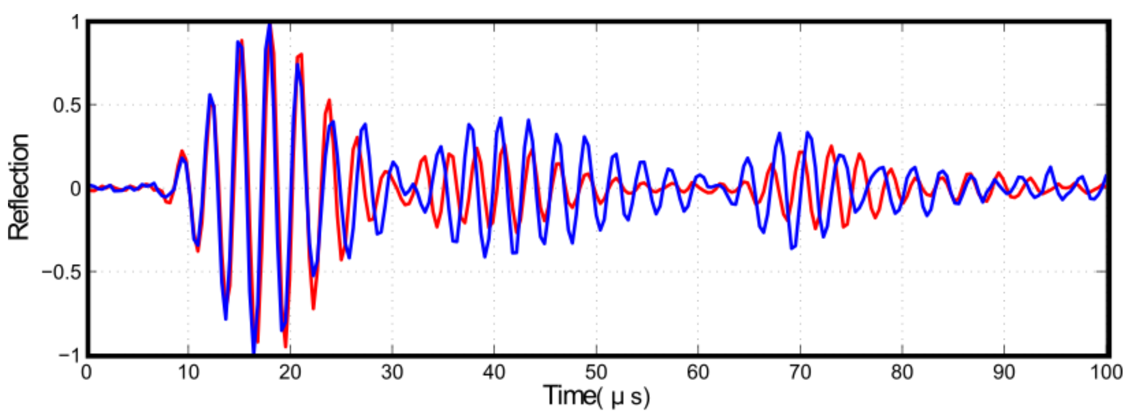

Figure 6.11. Out-of-plane velocity response to a seven cycles Hanning windowed burst at 300 kHz before the joint in the case of undamaged (blue) and damaged (red) stepped joint

The first visible wave packets corresponding to the in A0 incident mode are identical since the incident wave has not passed through the joint. The second wave packet associated with the reflection from the steps indicates the stronger amplitude of the reflected wave for the undamaged joint compared to the damaged reflection since a decrease of 45% is observed in the time-domain signal. This is in very good agreement with the previous frequency domain results in the experiments (Fig 6.10(top)) and numerical analysis as well (Fig. 6.5(top)).Thus, a reflection at the tip of each layer is observed and adding of each layer leads to the apparition of this reflection peak around 300 kHz, and confirms the ability of the system to detect the disbond, supported by the numerical predictions.

6.7 Conclusion

Finite element modelling of two scarf bonded composite plates is developed in this paper. The adhesively bonded joint is modelled, and disbond is simulated by introducing Teflon tape with the higher damping material. The A0 mode Lamb wave is excited by applying out-of-plane displacement, and measuring the transmitted and reflected wave fields. Results are presented in the form of wavenumber as well as reflection and transmission coefficient versus frequency. Comparison of both cases' results indicates a reflection peak at 300 kHz in the case of perfect bonding condition that is not observed in the case of partial disbond. This frequency corresponds to a wavelength of 3.1 mm, which corresponds to the size of the steps. The conclusion is that the steps' edges play a role like a tiny delamination through the thickness; however, its behavior depends on the location of the steps through the thickness. The dominant portion of the reflection comes from the steps near to the surface rather than those closed to the mid-plane. The numerical results on reflection from the steps and disbond have been validated by an experiment in the time and frequency domains, inferring the reflection at the tip of each layer and confirming that the quality of the joint can be assessed. Therefore, the first fundamental anti-symmetric mode with a frequency corresponding to a wavelength of each step length is a potential guideline for structural health monitoring of stepped bonded joints and scarf repairs.

6.8 Acknowledgments

This research was supported by the Natural Sciences and Engineering Research Council of Canada (NSERC) through the framework of the Consortium for Research and Innovation in Aerospace in Québec CRIAQ DPHM 501 project as well as Bombardier Aerospace and L-3 MAS.

6.9 References

[1] Soutis, C., Hu, F.Z. Design and performance of bonded patch repairs of composite structures, *Proceedings of the Institution of Mechanical Engineers, Part G: Journal of Aerospace Engineering* 1997; 211:263-71.

[2] Su, Z., Ye, L. Identification of Damage Using Lamb Waves, From Fundamentals to Applications. Berlin: Springer-Verlag GmbH & Co., 2009.

[3] Chang, F.-K. Introduction to health monitoring: context, problems, solutions, 1st European Pre-workshop on Structural Health Monitoring, July 9, 2002; Paris, France.

[4] Maio, L., Memmolo, V., Ricci, F., Boffa, N.D., Monaco, E., Pecora, R. Ultrasonic wave propagation in composite laminates by numerical simulation, *Composite Structures* 2015; 121: 64-74.

[5] Han, J., Kim, C.G., Kim, J.U. The propagation of Lamb waves in a laminated composite plate with a variable stepped thickness, *Composite Structures* 2006; 76: 388-396.

[6] Wang, D., Ye, L., Tang, Y., Lu, Ye. Monitoring of delamination onset and growth during Mode I and Mode II interlaminar fracture tests using guided waves, *Composites Science and Technology* 2012; 72: 145-151.

[7] Cho, Y., Rose, J.L. A boundary element solution for a mode conversion study on the edge reflection of Lamb waves, *Journal of the Acoustical Society of America* 1996, 99(4) 2097-2109.

[8] Jin, J., Quek, S.T., Wang, Q. Wave boundary element to study Lamb wave propagation in plates, *Journal of Sound and Vibration* 2005; 288(12):195-213.

[9] Ostachowicz, W.M. Damage detection of structures using spectral finite element method, *Computers & Structures* 2008; 86(35): 454-462.

[10] Sause, M.G.R., Hamstad, M.A., Horn, S. Finite element modeling of Lamb wave propagation in anisotropic hybrid materials, *Composites: Part B* 2013; 53: 249-257.

[11] Lee, B.C., Staszewski, W.J. Modelling of Lamb waves for damage detection in metallic structures: Part ii. Wave interactions with damage, *Smart Materials and Structures* 2003; 12(5): 815-824.

[12] Yang, C., Ye, L., Su, Z., Bannister, M. Some aspects of numerical simulation for Lamb wave propagation in composite laminates, *Composite Structures* 2006; 75(14): 267-275.

[13] Wilcox, P. Modelling the excitation of Lamb and SH waves by point and line sources. *AIP Conference Proceedings* 2004; 700(1): 206-213.

[14] Panda, R.S., Rajagopal, P., Balasubramaniam, K. An approach for defect visualization and identification in composite plate structures using air-coupled guided ultrasound, *AIP Conference Proceedings* 2015; 1650 (1299); 1299-1306.

[15] Matt, H., Bartoli, I., Lanza di Scalea F. Ultrasonic guided wave monitoring of composite wing skin-to-spar bonded joints in aerospace structures, *Journal of the Acoustical Society of America* 2005; 118: 2240-2253.

[16] Seifried, R., Jacobs, L.J., Qu, J. Propagation of guided waves in adhesive bonded components, *NDT&E International* 2002; 35: 317-328.

[17] Quaegebeur, N., Micheau, P., Masson, P., Castaings, M. Methodology for optimal configuration in structural health monitoring of composite bonded joints, *Smart Materials and Structures* 2012; 21: 1-11.

[18] Lowe, M.J.S., Challis, R.E, Chan, C.W. The transmission of Lamb waves across adhesively bonded lap joints, *Journal of the Acoustical Society of America* 2000; 107: 1333-1346.

[19] Scalea F.L.D., Rizzo, P. Propagation of ultrasonic guided waves in lap-shear adhesive joints: case of incident A0 Lamb wave, *Journal of the Acoustical Society of America* 2004; 115: 146-157.

[20] Hayashi, T., Kawashima, K. Multiple reflections of Lamb waves at a delamination, *Ultrasonics* 2002; 40: 193-197.

[21] Jang, I., Park, I., Lee, U. Guided waves in a Timoshenko beam with a bonded composite patch: Frequency domain spectral element modeling and analysis, *Composites: Part B* 2014; 60: 248-260.

[22] Takahashi, I., Ito, Y., Takeda, S., Iwahori, Y., Takatsubo, J., Takeda, N. Impact damage detection on scarf-repaired composites using Lamb wave sensing, 16th International Conference on Composite Materials, July 2007, Japan.

[23] Sherafat, M.H., Guitel, R., Quaegebeur, N., Hubert, P., Lessard, L., Masson P. Structural health monitoring of a composite skin-stringer assembly using within-the-bond strategy of guided wave propagation, *Materials and Design* 2016; 90: 787-794.

[24] Sherafat M.H., Guitel, R., Quaegebeur, N., Lessard, L., Hubert, P., Masson, P. Guided wave scattering behaviour in composite bonded assemblies, *Composite Structures* 2016; 136: 696-705.

[25] Habib, F., Martinez, M., Artemev, A., Brothers, M. Structural health monitoring of bonded composite repairs – A critical comparison between ultrasonic Lamb wave approach and surface mounted crack sensor approach, *Composites: Part B* 2013; 47: 26-34.

[26] Sherafat, M.H., Quaegebeur, N., Lessard, L., Hubert, P., Masson, P. Guided Wave Propagation through Composite Bonded Joints,7th European Workshop on Structural Health Monitoring; July 2014, Nantes, France.

[27] Ostiguy, P.C., Sherafat, M.H., Franca, D.R. , Bouslama, N., Quaegebeur, N., Maslouhi, A., Lessard, L., Hubert, P., Viens, M., Mofakhami, M.R., Hajjar, Z., Masson, P. Selection of structural features for the systematic study of guided wave propagation and interaction with damage; International Workshop on Structural Health Monitoring 2015, Sept. 2015, Stanford, USA.

[28] Ramadas, C., Balasubramaniam, K., Joshi, M., Krishnamurthy, C.V. Interaction of guided Lamb waves with an asymmetrically located delamination in a laminated composite plate, *Smart Materials Structures* 2010; 19: 65009-65020.

[29] Ramadas, C., Balasubramaniam, K., Joshi, M., Krishnamurthy, C.V. Interaction of the primary anti-symmetric Lamb mode (A0) with symmetric delaminations, numerical and experimental studies, *Smart Materials Structures* 2009; 18: 85011-85018.

[30] Guo, N., Cawley, P. The interaction of Lamb waves with delaminations in composite laminates, *Journal of the Acoustical Society of America* 1993; 94 (4): 2240-2246.

[31] Alleyne, N.D., Cawley, P. A 2-Dimensional Fourier transform method for the quantitative measurement of Lamb modes, *Ultrasonic Symposium*1990; 1143-1146.

[32] Ostiguy, P.C., Quaegebeur, N., Masson, P. Assessment of the excitelet algorithm for in-situ mechanical characterization of orthotropic structures, *SPIE Smart Structures and Materials/NDE* 2012; 83480N.

[33] Quaegebeur, N., Masson, P., Micheau, P, Mrad, N. Broadband generation of ultrasonic guided waves using piezoceramics and sub-band decomposition, *IEEE Transactions on Ultrasonics, Ferromagnetics and Frequency Control* 2012; 59: 928-938.

CHAPTER 7. CONCLUSIONS AND FUTURE WORK

7.1 Preface

This chapter summarizes the key findings of the research work described in the previous sections, presents the contributions to knowledge, conclusions and provide directions for future work.

7.2 Summary of key findings

7.2.1 Interaction of artificial delamination and impact damage with guided waves

Four laminates made of quasi-isotropic unidirectional CFRP were investigated. A circular disbond was placed through the thickness, one mid-plane Teflon tape for the first sample and one non mid-plane Teflon between the layers for the second coupon. The real damage was simulated by impacting the other two samples at high and low energy levels. The anti-symmetric plane guided wave was generated by piezoceramics in 180° and 135° directions. A 3-D LDV was employed to capture the signals for evaluation of reflection, transmission and scattering coefficients as a function of frequency. From the test results, the following points are noted:

1. The excitation angle has marginal influence on the wave behaviour in the pitch-and-catch (transmission) and pulse-echo (reflection) configurations.
2. The reflection increases with respect to frequency for both types of damage, while the transmission decreases with respect to frequency.
3. From the diffraction patterns, it is noted that the low energy impact and non mid-plane Teflon-type delamination induce very similar scattering behaviour. The mid-plane Teflon-tape diffraction pattern is entirely different from a real impact.

7.2.2 Within and across the bondline strategies of guided waves propagation in composite skin-stringer assembly

The structure of interest was a composite bonded joint, composed of carbon fibre reinforced polymer (CFRP) plates bonded together by an adhesive film. The assembly consisted of a skin bonded to two stringers incorporating two joint conditions, namely a pristine and damaged joint configuration, with inserted Teflon tape as a disbond. Plane guided waves were generated using rectangular piezoceramics within and across the bondline. An LDV was employed to capture the A0 and S0 mode signals. The reflection, transmission and scattering behaviour of the plane guided waves were studied as a function of mode, frequency and the quality of the joint. It was noted that the A0 mode was more directional while the S0 was more scattered.

For inspection within the bondline:

1. In a pitch-and-catch configuration, the A0 mode is highly sensitive to the disbond for frequencies below 350 kHz and a decrease of 10% of the transmission is observed.
2. In a pulse-echo configuration, the S0 mode around 200 kHz could be used for monitoring an echo induced by the presence of a disbond.
3. Based on the scattering of the wave at the disbond, S0 mode below 350 kHz appears as the best candidate for damage imaging, since an increase of 60% of the scattered field is observed in the presence of a disbond, modifying the diffraction pattern of the joint.

For inspection across the bondline:

4. Excitation of guided waves in the low-frequency range (below 150 kHz) ensures that the energy of diffracted waves is strong enough to be used for inspection.
5. The symmetric mode is more prone to excitation angle, while anti-symmetric mode scattering is less affected by the orientation of the excitation; as the plane wave beam is rotated from 180° to 135°.
6. For damage imaging, the S0 mode appears to be the good candidate at low frequencies, since an increase of 30% of the scattered coefficient is observed in the presence of a disbond.
7. Monitoring the assembly in anti-symmetric excitation around the orientation of the excitation (0°, 180°) at low frequencies helps to investigate the quality of joint, by incorporating just a few sensors. Whereas for the symmetric excitation, more sensors must be employed around the targeted zone for damage imaging.

7.2.3 Guided waves propagation in composite scarf repair

The integrity of a composite patch repair was evaluated using Finite Element (FE) analysis and experimental assessment. The structure of interest was composed of two stepped CFRP plates bonded together by an adhesive film, with two bonding conditions, pristine and disbonded. In the FEM, the anti-symmetric mode Lamb wave was excited by applying out-of-plane displacement, and A-scan was performed for extraction of reflection and transmission coefficients. The experiments were also conducted using two co-localized rectangular piezoceramics for plane wave generation and a LDV for non-contact measurement of the in-plane and out-of-plane velocity.

1. Comparison of the undamaged and damaged cases indicates a reflection peak at 300 kHz in the case of perfect bonding which is not noted in the case of partial disbond. This frequency corresponds to a wavelength of 3.1 mm, which corresponds to the size of the steps. The dominant portion of the reflection comes from the steps near to the surface rather than those closed to the mid-plane.
2. Thus the reflection at the tip of each layer in the scarf (the reflections from the steps' edges) can be an indication for evaluation of the quality of the joint.

7.3 Conclusions

Guided wave propagation was investigated in composite structures to detect delamination, disbond and impact damage. The damage parameters and structural features were typical representatives of those found in aircraft composite structures. The research was initiated by investigating the guided wave interaction in simple composites with artificial delamination and damage due to impact. An inspection methodology was developed, and then applied in two more complex structures, skin-stringer assembly and scarf joint, to detect disbond. The most sensitive guided wave features including reflection, transmission and scattering, along with the best mode and frequency range, excitation approach, and incident angle are identified and developed.

It is noted that the low energy impact and non mid-plane Teflon-type delamination induce very similar scattering behaviour. The reflection increases with respect to frequency for both types of damage, while the transmission decreases. For the skin-stringer assembly, it was noted that the A0 mode was more directional and highly sensitive to the disbond in transmission for frequencies below 350 kHz. The S0 was more scattered, and appears as the best candidate for damage imaging below 350 kHz, since an increase of up to 60% of the scattered field is observed in the presence of a disbond. In the scarf joint, the reflection at the tip of each layer in the scarf (the reflections from the steps' edges) is observed in the undamaged repair, which can be an indication for evaluation of the quality of the joint. The results verified that guided wave propagation approach is very efficient for disbond detection in composite bonded joints and scarf repairs.

7.4 Publications and presentations

Referred Journals

1. Sherafat, M.H., Quaegebeur, N., Hubert, P., Lessard, L., Masson, P. A comparative study of guided wave interaction in composites with artificial delamination and impact damage, submitted to *Structural Health Monitoring, an International Journal*.
2. Sherafat, M.H., Guitel, R., Quaegebeur, N., Hubert, P., Lessard, L., Masson, P. Structural health monitoring of a composite skin-stringer assembly using within-the-bond strategy of guided wave propagation, *Journal of Materials and Design* 2016; 90: 778-794.
3. Sherafat, M.H., Guitel, R., Quaegebeur, N., Lessard, L., Hubert, P., Masson, P. Guided wave scattering behaviour in composite bonded assemblies, *Composites Structures* 2016; 136: 696-705.
4. Sherafat, M.H., Quaegebeur, N., Hubert, P., Lessard, L., Masson, P. Finite element modelling of Lamb wave propagation in composite stepped joints, *Journal of Reinforced Plastics and Composites* 2016*;* 35(10) 796-806.

Conference Papers:

5. Sherafat, M.H., Quaegebeur, Lessard, L., N., Hubert, P., Masson, P. Guided wave propagation through composite bonded joints, EWSHM-7th European Workshop on Structural Health Monitoring, 8-11 July 2014, Nantes, France.
6. Sherafat, M.H., Lessard, L., Hubert, P. Damage detection in a composite skin-stringer panel using lamb wave propagation technique: a numerical study, 20th International Conference on Composite Materials, 19-24 July 2015, Copenhagen, Denmark.
7. Sherafat, M.H., Guitel, R., Quaegebeur, N., Lessard, L., Hubert, P., Masson, P. Characterization of guided waves propagation in a composite skin-stringer

assembly, 10th International Workshop on Structural Health Monitoring , 1-3 September 2015, Stanford, CA, USA.

8. Ostiguy, P.C., Sherafat, M.H., Franca, D.R., Bouslama, N., Quaegebeur, N., Maslouhi, A., Lessard, L., Hubert, P., Viens, M., Mofakhami, M.R., Hajjar, Z., Masson P. Selection of structural features for the systematic study of guided wave propagation and interaction with damage, 10th International Workshop on Structural Health Monitoring, Sept. 2015, Stanford, CA, USA.

7.5 Future Work

Aircraft structures are increasingly incorporating hybrid (bolted-bonded) joints as composite principle structural elements. Thus, for future work, the methodology of using guided wave propagation in composite bolted joints, and hybrid joints should be developed. The effects of diameter and location of the hole as well as the bolts on the wave behaviour, are the key elements that need to be assessed. Other complex features such as the monolithic to honeycomb transitions, and metallic-composite joints are also other common features in the aircraft structures for which the methodology developed in this research can be applied.

As aircraft structures experience a broad range of temperature, pressure and moisture gradients during their service, the influence of environmental conditions on the quality of the guided wave behaviour should also be investigated. The quality of the joints before and after the environmental damage (ED) is a research question which should be addressed.

It was shown in the presented work that the developed methodology assists inspection of composite joints regarding damage detection. A strategy for damage localization with the present methodology should be developed. Moreover, the severity and size of the damage and their attribution to the level of the scattering, refraction or transmission coefficients should also be considered.

These research developments assist comprehensive understanding of guided wave behaviour in composite assemblies, thus helps to facilitate the verification, validation and certification process of application of such a technique on real aircraft structures.